Lasse Skogström

A Novel Approach for Rapid Reliability Assessment of Power Electronics under Combined Vibration and Thermal Loading

School of Electrical Engineering

Thesis submitted for examination for the degree of Master of Science in Technology.

Espoo 5.5.2014

Thesis supervisor:

Prof. Mervi Paulasto-Kröckel

Thesis advisor:

D.Sc. (Tech.) Jue Li

Aalto University
School of Electrical
Engineering

AALTO UNIVERSITY
SCHOOL OF ELECTRICAL ENGINEERING

ABSTRACT OF THE
MASTER'S THESIS

Author: Lasse Skogström

Title: A Novel Approach for Rapid Reliability Assessment of Power Electronics under Combined Vibration and Thermal Loading

Date: 5.5.2014 Language: English Number of pages:8+88

Department of Electrical Engineering and Automation

Professorship: Electronics integration and reliability Code: S-113

Supervisor: Prof. Mervi Paulasto-Kröckel

Advisor: D.Sc. (Tech.) Jue Li

This thesis develops a method for comprehensive reliability assessment. The method is developed to assess the lifetime of power electronics under concurrent vibration and thermal loading. The approach is based on experimental reliability tests, Weibull model, and a simple modified Coffin-Manson lifetime prediction. The method can be used to predict component or system lifetime under vibration excitation at different temperatures. It is designed especially for industrial applications, where development cycles are short.

To validate and improve the developed approach, lifetime prediction for experimentally tested D^2PAK power electronics component was generated, accompanied by an in-depth failure analysis. Based on these results the influence of temperature on the failure characteristics was analyzed. It is widely recognized that the temperature has a significant effect on the material properties. The changing material properties can affect the mechanical response of the system, thus substantially influencing the vibration lifetime. Different temperatures can even induce new failure modes. Because of these effects, comprehensive understanding of temperature's influence on vibration lifetime is vital.

Outdoor environments for applications, such as automotive drive systems, are notably harsher compared to traditional indoor applications. In addition to harsh environment, also long-term reliability is required; e.g., the lifetime of automotive electronics is often standardized to be at least ten years. Temperature cycles and high operational temperatures combined with vibration and shock impacts can pose a significant reliability threat. Furthermore, moisture and contaminants make the environment even more hostile for the electronics.

Results obtained in this study, indicate that rapid, comprehensive and accurate reliability assessment can be conducted by following the provided guidelines.

Keywords: reliability, reliability assessment, power electronics, electronics, vibration, lifetime, lifetime prediction, lifetime model, temperature, combined loading, concurrent loading

AALTO-YLIOPISTO
SÄHKOTEKNIIKAN KORKEAKOULU

DIPLOMITYÖN
TIIVISTELMÄ

Tekijä: Lasse Skogström

Työn nimi: Uusi menetelmä nopeaan tehoelektroniikan luotettavuusarviointiin yhdistetyssä tärinä- ja lämpötilarasituksessa

Päivämäärä: 5.5.2014 Kieli: Englanti Sivumäärä:8+88

Sähkötekniikan ja automaation laitos

Professuuri: Elektroniikan integrointi ja luotettavuus Koodi: S-113

Valvoja: Prof. Mervi Paulasto-Kröckel

Ohjaaja: TkT Jue Li

Tässä työssä on kehitetty menetelmä kattavan luotettavuusarvioinnin suorittamiseen. Menetelmä on suunniteltu tehoelektroniikalle yhdistettyyn tärinä- ja lämpörasitusympäristöön. Se perustuu kokeellisiin mittauksiin, Weibull malliin ja muokattuun Coffin-Mansonin elinikäennusteeseen. Menetelmän avulla voidaan ennustaa komponentin tai järjestelmän elinikä tärinärasituksessa eri lämpötiloissa. Se on suunniteltu erityisesti teollisuussovelluksiin, joissa kehityssyklit ovat tavallisesti nopeita.

Menetelmän kehittämiseksi ja arvioimiseksi luotiin elinikäennuste ja suoritettiin vikaantumisanalyysi kokeellisesti testatulle D^2PAK tehoelektroniikkakomponentille. Tulosten perusteella analysoitiin lämpötilan vaikutusta vikaantumiseen. Lämpötilalla on tunnetusti merkittävä vaikutus materiaaliominaisuuksiin. Materiaaliominaisuuksien muutos voi muuttaa systeemin mekaanista vastetta, ja täten merkittävästi vaikuttaa elinikään tärinärasituksessa. Lämpötilan muutos voi jopa johtaa uusiin vikaantumismekanismeihin. Näiden vaikutusten johdosta on olennaista ymmärtää lämpötilan vaikutus elinikään tärinärasituksessa.

Ulkoilmaympäristöihin suunnitelluissa sovelluksissa, kuten ajoneuvojen voimansiirtojärjestelmissä, ympäristö voi olla huomattavasti perinteisiä sisätilasovelluksia rankempi. Haastavan ympäristön lisäksi näissä sovelluksissa vaaditaan pitkäaikaista luotettavuutta, esim. ajoneuvosovelluksissa tavallisesti vähintään kymmenen vuotta. Lämpösyklit ja korkeat käyttölämpötilat yhdistettyinä tärinään ja iskuihin muodostavat merkittävän uhan luotettavuudelle. Lisäksi kosteus ja epäpuhtaudet tekevät ympäristöstä entistä haastavamman.

Tämän työn tulokset osoittavat, että on mahdollista luoda kattava ja tarkka luotettavuusarvio seuraamalla luotuja ohjeita.

Avainsanat: luotettavuus, luotettavuusarviointi, tehoelektroniikka, elektroniikka, elinikä, elinikäennuste, elinikämalli, tärinä, lämpötila, yhdistelmätestaus

Preface

This work has been done in the Aalto University School of Electrical Engineering at the department of Electrical Engineering and Automation in the unit of Electronics integration and reliability. Work was a part of a project to develop methods and guidelines for rapid reliability assessment and improvement of commercial harsh environment inverter.

I would like to thank my supervisor Prof. Mervi Paulasto-Kröckel and advisor D.Sc. Jue Li for the opportunity and the valuable guidance with this thesis. I also appreciate the numerous discussion with the personnel of our unit, especially D.Sc. Vesa Vuorinen. Special thanks to D.Sc. Jue Li for FE-modeling and Nikolai Mäntyoja for help in conducting experimental testing and sample preparation as well as for the valuable comments and proof reading. D.Sc. Juha Karppinen is also acknowledged for participating and leading the previous part of this project.

I would also like to thank my partner, family and friends for the understanding and support during the work with this thesis.

Otaniemi, 21.3.2014

Lasse Juhani Skogström

Contents

Symbols and abbreviations

Symbols

a	Experimental power law lifetime model coefficient
A	Pre-exponential factor
b	Experimental power law lifetime model exponent
b_f	Fatigue strength exponent
c	Experimental coefficient for Coffin-Manson model
E	Young's modulus
E_a	Activation energy
f_r	Frequency in field conditions
f_t	Test frequency
$F(t)$	Weibull cumulative density function
k	Acceleration factor
k_b	Boltzmann constant
N_f	Lifetime in cycles
s'_f	Fatigue strength coefficient
t	Time
t_c	Time conversion coefficient
T	Temperature
T_g	Glass transition temperature
T_h	Homologous temperature
T_m	Melting point temperature
$P(c)$	Probability of component failure
$P(p)$	Probability of product failure
R^2	Goodness of fit, describes how well statistical model fits to a set of observations
x	Stress or strain in component lifetime model
α	Usage coefficient
α_l	Thermal expansion coefficient of length
β	Weibull shape parameter
γ	Weibull location parameter
$\Delta\varepsilon'_p$	Plastic strain range
Δl	Change of length
ΔT	Change of temperature
ε	Strain
ε'_f	Fatigue ductility coefficient
η	Characteristic lifetime, i.e. point where 63,21% of the population have failed
σ	Stress

Abbreviations

2D	2-dimensional
3D	3-dimensional
AC	Alternating Current
AEC	Automotive Electronics Council
BGA	Ball Grid Array
BJT	Bi-Junction Transformer
CABGA-256	ChipArray® Ball Grid Array surface mount component with 256 I/O's
CTBGA	ChipArray® Thin Ball Grid Array
CTE	Coefficient of Thermal Expansion
D^2PAK	Surface mount component package type
DC	Direct Current
DUT	Device Under Testing
EDS	Energy-Dispersive X-ray Spectroscopy
ENIG	Electroless Nickel and Immersion Gold
ESD	Electrostatic Discharge
EV	Electric Vehicle
FE	Finite Elements
FEA	Finite Elements Analysis
FEM	Finite Elements Method/Modeling
FIT	Failures In Time
FPGA	Field Programmable Gate Array
FR4	Common printed wiring board material consisting of resin, glass fibers and copper
G	Acceleration of $9,81 m/s^2$
HALT	Highly Accelerated Life Testing
HASS	Highly Accelerated Stress Screening
HCF	High Cycle Fatigue
HETB	Harsh Environment Test board / name of used test board
IC	Integrated Circuit
IDSA	Incremental Damage Superpositioning Approach
IEC	International Electrotechnical Commission
IGBT	Insulated-Gate Bipolar Transistor
IMC	InterMetallic Compound
IPC	Association Connecting Electronics Industries
JEDEC	Solid State Technology Association
JESD	JEDEC reliability standard series
LCF	Low Cycle Fatigue
LDSA	Linear Damage Superpositioning Approach
LED	Light Emitting Diode
MIL-HDBK	Series of handbooks for various purposes produced by United States department of defense
MOSFET	Metal-Oxide-Semiconductor Field-Effect Transistor
MTBF	Mean Time Between Failures

MTTF	Mean Time To Failure
OSP	Organic Solderability Protector
PoF	Physics of Failure
PWB	Printed Wiring Board
QFP	Quad Flat Package
RMS	Root Mean Square, i.e. quadratic mean
SAC305	Solder with 96,5 wt.% tin (Sn), 3,0 wt.% silver (Ag) and 0,5 wt.% copper (Cu)
SAC387	Solder with 95,5 wt.% tin (Sn), 3,8 wt.% silver (Ag) and 0,7 wt.% copper (Cu)
SEM	Scanning Electron Microscope
TR332	Telcordia, US Commercial Telecommunication Standard
SR332	Telcordia, US Commercial Telecommunication Standard
TSOP	Thin Small Outline Package
US	United States
USA	United States of America
wt.%	Percentages in weight

1 Introduction

Design for reliability is a vital part of product development, as reliability is always a financial concern and often a safety issue. Poor reliability causes more returns and costs in fixing or replacing returned products. Reliability problems will increase customer dissatisfaction, resulting in the loss of reputation and decreasing brand value. In a worst case scenario, one seemingly tiny mistake in the design may damage the company dramatically. In many applications, such as in automotive and aviation applications, electronics control multiple safety-critical systems, where the failure may have catastrophic consequences to the people concerned and to the company itself.

During recent years power electronics are being applied to harsher environments. Traditionally many of the applications have been stationary with stable conditions, such as indoor industrial applications. Nowadays, for example in electric- and hybrid-electric vehicles, wind turbines, or seafaring applications, power electronic systems are commonly used also in very harsh environments. [1] In the harsh environments, such as in automotive applications, numerous stresses; e.g., large temperature variations, vibration, shock impacts, moisture, and contaminants are constantly present [2]. These stresses can originate from the device itself as well as from the external environment. The environment like this combined with the heat generation resulting from the high power levels, makes the reliability a key concern. Moreover, stresses usually affect the device concurrently or consecutively; despite this, most of the reliability tests focus only on a single stress.

Single parameter stress tests are often used to simplify and speed up the reliability evaluation. Accelerated tests are used to simulate the stresses faced by the product during its lifetime. The acceleration is achieved by increasing the stress level and frequency of occurence. [3] The analysis of single parameter tests is relatively simple as only one changing parameter needs to be considered, and all changes in behavior and lifetimes can be expected to be dependent on that parameter.

However, in many cases, these single parameter reliability tests do not represent the reality sufficiently. Often, some failure mechanisms may only appear under certain more complex conditions. It is known that temperature has a considerable effect on material properties [4]. Many of the materials e.g., solder alloys, used in electronics often operate at high homologous temperatures (relative temperature from 0 K to melting point), generally $T_h > 0,4T_m$, which results in a larger temperature effect compared to traditional engineering materials; e.g., copper or steel. For example, vibration testing under high or low temperatures may yield different failure modes, due to changing material properties of certain materials or relative change between several materials [5]. Even if the failure modes remain the same, the lifetime will most likely change.

To gain profound knowledge of the products lifetime and reliability, comprehensive and well designed testing is required [3]. Experimental testing program should be designed based on the real usage environment. The results obtained from a poorly designed test are a waste of resources. A Test conducted in too harsh or tender environments may lead to erroneous improvements or give overly confident results.

For example, some failure mechanisms may occur only under very high stresses, if the product never faces as high stresses, fixing these problems is irrelevant. When considering the combined loading, test design is even more critical, and requires in-depth understanding of the underlying mechanisms and the product itself.

With combined loading approach, testing time and required resources can be saved, even though the test design and interpretation is more difficult compared to single load tests [6]. Due to market competition, development cycles are constantly shortening, whereas functionality increases and size decreases. Therefore, the reliability is increasingly critical issue but available testing time is scarcer.

Under the combined vibration and temperature loading, failure modes can be the same as under single loading conditions. Failure modes depend on the dominant loading parameter. In addition, they can also be combinations of failure modes seen under the single load conditions. [5, 7]

This thesis develops a method for comprehensive reliability assessment under combined vibration and thermal loading. The approach is developed primarily for studying solder interconnection reliability in power electronics. The goal of the method is to generate a component based lifetime prediction model in a short time. The approach is designed to serve especially the needs of the industry, where the development cycles are short. In the method, vibration excitation tests are conducted in various temperatures. A specific test board was designed to maximize the efficiency and to provide high amounts of reliability data.The developed setup maximizes the reliability data from each test run, i.e. orientation specific results can be obtained with several strain amplitudes within a single test run.

Although the test method aims for the power electronics it can also be applied to other applications, such as consumer electronics. No exact test parameters are defined, parameters such as test temperatures and vibration excitation levels are case specific, and should be designed with the real field conditions in mind.

The designed test method is utilized to produce a lifetime prediction for a D^2PAK power electronics component. This test method execution will work as a validation of method, as well as be an example of the recommended workflow. To ensure efficient usage of the method in the future, major pitfalls and aspects worth considering were mapped out during the validation testing. Comprehensive failure analysis will be conducted to investigate the failure modes. The results obtained through comprehensive failure analysis can increase the knowledge of the fracture characteristics under combined load testing. For the further development of the method, new test program is developed based on the findings of this study.

This thesis consists of the background, developed method, and experimental analysis. Background part covers the effects of temperature and mechanical stresses, as well as the reliability, power electronics, and lifetime modeling. They are followed by the review of the relevant parts of accelerated reliability testing. Secondly, the workflow of the developed method is presented. Lastly, the experimental part explains the application of the method, accompanied by the results and discussion.

2 Background

2.1 Reliability in electronics

Reliability can be defined as follows: "Reliability is the probability that an item operating under stated conditions will survive for a stated period of time" [8]. However the reliability from the user point of view can differ. User may often ignore the stated conditions or time. From a customer's point of view reliability can be defined as simply as "does the product do what is expected." Even this may be different with different customers, small fault may make one user consider product to be faulty, whereas others may still consider it as working. Especially consumers often blame the manufacturer for faulty product, even if the failure occurs due to misuse e.g., exceeding the stated conditions. To minimize the costs of failures reliability has to be considered throughout the whole process from design to manufacturing and usage.

The potential cost of failures increases throughout the process. Generally accepted guideline is that the cost of one failure increases by one order of magnitude after each process stage. If faulty component can be picked out before assembly, fixing is simple and easy, only the replacement of the component is necessary. If failure can be detected after component board (printed wiring board, PWB, with components) assembly, the price has increased to tenfold. After product assembly the price has increased to hundred times the price of the first step. Finally, if the failure is detected by the user, the price is already thousandfold. In case of user detecting the failure, increased repairing and/or warranty costs are not the only concern. The cost of lost reputation and brand value are often even more significant compared to the other costs of failure.

In many applications, such as automotive and avionics, electronics control multiple safety critical systems. Failures in these may have catastrophic consequences to people concerned as well as to the company. A catastrophic event can lead to deaths of passengers or bystanders. In such cases, also lost reputation and brand value with high indemnities can cause damage large enough to bring the whole company down to bankruptcy. In addition flaws in design, once discovered, may lead to large and costly callback campaigns, especially in automotive industry. However callback campaigns do not usually concern the actual electronics. Around 30 % of callbacks in Finland are due to electrical system, but this also concludes software updates and many of rest are due to wiring and connector problems [9, 10].

Three fundamental activities are required for reliable product development. Design for reliability, reliability verification and analytical physics tools should be used during the whole product development. Design for reliability is a method utilized to improve the design and reduce the potential problems using physics-of-failure knowledge. Product and process reliability should be analyzed and proved to meet or exceed the customer requirements during the verification stage. With the help of analytical physics, possible failures should be analyzed and understood. With this knowledge, improving the reliability design of the product and the future products is more efficient. [11]

Understanding the effect of design to reliability is critical. If everything is not designed with reliability in mind, product reliability may be compromised. Overlooking a small detail may result in the poor reliability of the whole product. Whole assembly should always be considered, for example the effect of component board mounting can have immense effect on the stresses occurring. Even if the stresses on the component board alone are small with assumed excitation levels mounting can increase these notably. For example, if mounting mechanics and component board have overlapping resonant frequencies, stresses may multiply compared to the component board being alone. FE-modeling is often used to analyze effects like these, as prototype building and analysis is time consuming, especially if it has to be repeated numerous times.

Product lifetime can be divided into three stages, where different failure types affect the reliability. These three stages are infant mortality, normal life and wear-out. During these stages product failure rate is commonly described to follow bathtub curve behavior [8, 11]. A schematic representation of the bathtub curve is presented in figure 1.

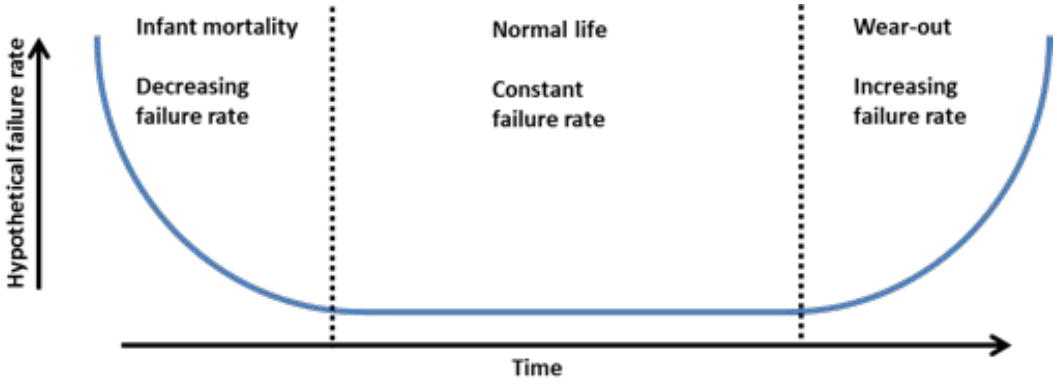

Figure 1: Bathtub curve, failure rate as a function of time.

During the early life of the product failures are dominated by defective components and problems due to manufacturing process. Failures during the first stage are usually referred to as infant mortality. Screening processes are used to screen out at least most of the products containing defects. After defective components have failed during the early life of the product failure rate will decrease. In second stage, most of the failures are random failures occurring on a steady rate. Rate of the random failures is usually dependent on the component type and environment and is described by FIT (Failures-In-Time) or MTBF (Mean Time Between Failures). During the last stage of product lifetime failure rate starts to increase due to wear-out mechanisms. [8, 11]

Common locations for failures are the various interconnections. In this thesis main focus is on the board level interconnection reliability. In addition to this, IC-level, package level and system level interconnections can be distinguished.[12] IC- and package level interconnection reliability is usually the focus of the component manufacturer. Board and system level interconnection reliability is the responsibility of the company manufacturing and designing the assembly and/or product.

Naturally weak reliability in the two lower levels is also problem for the product manufacturer. In these cases it is beneficial to discuss with component manufacturer. Other options are changing the component supplier or choosing a more reliable package type.

On board level solder interconnection is usually considered to be the weak point, especially with surface mount components. In addition, failures may occur on the PWB copper traces or in the component lead. During product lifetime, many environmental aspects affect the reliability and the failure location. Two of these, namely temperature and mechanical stresses are discussed in the following sections.

2.2 Power electronics

Power electronics are solid-state electronics used to convert the electric power of source to suitable form for the load. Semiconductor devices such as switches are used to alter the voltage and current. [1] Relevant power levels can range from milliwatts used in small battery powered equipment to gigawatts used in power plant applications [13]. In this study we are mostly interested in challenging mobile applications such as automotive. Relevant power in these applications is usually measured in tens or hundreds of kilowatts.

Power converters can be divided into four groups according to their input and output [1]:

- AC/DC, Input AC (alternating current) is converted to the DC (direct current) of desired level. For example standard outlet 230V/50Hz is converted to 5V DC for mobile phone charging.
- DC/AC, Input DC converted to AC. For example, the DC of a battery pack of an electric vehicle (EV) is converted to the AC of the desired amplitude and frequency for driving an electric motor.
- DC/DC, Input DC is converted to a regulated amplitude of DC. For example, the conversion of DC from the battery to lower or higher amplitude, required by the drive system.
- AC/AC, Input AC is converted to the AC of different amplitude and/or frequency; e.g., to control the power and frequency of an electric motor.

For automotive applications all of these conversions are relevant. In an EV, a battery pack is normally used for energy storage and electric motors that power the wheels. Different conversions are required in various parts of the system. Firstly DC/AC conversion is required to convert the DC power from the battery pack to the AC powered induction motors. With AC/AC conversion it is possible to control the speed and power of the motor. In traditional internal combustion engine vehicles, most of the electric systems are 12 V or 24 V systems. The voltage of the battery pack in an EV is usually higher to serve the needs of the electric motors, thus DC/DC conversion is needed to adjust the voltage levels for other systems. The charging of the battery module is conducted by using the 230 V/50 Hz or higher

power networks. To charge the battery module by using the power network, the AC power has to be converted to DC, as well as when using the braking enegy for charging. [14, 15]

Semiconductor devices used in power electronics are commonly diodes, thyristors and transistors. Diodes and thyristors are used as switches, diodes being uncontrollable and thyristors controllable. Transistors, such as MOSFETs (Metal-Oxide-Semiconductor Field-Effect Transistor), BJTs (Bipolar Junction Transistor) and IGBTs (Insulated Gate Bipolar Transistor) are also used as switches, but they allow the complete control of on- and off-states [1]. High power IGBT modules can operate at voltages up to 6,5 kV and currents up to 1,2 kA [16].

Similar systems to drive electric motors have traditionally been used in static environments, such as in the industry. In the industrial applications systems are for examples used to drive electric motors controlling machines like robots or other production equipment. In these applications the usage environment is commonly very mild. External temperatures are relatively constant, systems are not subjected to high vibration excitation levels or impacts.

Environments in automotive applications and other harsh environments are more dynamic. External temperatures can range from -40 $°C$ to 50 $°C$. Furthermore, the changes of external temperature can be rapid; e.g., driving outside from a garage during the winter can result in large temperature change. While driving, constant vibration and shock loads are expected. During operation power levels can vary constantly from near zero, while coasting, up to hundreds of kilowatts consumed by full acceleration.

The efficiency of a system is never ideal, thus a fraction of the power will be consumed by heat generation. This can result in substantially high temperatures. In industrial applications, due to less strict space requirements, powerful cooling systems can be used to manage the heat generation. Whereas, in the automotive applications the usage of similar cooling systems is more difficult, due to space restrictions. Local ambient temperatures in automotive applications can reach 150 $°C$ and local operational temperatures 200 $°C$ [2]. In addition, high temperature gradients and temperature cycles are present due to heating of certain components. Moreover, the vibration levels of 10 G RMS are common [2]. As a conclusion, automotive environment is very harsh compared to traditional indoor industrial environments.

Power electronic components are often very large and rigid, due to the requirements of the high powers, and thus, quite reliable. However these systems require control systems such as large FPGA components (field programmable grid array). These components are commonly BGA (Ball Grid Array) components, where the size of a single interconnection is relatively small. Even if the power components can handle the stresses, controlling components can raise a reliability concern.

2.3 Lifetime modeling

Lifetime models are a crucial part of the reliability studies. Lifetime models are commonly used to assess the product reliability. Additionally to the importance,

lifetime predictions are one of the most challenging parts of the reliability assessment. The extrapolation of the accelerated results requires knowledge and understanding of the field conditions and acceleration factors [6]. For accurate predictions, an immense amount of factors has to be considered.

Lifetime models are based on experimental data from accelerated tests and/or actual field reliability data. More advanced models also incorporate the accumulating damage properties during cyclic loading conditions. [6] In this thesis several prediction methods are described (namely failure rate models and Coffin-Manson model). Additionally some other popular methods are briefly presented, more detailed descriptions can be found in references. In addition to models presented here, Arrhenius model presented in section 2.4 can be categorized as lifetime model for certain temperature dependent mechanisms.

Failure rate models

Failure rate models are often used to calculate the component normal life failure rate. Commonly used terms are FIT (Failures In Time, failures per 10^9 h) and MTBF (Mean Time Between Failures) or MTTF (Mean Time To Failure).

FIT and MTBF values are a common base for reliability predictions. During the useful life, failure rate is usually considered to be constant and component type specific, thus values for different components can be found from literature. One of the most comprehensive sources for failure rate data is the MIL HDBK217 [17]. It allows the calculation of failure rate for active and passive components and also for connectors and other appliances, such as electric motors. The standard provides two methods: parts count and detailed stress method. Of these two, the parts count method is simpler and optimal for early design phase analysis. The detailed stress method on the other hand is more accurate as it considers the actual stresses but is also more labor intensive.

As the MIL-standards are designed for military applications, which have very high reliability requirements, they can be pessimistic for consumer product applications. For this reason other standards have been developed; for example, Tellcordia (Bellcore) TR-332 and SR-332. Tellcordia methods are based on the MIL-HDBK217, but are optimized and simplified for more commercial applications. Additionally to given data, methods for utilizing laboratory test and field data are given in the Tellcordia methods.

As these are predictions based on assumptions, the effect of different factors should always be considered to evaluate the reliability and accuracy of prediction. Care should be taken always when choosing the parameters for predictions. Despite the known weaknesses, when properly executed, these methods are shown to work as a good guideline when designing reliability. [11] One of the largest benefits of failure rate approach is the easy usage. Lifetime prediction can be established without experimental testing, based solely on the know or assumed conditions. However, the accuracy of these predictions should always be critically reviewed.

Weibull distribution

One of the most versatile and used statistical tools in reliability prediction is Weibull distribution developed by Waloddi Weibull in 1951. It was developed for describing material breaking strength and ball-bearing lifetimes. It is nowadays widely used in various reliability applications. [8]

Most often, two parameter Weibull distribution is used. Cumulative probability density function $F(t)$ is presented in equation 1, where η is the characteristic lifetime and β is the shape parameter. The shape parameter β corresponds to the failure rate of the test specimen and is expected to correlate with different failure mechanisms. For full three parameter Weibull, γ parameter is also included. This parameter is called as the location parameter or minimum life.

$$F(t) = 1 - e^{-(t/\eta)^{\beta}} \tag{1}$$

For lifetime applications cumulative Weibull curves are usually plotted on charts where the percentage of failed population is presented as a function of time. Lifetime parameter η represents the point where 63,21 % of the population have failed. Shape parameter β defines the shape of the distribution. Some basic characteristics can be recognized as follows:

- $\beta < 1$: decreasing failure rate
- $\beta = 1$: constant failure rate
- $\beta > 1$: increasing failure rate

In addition, Weibull shape parameter is said to correlate with the failure mode [5]. This allows; for example, comparison between different conditions or helps detecting the changes in failure modes under different conditions. For example, if testing is conducted under several different stress levels, we can create Weibull model for each magnitude of stress. It is possible, that β-value can change between different test amplitudes or during a same test condition. Results like this suggest that there can be a change in the failure mode between the lower amplitude and the higher amplitude tests. However often failure analysis is required to confirm these findings.

As Weibull model can correlate with failure mode, cases with numerous failure modes can be problematic. If the goodness of fit between the model and the observations is weak, the possibility of multiple failure modes should be considered. It can be problematic to compare the different Weibull model cases, where multiple failure modes exist. For the actual lifetime prediction all of the failure modes need to be considered.

Coffin-Manson model

Coffin-Manson lifetime model is strain based power law model developed by Manson [18] and Coffin [19]. Similar models based on the power law are often referred to as "Modified Coffin-Manson equations". Coffin-Manson equation (equation 2 and similar models are widely used for predicting lifetime in electronics [6]. The simple

power law lifetime model used in this thesis is essentially a modified Coffin-Manson model. In equation 2 N_f is the lifetime in cycles, ε'_f the fatigue ductility coefficient, $\Delta\varepsilon_p$ the plastic strain range and c is the experimental coefficient. Model considers only plastic strain, thus being optimal for modeling low cycle fatigue.

$$\frac{\Delta\varepsilon_p}{2} = \varepsilon'_f(2N_f)^c \tag{2}$$

To incorporate the high cycle fatigue on the model Basquin equation [20] can be combined with Coffin-Manson model. Model is presented in equation 3 is often called the Total strain model [21]. Additional terms s'_f, E and b_f are the fatigue strength coefficient, Young's modulus and fatigue strength exponent respectively.

$$\frac{\Delta\varepsilon_p}{2} = \frac{s'_f}{E}(2N_f)^b_f + \varepsilon'_f(2N_f)^c \tag{3}$$

Engelmaier model

Engelmaier model [22] is based on the Coffin-Manson model, and is developed for the lifetime prediction of solder joints. Even though, it is very popular model, it still has some disadvantages. Due to simplified assumptions it cannot be used for creep, and it does not consider the joint geometry and is usable only with certain package types. [23]

Energy-based models

Compared to strain based models presented earlier, energy based model are newer and more accurate. They are based on the stress-strain hysteresis energy of interconnection or system[6]. Several widely used models are, first of which possibly the most popular one:

- Darveaux [24], separates crack initiation and growth.
- Liang [25], Engelmaier based, but strain-stress energy as a criterion.
- Syed [26], designed for creep deformation.

Multiparameter lifetime models

To predict lifetime under multiple loading conditions, several methods have been developed. Firstly, the Linear Damage Superposition approach (LDSA) by Palmgren [27] and Miner [28]. Due to several shortcomings of LDSA second method called the Incremental Damage Superposition Approach (IDSA) has been developed by Dasgupta and Upadhyayula [3].

In LDSA, it is expected that multiple normalized damage fractions can be superimposed. The damage fraction of any stress is assumed to be linearly dependent on the ratio between number of cycles and the number of cycles required for failure. Major shortcomings of the model are: i) load sequence has no effect, ii) only one

damage mechanisms is assumed to exist, iii) the interactions of different loads are not considered. [6]

Afore mentioned shortcomings are addressed in the IDSA. It can be considered as the LDSA broken down in small parts, each of which represents one stress cycle. Incremental parts account for different stress levels and time scales. In addition, other stress parameters are considered as a function of temperature, which for solder interconnections is essential. [6] As a result, IDSA is superior, but more laborious method, compared to LDSA.

Physics of failure (PoF) based lifetime prediction

Lifetime prediction can be taken even one step further by accounting the actual physical reasons leading to failures. Above presented approaches are based on experimental data, which is fitted to curves. For more comprehensive reliability predictions, actual physical and microstructural phenomena should be considered during the modeling process[6].

One PoF based approach is developed by Upadhyayula and Dasgupta [3]. In the model, the whole stress history, microstructural evolution and damage accumulation is analyzed for each loading cycle. Due to its nature, the model will consider the interactions of different loads during the process and can reduce the uncertainties of damage superposition methods. However, it requires an immense amount of computational power and comprehensive material models. Due to the rapid evolution of electronic materials many material models are inaccurate or inexistent. However, in the future it is possible that PoF based lifetime modeling methods will emerge as feasible option for large scale analysis. [6, 3]

2.4 The effect of temperature

In electronics, a large array of different materials is commonly used. Based on their chemical & physical properties and structure, materials in general can be divided into following groups:

- Metals
- Polymers
- Ceramics
- Semiconductors
- Combinations of above, composites

All of these groups are used in electronics; often even a single component can contain materials from all these groups. Most common PWB material FR4, is a composite material consisting of glass fibers, resin, and copper metallizations. In addition, to PWB metallizations, metals are used as solders and component leads and metallizations. Polymers are often used as adhesives and for component packaging.

Ceramics can be used also as a PWB's base material and for component packages in applications, where very high reliability is required. Semiconductors are used for semiconductor components, such as IC's and diodes. The usage of materials with very different material properties makes reliability designing difficult [4].

Electronic assemblies are commonly multi-material systems, i.e. different structures are composed of multitude of materials. A simplified illustration of the multimaterial system is shown in figure 2. Interconnection is formed by the component lead, PWB pad, and solder. Most of the interconnection will be bulk solder; e.g., Sn with small amounts of Intermetallic compounds (IMC), mostly on the grain boundaries and as small colonies. In addition, IMC layers will form on the interfaces.

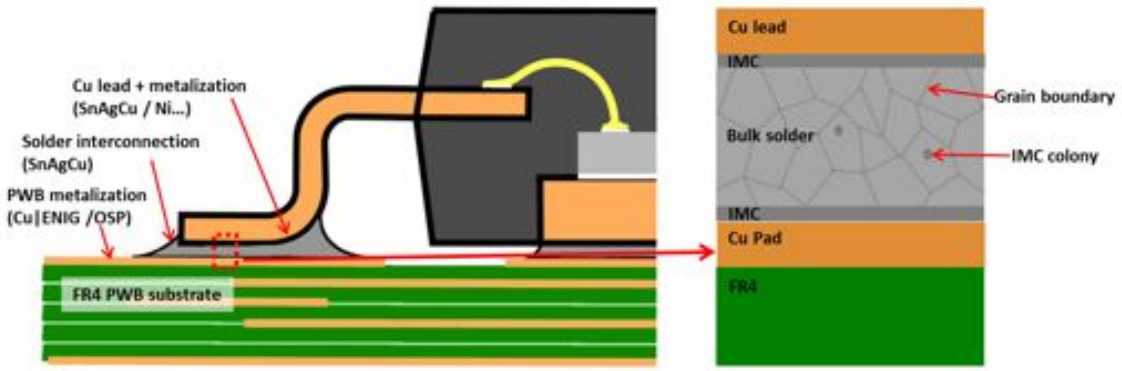

Figure 2: Simplified schematic representation of multimaterial system in solder interconnection, illustrated by a D^2PAK component. Drawn based on [29]. Images not in scale.

Intermetallic layers start forming during the re-flow soldering. In a simple SAC solder and Cu pad system, Cu_6Sn_5 forms first during the reflow. The other observable IMC, Cu_3Sn can usually be detected only after further annealing or thermal cycling. In more complex material systems, IMC formation is often more complex, but in most cases the material properties of intermetallic layers differ notably from bulk solder's properties. [30] Compared to annealing IMC layer growth is accelerated by thermal cycling due to thermomechanical stresses [31]. Intermetallic layers play a critical role especially during mechanical loading conditions, such as shock impact or vibration excitation;however, bulk solder microstructure is less significant in these conditions [5].

Due to its nature, temperature affects electronic assemblies, components and their reliability in a multitude of mechanisms. These mechanisms can be divided into three groups: the effect on material properties, acceleration of chemical reactions, and thermal stresses. All of these mechanisms may have a tremendous effect on reliability, especially during a long lifetime.

Material properties, such as Young's modulus, strength, plastic properties and CTE define material behavior and thus also their reliability. Material properties are dependent on the temperature and on the homologous temperature (T_H). T_H is

defined as the relative temperature of material i.e. ratio of the temperature and the material melting point temperature in Kelvin (K). Solder materials have relatively low melting points; i.e., SAC305 T_m = 217 °C. Whereas many metals used in electronics have substantially higher, for example, copper (T_m= 1085 °C). Respectively for SAC305 and copper homologous temperatures in -40 °C are T_H=0,48 & T_H=0,17 and in 100 °C T_H=0,76 & T_H=0,27. Conclusively with same absolute change in temperature, in the terms of the homologous temperature, solder materials temperature change is notably higher compared to copper.

Differences in the change of material properties as a function of temperature can be large. For example, SnAgCu solder alloy's Young's modulus drops from 47 GPa by 10 % to 28 % depending on the composition when increasing the temperature from 20 °C to 100 °C [32]. Whereas, the Young's modulus of copper (Cu) will drop only by 2,5 % from 110 GPa at the same temperature range [33]. This means that at different operational temperatures copper will be basically the same across the temperature range, while solder alloy may be notably harder or softer depending on the temperature. Difference like this can have a tremendous effect on the failure mode and lifetime under different temperatures.

Mechanisms, such as, diffusion, microstuctural evolution, electromigration, and corrosion are temperature dependent. Aging and evolution of the solder interconnection can have a substantial effect on the reliability during a long lifetime. However, these effects are not in the scope of this study but will be addressed in the future project.

The third effect of temperature is the stresses inflicted due to global or local temperature changes/differences. Temperature changes and differences occur due to internal and external factors. Internally, operational electronics produce heat. As different components and regions produce varying amounts of heat, temperature gradients are formed. As components are seldom operated at constant power level, also cyclic changes in the temperature gradients will occur. External temperature usually is not a constant but varies due to different factors, especially in mobile applications such as automotive or portable applications. Temperatures may vary simply due to weather or due to engine heating up or cooling down.

Thermal expansion can result in significant stresses, as CTE's of materials differ from each other. For example, FR4 has a CTE of 14 - 17 ppm/°C and silicon (Si) that is used for IC components has a CTE of 2,5 ppm/°C. Due to the CTE mismatch, the different parts of the assembly will deform different amounts, which results in stresses. Deformation under temperature cycle is presented in figure 3. In the figure, we can see bending, which occurs due to components restrictive effect on deformation. Bending will increase during temperature ramp-up and -down stages. During dwell-times i.e. high or low temperature holding time, the amount of bending will reduce due to relaxation. During the relaxation solder joints will plastically deform reducing the stresses in the system. Due to high homologous temperature, creep is the major factor affecting the relaxation[4]. At homologous temperatures above 0,5, creep will dominate the plastic deformation [34]. Moreover, it can even be a major failure mechanism [35]. Most of the deformation will occur in solder, as other materials are usually have lower homologous temperature. Thus the solder

interconnection is often the critical location.

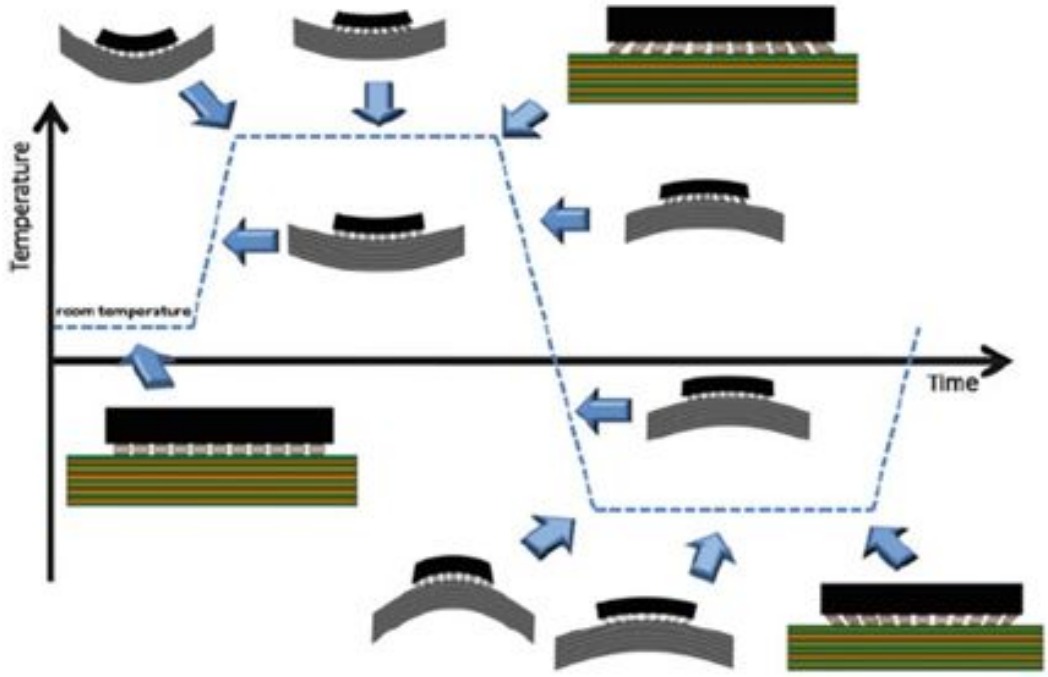

Figure 3: Deformation under temperature change in electronics assemblies[4]. During temperature ramp up/down bending increases, due to CTE missmatch. During dwell time relaxation occurs, resulting in plastic deformation and reducing bending.

Within this thesis, no cyclic thermal loads are utilized. However thermal stresses are expected to affect the system due to the temperature ramp up. Thermal expansion will change the behavior of the test setup between different temperatures. Solder joint will be stressed and some relaxation is expected to occur.

The amount of the plastic work done on the interconnection can be calculated by the area inside stress-strain hysteresis loop [4, 36]. During temperature cycles, a large span of homologous temperature has to be concerned, especially with solders. For example, in figure 4 a) a calculated stress-strain hysteresis loop is presented under thermal cycle from -55 $°C$ to 125 $°C$, in terms of homologous temperature from 0,45 to 0,82. Due to long temperature range, the material properties of solder vary notably. At higher homologous temperatures, the strength of solder is substantially weaker and creep is much more effective.[4] It can be seen that stresses are higher on lower temperatures, this can be explained by the difference in material properties. In higher temperatures, softer solder and faster creep rate will allow more rapid relaxation of the stresses during cycling. Creep and relaxation will occur during the whole cycling phase, but effect can be clearly seen during the dwell-times. Creep is plastic time dependent monotonous deformation under stresses, grain boundary sliding being the dominant mechanism [37].

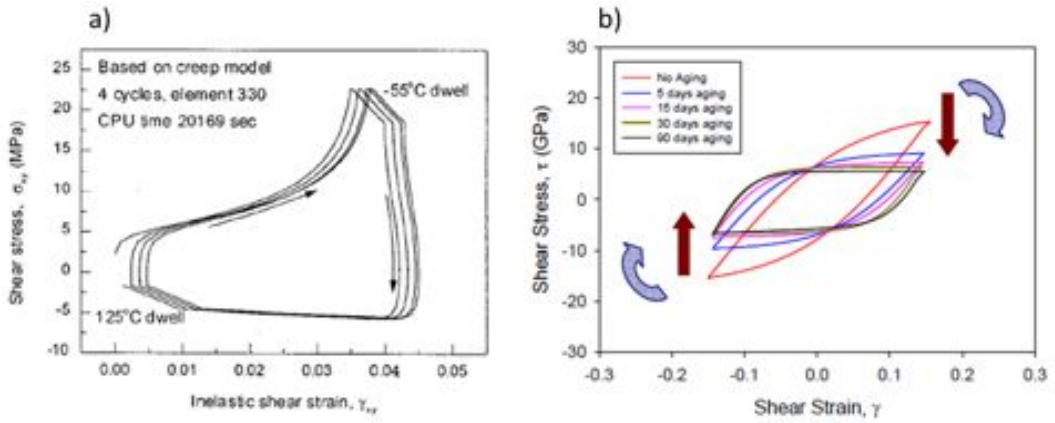

Figure 4: a) Calculated stress-strain hysteresis loop of solder under thermal cycling [38].b) The evolution of the stress-strain hysteresis loop under isothermal aging [36].

As stated earlier, aging will occur in materials under temperature exposure. In figure 4 b) the effect of isothermal aging on stress-strain hysteresis loop is presented. Due to isothermal aging in 125 $°C$, with strain controlled testing maximum stress will decrease. Equally, with stress controlled test, strains will increase. During isothermal aging, the shear strength of the solder will drop. As a conclusion, we can say that if strain is constant, isothermal annealing will reduce the amount of accumulating damage and if stress stays constant, isothermal annealing will increase the accumulated damage. [36] Even annealing of few days has notable effect on the stress-strain relationship. It is possible that in longer vibration tests at elevated temperatures, this will have an effect on the system behavior.

Stress-distributions in the interconnections are seldom evenly distributed. Due to the geometry of the interconnection and the whole system, stress concentrations can be found in certain locations. Most of the plastic deformation will occur in these concentrations, leading to microstructural evolution, such as recrystallization, and crack initiation and propagation [4].

In addition to solder, PWB or other polymer materials can also cause notable problems in higher temperatures. Glass transition temperature T_g is the temperature where the rigidity; e.g., the elastic modulus, of polymer materials drops significantly. For the standard FR4 PWB material $T_g = 130°C$ and for the high T_g FR4 $T_g = 180°C$. However, differences between manufacturers exist. Commonly high T_g FR4 boards also have higher elastic modulus and lower CTEs. [39]

2.5 The effect of mechanical loading

Electronic products often face mechanical vibration and shocks. Especially, as the amount of electronics increases constantly in mobile applications such as automotive, avionics and portable consumer electronics, understanding the effects of mechanical stresses is important. Failures occurring due to mechanical loading are often fractures around the interfacial region.

Similarly to thermal loading, mechanical loading results in PWB bending, thus inducing stresses to interconnections between components and PWB. Thermal stresses are dominantly shear stresses, whereas in mechanical loading normal stresses are dominant. The change of the main stress component can have large effect on the failure mode of the interconnection. [4] Furthermore, despite the similar cyclic bending behavior as under thermal cycling, due to faster bending rate, the amount of recovery is normally negligible.

Mechanical loading usually results in fatigue cracking. With very high stresses, like in drop testing, failures can also occur due to sudden overstress failures. Based on the amount of stress cycles, fatigue can be either low cycle fatigue(LCF) or high cycle fatigue(HCF), lifetimes being commonly below 10 k cycles and above 10 k cycles respectively. fatigue fracture starts with crack initiation phase, followed by crack propagation and in the last phase after the sufficient weakening of the interconnection, sudden overstress failure will occur. During LCF, plastic deformation is present whereas with HCF only elastic deformation will occur.[40] During thermal cycling or high amplitude mechanical loading, fatigue is usually LCF. Whereas with lower amplitude mechanical loading, like common vibration tests, HCF should be the main failure mode.

Fatigue is a damage mechanism that occurs at stress levels below the nominal strength of the material. Fatique cracks initiate at local defects, such as scratches or impurities. In locations like this, the local strength of the material can be lower. During the cyclic loading crack will open and close constantly. Due to cyclic loading, crack will slowly propagate as the constant opening and closing of the crack will deform the crack tip. [41, 42]

Drop impacts will induce large bending and excite the board to vibrate on its natural modes. Total PWB deformation is the sum of the different bending modes of the PWB or assembly [4]. With the vibration excitation it is possible to dominantly excitate certain frequencies, in addition other significant resonant modes may be excited even if the point frequency excitation is used. Depending on the application product can face, constant point frequency, varying point frequency sweep or random vibration, where multiple random frequencies are present simultaneously. Independent of the mechanical stress generally cycle frequency is from several hertzes to even thousands of hertzes. For comparison, in thermal cycling, cycle time normally ranges from tens of minutes to days. In terms of strain rate values respectively are in the range of 1-100 /s and 10^{-4} - 10^{-6} /s [4].

For solder materials, strain rate has large effect on the ultimate tensile strength and especially on the yield strength [4]. Similarly shear strength will also increase due to strain-rate hardening. While strain rate is increased from 10^{-6} to 10^{-1} ultimate shear strength will increase from 30 MPa to 80 MPa respectively as presented in figure 5. [43] Naturally behavior like this can have a marked change on the failure mechanisms under different strain-rates. The deformation rate dependency of material properties is dependent on homologous temperature [5]. As solder operates at high homologous temperatures, strain-rate hardening is especially important for bulk solder. For copper and common IMC's, melting point temperature is higher. And thus their homologous temperatures are also lower.

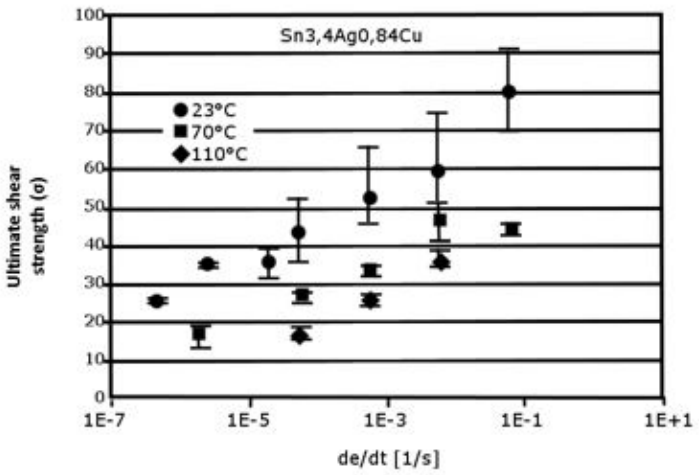

Figure 5: Experimental ultimate shear strength as a function of strain rate. Sn3,4Ag0,8Cu solder in several temperatures. [43]

As stated earlier, only negligible amounts of recovery and thus recrystallization normally happen under fast deformation rate mechanical stresses. In addition, strain-rate hardening also prevents the microstructural evolution to occur. Strain-rate hardening will also results in higher stress concentrations at interconnection corner regions. As these local stresses increase, they can exceed the yield strength of the intermetallic layers at the solder and pad interface, usually on the component side. [43]

Highest deformation rates are usually achieved with drop impacts. With vibration excitation strain-rate is usually slightly lower, but still notably above thermal cycling. Drop impacts commonly result in IMC cracking or copper trace fracture, especially in elevated temperatures. With the vibration excitation, failure modes can be similar to the drop impacts or solder fatigue cracking, depending on vibration amplitude. Compared to thermal cycling, failures due to vibration excitation usually have no recrystallization and cracking is ductile and transgranular. [5]

3 Accelerated reliability testing

Accelerated reliability testing is used to simulate the stresses occurring during the product lifetime in a significantly shorter time. With a large array of different testing methods and standards, basically everything that happens during product lifetime can be investigated.

Accelerated reliability testing is an essential part of the product development. With comprehensive testing, product reliability can be improved and estimated accurately. For designing a proper test, field use conditions and requirements have to be recognized. Incorrect test methods or stress-levels can lead to pessimistic, or even worse, optimistic reliability predictions. Concentrating on irrelevant failure modes is mostly a waste of money, thus the most critical stresses have to be distinguished.

Usually the customers require the filling of the reliability requirements according to certain standards. In addition to these, it may be beneficial to use specifically designed test methods to generate comprehensive lifetime and reliability predictions. As the standards often focus on single parameter stresses they may be inefficient during the development phase. Using well designed combined loading tests, reliability analysis can be made more efficient and relevant. After the internal reliability requirements have been met, standardized test can be used to prove reliability to the customer.

In addition to the reliability assessment, similar testing methods can be used for qualification and monitoring purposes [3]. Many of the standardized test are used for qualification, where a certain amount of products or components have to withstand a certain amount of stresses. Monitoring or screening is mostly used to observe process quality and to detect the faulty products in as early stage as possible.

Focus of this chapter will be on temperature related test and mechanical loading tests. These two are the most relevant for the method developed in this thesis. In addition, some other methods are briefly presented.

3.1 Single load testing

Most of the traditional and standardized test methods used are single parameter tests. They are preferred due to easier analysis and parameterization. In single load tests, the effect of certain stress condition parameter can be distinguished. However, as combined stresses may have marked effects on the behavior, lifetime and failure mechanisms, single parameter tests can not offer a complete understanding of the reliability.

Temperature and mechanical testing will be covered in following subsections. In addition, to these two groups, numerous other tests are commonly used. For example, different electrical tests e.g., power cycling & electrostatic discharge (ESD) and corrosion tests where DUT (device under test) is subjected to different corrosive agents e.g., humidity and corrosive gases.

Power cycling results in similar effects as temperature cycling, but heating is usually very localized and temperature gradients can be large. Additionally, power cycling can be used to investigate electromigration. Electromigration is usually a

problem in components with very thin aluminum and copper metallizations. High enough current densities lead to atomic movement potentially resulting in voiding and hillocking. In addition, it has been shown that as solder interconnection size reduces and current densities increase, the electromigration of solder joints may become a problem. [6]

ESD occurs due to internal or external voltage spikes. These sudden voltage spikes can easily harm sensitive IC-components. Sources can be e.g., a malfunction in component or a person touching the unprotected product or component. Due to static charging person touching the component can result in a surge of multiple kilovolts. [8]

Corrosion tests usually have defined environment, which is observed by reference samples. Test usually have certain temperature humidity and corrosive gas concentrations. The corrosion testing of electronics is important especially in outdoor applications and areas near seas, as in these regions conditions for corrosion are often good. [41]

Numerous test standards for the presented tests and many others can be found. For example, following parties have published test standards for various applications:

- US department of defense (MIL-standards)
- JEDEC (Solid State Technology Association)
- IPC (formerly: Institute for Interconnecting and Packaging Electronic Circuits)
- IEC (International Electrotechnical Comission)
- Telcordia
- AEC (Automotive Electronics Council)
- ...

JEDEC and MIL standards are probably the most widely used standards. MIL-standards and handbooks by the USA department of defense originating from the 1960's and 1970's were the first ones to aim for comprehensive reliability development and assessment. MIL standards have been revised through the years and are still widely used along the field. Many reliability prediction and test methods are based on them. The whole science behind electronics' reliability is considered to originate from these standards. The reliability of electronics was originally a concern especially in military applications.

Dozens of different standards for varying applications can be found. Different organizations may have similar standards which are optimized for certain applications. Many of the standards are defined for certain component type e.g., semiconductors, capacitors, or PWB. In addition, also product level standards exist.

Most of the standardized tests are used to investigate the sufficiency of the product reliability. Thus, they are not commonly used for lifetime testing. However, same procedures can be used as lifetime tests by simply testing until failure. In

lifetime testing acceleration factors should be considered. If too high stresses are used, the risk of changing failure mode and inaccurate results increases.

Temperature related testing

Temperature related tests can be divided into dynamic and static tests. In dynamic tests, temperature is changed constantly. Static tests are based on constant high or low temperature. Dynamic tests are usually conducted to simulate thermal stresses whereas static ones are used to accelerate temperature dependent mechanisms.

Dynamic tests are usually based on either temperature cycling or temperature shocks, for example, standards JEDEC JESD22-A104 [44] for the cycling and JESD22-A106 [45] for the thermal shock. Both of these tests are used to determine component's and interconnection's ability to endure thermal stresses. In addition, microstructural changes can be observed.

Temperature cycling test are usually conducted in one or multi chamber systems with air flow. Whereas in temperature shock tests, higher ramp rate is achieved with hot and cold fluids. For temperature cycling, usually maximum and minimum temperatures with ramp and dwell times are defined. In JESD22-A104, 11 temperature combinations are defined, minimum temperatures ranging from -65 $°C$ to 0 $°C$ and maximum from 85 $°C$ to 150 $°C$. Cycle times are from 20 minutes to 1 hour+ and dwell times from 1 minute to 15 minutes. As discussed earlier, solder joint microstructural evolution happens mostly during dwell times, thus 5 min - 15 min dwell times are recommended for these tests. Shorter dwell times can be used when only components are investigated, due to absence of plastic behavior in silicon (Si). An example of temperature cycling profile is presented in figure 6.

The main effects of temperature related testing are discussed in section 2.4. Failure modes resulting in temperature cycling are usually related to fatigue and delamination. Failure criterion for both tests should be case specific, usually either a complete failure e.g., open circuit due to fracture or a change in electrical properties. In solder interconnections the most common failure mode is recrystallization assisted intergranular cracking [5].

Hot and cold storage tests are examples of static temperature testing; e.g., standards JEDEC JESD22-A103 [46] and JESD22-A119 [47] respectively. Both of these tests are used to accelerate time and temperature dependent reactions under long storage times. In addition, they can be used as preconditioning for other tests to simulate the effects of long lifetime. When choosing the test condition, material properties such as melting points and glass transition temperatures have to be considered.

Mechanical testing

Mechanical testing is used to simulate mechanical stresses that occur during product lifetime as well as to characterize the production quality. Mechanical shocks, due to drop impacts, and different vibration excitation profiles are commonly used. In addition to these, shear, tensile and bending tests are used.

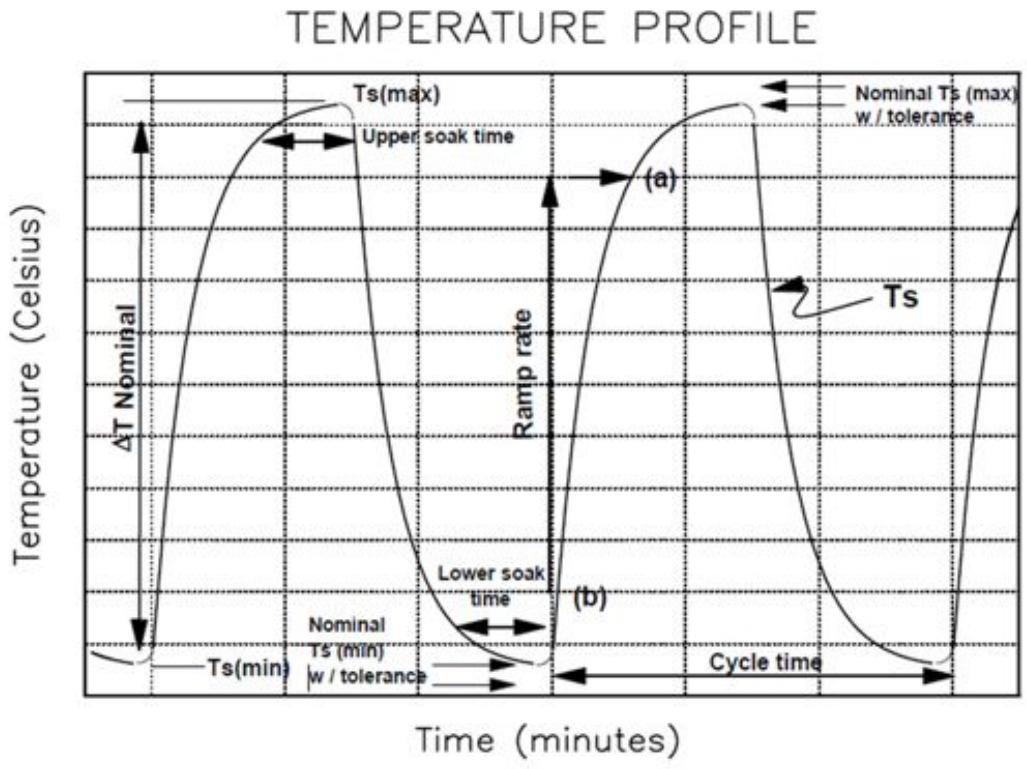

Figure 6: Schematic temperature cycling profile according to [44]

Mechanical shock test are commonly drop tests, where high deceleration exerts force on the tested structure, resulting for example, in PWB bending. Test procedure is presented in standards JESD22-B111 [48] and JESD22-B104 [49]. JESD22-B111 defines a test setup where component board mounted in sleigh is dropped onto strike surface. By altering the drop height and strike surface, peak acceleration and pulse width can be adjusted. For board level tests, also specific test PWB design is defined.

Only one drop impact at a time is conducted, i.e. drop table may only hit the impact surface once per drop. Standardized amount of drops is a maximum of 30 [48], but if larger amount of drops is conducted, testing time may be long as after each drop, drop sleigh has to be risen to desired drop height. It has been shown that also powerful vibration shakers can be used to produce similar pulses, which potentially reduces the required testing time [5, 50].

Vibration testing can be used to simulate vibration under product loading conditions. Vibration shakers are either electrodynamic or pneumatic and uni- or multi-axial [3]. JEDEC JESD22-B103[51] defines a component level vibration test procedure where either frequency sweep or random vibration is used. Each axis is separately excited by decided profile. Frequency sweep profiles are generally defined by the displacement and acceleration. On lower frequencies, vibration is displacement controlled and on higher frequencies acceleration controlled. Random vibration on the other hand, is defined by the power spectral density and the amplitude is

gauss-distributed.

Failure mode under drop testing is often brittle or ductile cracking, and with vibration fatigue cracking. Failure modes are dependent on the strain rate and the stress level. Drop impact tests commonly result in higher strain rates (from 1 to 100 /s) and with vibration strain rates are lower (0,001 - 1 /s) [5]. However, with vibration testing it is also possible to achieve strain rates similar to drop testing, if high amplitude and/or frequency is used.

Failure criterion with the mechanical tests is an open circuit or a substantial increase of resistance. This failure occurs commonly due to PWB trace, solder interconnection or component lead fracture by the mechanisms discussed in section 2.5. Additionally, internal component structures may be damaged. As cracks may be open only at the maximum bending situation, high speed measurement is required to monitor the test samples. For example, in [48] event detectors with capability to detect discontinuities of 1 microsecond or high speed data acquisition device with a sampling rate above 50 kHz is suggested. To rule out errors, three failure indications during five drops is considered as a failure in drop testing.

Shear and tensile pull tests are commonly used to investigate internal component interconnections, such as wire bonds. They are also applicable for testing the solder balls of BGA components. They are usually used to characterize the interconnection strength. In standards requirements for minimum strength is usually defined. Cyclic bending tests are often used to test component lead and interconnection fatigue properties.

3.2 Combined load testing

Combined loading tests are tests in which two or more loading conditions are used consecutively or concurrently. Combined tests are gaining popularity, due to several reasons. Firstly, especially with the concurrent loading, testing time can be reduced, thus reducing the amount of required time and resources. Secondly, they match the real loading conditions more accurately[5, 6].

During recent years, numerous papers on combined loading have been published. General conclusion across the field is that combined loading testing is a beneficial, despite the more complex analysis. There is clear evidence that failure modes can change drastically between single load and combined load test [5, 6]. It has also been shown that isothermal aging and electrical loading as preconditioning can have a substantial effect on the behavior of the interconnections under slow cyclic loading [52] and vibration loading[53]. In this thesis, main focus is on the concurrent thermal and vibration excitation loading and the reliability of solder interconnections.

In consecutive testing first loading parameter is used as preconditioning, commonly electrical or thermal loading. Using these as preconditioning is based on the irreversible material evolution occurring due to thermal and/or electrical loading. The second parameter is commonly mechanical loading. The benefit of the consecutive testing is that the effect of different parameters can be easily observed. For example, part of the population can be analyzed using cross-sectional analysis before, between and after the two tests.

In concurrent load testing, two or more loading conditions are applied simultaneously. They offer the highest acceleration factors and can be used to represents harsh field conditions[6]. However, designing concurrent loading tests is notably more difficult compared to single parameter or consecutive load tests. Interactions between different loads should be profoundly understood. In combined thermal cycling and vibration excitation tests, adjustment of proper vibration level is critical. Temperature cycling tests are long duration tests (1000 h+), whereas vibration tests can be very short or long depending on the acceleration level. If we want to consider the combined effect of these factors we need to adjust the vibration level low enough to allow thermal cycling related mechanisms to affect the system. Additionally we can use vibration sweep or vibrate only for a certain time per thermal cycle.

Usually combined loads, independent of being consecutive or concurrent, have a negative effect on the lifetime. However, this is not always true, 1000 h power cycling or 750 thermal cycles prior to drop testing can increase the interconnection lifetime [54, 55]. However, longer testing led to a rapid decrease of lifetime. On the contrary, 500 h of isothermal annealing at 125 $^{\circ}C$, resulted in drastic decrease in drop reliability [55]. It seems that a certain amount of microstructural evolution can increase drop reliability.

Combined vibration and power cycling test has been shown to have significant effect on the failure modes and lifetime [7]. It can be assumed, that electrical loading essentially led to thermal stresses, electrical effects on solder interconnection, like electromigration were presumably negligible. Constant power and power cycling were combined with various vibration strain amplitudes. Three different failure modes were found to occur depending on electrical stress and vibration excitation amplitude:

- Ductile crack propagation through bulk solder, present at highest vibration levels. No notable changes in solder microstructure were observed, thus vibration was dominant factor on reliability.

- Local recrystallization with crack path propagating locally along grain boundaries, present at medium vibration levels. Vibration dominated crack propagation, but thermal stresses contributing significantly.

- Recrystallization assisted crack nucleation and propagation. Similar to thermal cycling failures, thus thermal stresses have started to dominate.

Observed failure modes and respective stress conditions are presented in figure 7. [7]

Combined power and vibration loading can result in substantial acceleration factors, as presented in [7]. With single load vibration, acceleration factors up to 41 and 88 can be achieved, as shown in figure 8 a). Whereas with the combined loading conditions acceleration factors up to several hundreds can be achieved. In figure 8 b) acceleration factors between combined loading conditions and single load vibration are presented. It is shown that with combined power cycling and vibration excitation, failure mode can be accelerated with a factor of nearly 2500 compared to

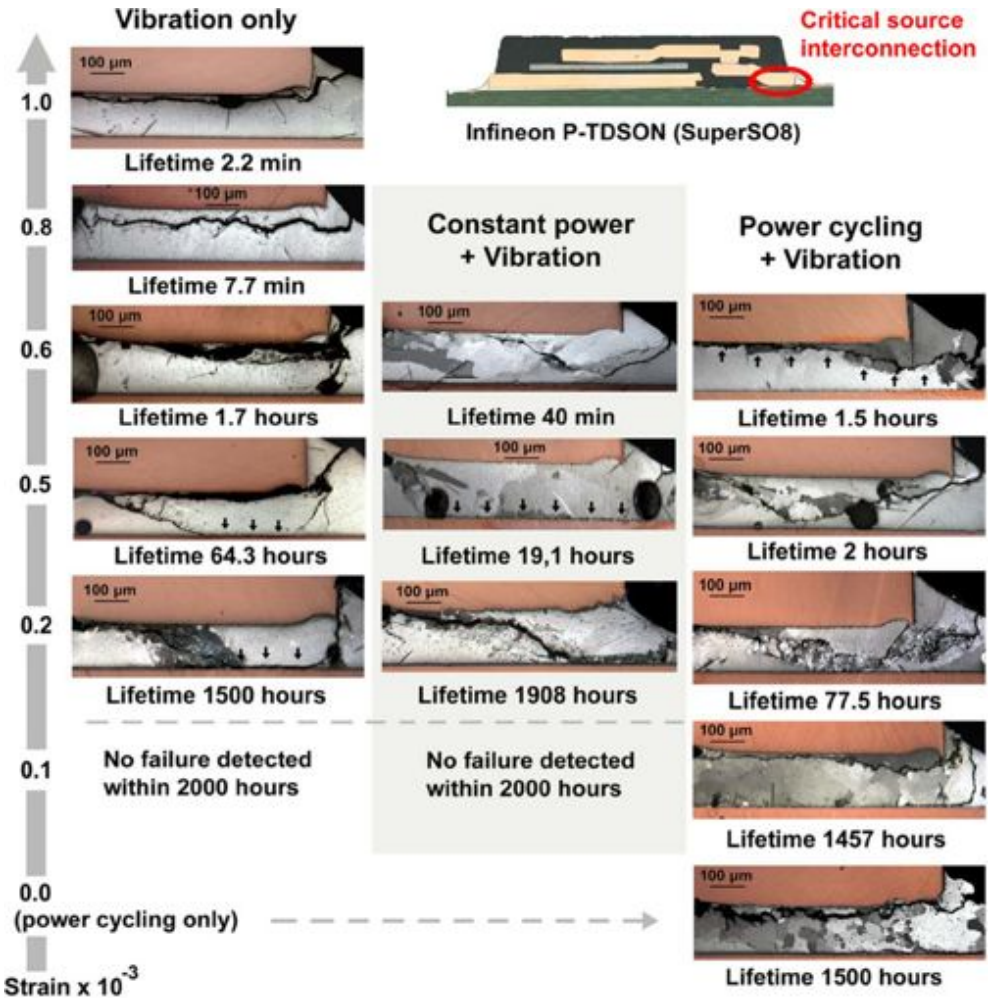

Figure 7: Failure modes under various vibration amplitudes, under single load, combined constant power and combined power cycling.[6]

single load vibration. [7] Based on these results the importance of combined loading testing can be emphasized. If product is tested only with single load vibration, acceleration caused by the thermal stresses and change of material properties is ignored. However, in the study the effect of different temperatures was not investigated.

High acceleration factors also makes the combined testing an interesting approach for test acceleration. However, acceleration factors and failure mode transitions are component and system specific. When designing the acceleration of vibration tests, extensive preliminary testing may be required to determine the acceleration factors and failure modes. Accuracy of the prediction can be reduced, if the failure mode is different from the failure modes observed/expected under field conditions.[7]

Elevated temperature combined mechanical loading has shown a drastic effect on the lifetime under vibration [56, 57] and drop impacts [5]. Largest drop in lifetime has been observed between room temperature and 70 - 85 $°C$, the change is less significant between 70 - 85 $°C$ and 110 - 125 $°C$ [5, 57]. In-depth failure analysis

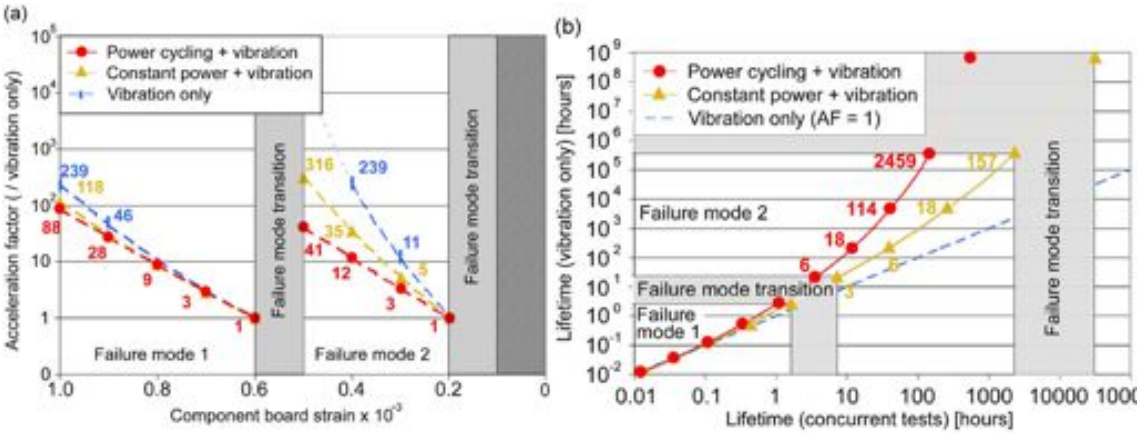

Figure 8: a) Achieved acceleration factors by increasing vibration amplitude. b) Interconnection lifetime under different conditions, with acceleration factors.[6]

was conducted only in drop impact study, with several test board designs also change of failure mode was observed [5]. At sub-zero temperatures the behaviour of the test system can change the behavior of the setup significantly, thus making the analysis difficult [56].

Several studies on the modeling of combined thermal and vibration loading tests can be found in the literature. General conclusion in all of the studies is that combined loading has a significant negative effect on the lifetime [58, 59, 60]. Studies were supported by experimental testing, but no in-depth failure analyses were conducted. LDSA and IDSA were both shown to yield good predictions [58, 59, 60], IDSA is superior method compared to LDSA [61]. On lower excitation amplitudes importance of comprehensive material models [58] and vibration related creep damage [60] has been emphasized. The usage of experimentally determined parameters increases the accuracy substantially [58]. Simplification of the model can be used to reduce the required computational resources. Global-local approach and using symmetry planes to halve the joint have shown to be effective [62].

Highly Accelerated Life Testing (HALT)

Probably one of the most commonly known combined loading test method is HALT testing, developed by Hobbs [63]. Despite its name it is not used for lifetime assessment. However, some statistical methods for lifetime assessment have been developed.

HALT procedure contains temperature and vibration step-stress tests and their combination. The goal of the testing is to find product weaknesses in as short time as possible. Loading is increased step by step until failure occurs. After failure detection corrective measures should be done and test repeated.[11]

In addition to reliability improvement, HALT is used to determine product operational and destructive limits [11]. Operational limit is stress value above which product will stop working but will recover after stress is reduced. After exceeding destructive limit, product will not be recovered even if stresses are released. For this

purpose HALT testing is a very good tool.

Criticism towards HALT testing lies in the very high acceleration factors. As testing times are very short, they cannot really be used to simulate failure modes affected by microstructural evolution. Even if the product can withstand very harsh HALT conditions, it can still be very unreliable. Continuing to pursue HALT testing reliability too far, can waste resources, as corrective actions can be conducted on irrelevant failure modes. If product will never faces stresses as high as in HALT, there is no need to continue improving. Failure modes in HALT are usually over-stress failures, while fatigue failures are mostly neglected. In addition, as HALT testing is usually very rapid, no microstructural changes will happen at the interconnections, as a result failure modes are likely vibration dominated [5]. Even if the product can withstand certain stress, it may fail under notably lower stress due to long-term cyclic loading.

HALT is a good tool for determining the operational and destructive limits. For screening purposes similar approach is optimal. Highly Accelerated Stress Screening (HASS) can be effectively used to screen out defective products thus reducing the on-field infant mortality. HASS limits are usually chosen slightly below operational limits. This test should fail most of the defective population.

3.3 FE-modeling

Finite element analysis (FEA) or modeling/method (FEM) is a numerical computation method for structural simulations. Even though it is not an actual lifetime test, it is commonly a important part of reliability analysis. It is commonly used in a wide variety of engineering applications. It is used to analyze various systems such as structural mechanics, fluid dynamics and electromagnetics in fields from electronics to civil engineering [31, 64]. It is applicable from nanoscale systems to largest structures known to man.

FEA is based on work done by Hrennikoff [65] and Courant [66]. More comprehensive mathematical foundation was provided by Strang and Fix in the 1970's [67]. Since then, due to the increasing amount and reducing price of the computational power, FEA has become an industry standard for analyzing the behavior of complex systems. Numerous calculation software have been developed for analysis(e.g., Abaqus, Ansys and Comsol multiphysics).

Finite element analysis is based on discretizing the studied system into a finite number of elements. The elements are connected to each other by nodes, usually located at the element boundaries. The behavior of these nodes is studied by calculating approximate solutions for partial differential equations. [31] As the calculation is based on the nodes, defining them is an important factor.

Structure under interest is divided to elements in a step called meshing. In most cases, the finer the mesh and higher the amount of nodal points, the more accurate solution will be achieved. However, the calculation speed is dependent on the amount of nodal points. Thus, mesh density is usually a compromise between model accuracy and calculation time. Often, some simplifications can be used to reduce model complexity e.g., 2D model instead of 3D, symmetry axises and global-

local approach [64].

Global-local or submodeling approach is based on modeling only a certain part of the model accurately [31]. This approach is used also in this thesis. For example, when interested in stresses on the solder interconnection of a certain component in the component board it is usually sufficient to accurately model only that certain component and interconnection or alternatively even only the interconnection. The rest of the PWB and other components can be just roughly modeled. Rough model and even coarse mesh should give a good representation of the system's behavior affecting the detailly modeled area. Calculation time for model like the one presented here is often measured in hours or even days. Global-local approach results in notably shorter calculation time, compared to the full detailed model of the whole complex component board.

As with all calculations, results can be only as good as the model and the input data[64]. Due to this, care has to be taken when defining the material properties and load parameters, as well as the boundary conditions. Every calculation should be critically considered in respect to limitations and assumptions lying in the FEA and the model. Model is never an exact representation of the reality. In addition, the model should only consider the effects that are relevant, since this can reduce the amount of possible errors and optimize the model complexity[68]. The critical steps for successful FEA listed by Li [31] are following:

- Establishing a simplified and approximately accurate representation of the geometry.
- Choosing correct element types, mesh, material properties and material models in respect to desired analysis.
- Determining and applying accurate loading and boundary conditions.
- Using appropriate analysis type and error control.

In the reliability analysis of electronics FEA is commonly used to calculate the stresses due to a variety of loading conditions. As interconnections and component internal structures are out of scope of experimental measurements, FEM is essentially the only method of analyzing stresses in these structures. These stress parameters are crucial for generating the actual lifetime models. It is a common method that for a lifetime model several experimental tests are conducted to experimentally analyze the lifetime of the component or product under certain loading condition. Used stress conditions are characterized using accelerometer and strain gauge measurements. Generated FE-model is calibrated to match the loading conditions of the experimental tests. The stresses at the failure locations can then be determined using the generated FE-model .

By using the experimental lifetime data and calculated stress values, component specific lifetime model can be created by using the models presented in section 2.3. After the product level FE-model is generated, field condition specific stresses can be analyzed. By applying the created lifetime model on the field condition specific

stress results, lifetime prediction for the component in the real usage environment can be established.

Building accurate prediction for whole product can be too time consuming, as the products can be extremely complex. However, with an in-depth understanding of the product and component behavior critical components and locations can be estimated with the aid of simple FE-model. This information can be used to generate lifetime predictions only for the components that are considered to be critical. It should be noted, that error in determining these components can result in ignoring certain component, that contrary to the initial assumption, is critical to product reliability. With proficiency in FE-modeling and reliability analysis combined with understanding gained from other products, the amount of these errors can be minimized.

In addition to simple mechanical stresses induced by vibration excitation or drop impacts, more complex cases can be studied. Stresses by thermal loadings are a common scope of FEA. Stresses inflicted by CTE mismatches during static and dynamic uniform temperature loads or the effects of temperature gradients due to power on conditions can be investigated relatively easily. Also whole complex systems can be analyzed; e.g., the effects of the whole system can be analyzed. For example, the component board loading input can be modeled based on the loading conditions of the system where the component board is mounted on.

The complex combined loading conditions can also be analyzed using FEA. Analysis like this can give good insight on the effect of different loading conditions on the combined stresses. As in any other FE-calculation, the importance of accurate and comprehensive material models is vital for accurate analysis [31]. However, when the amount of loading conditions is increased also more complex material models may be needed. For example, simple vibration analysis may only need constant material properties for accurate analysis. In the more complex analysis it may be necessary to consider also temperature and strain-rate dependencies in addition to creep and microstructural evolution.

FEA can be only used for macroscale structural simulation, thus microstructural evolution is out of FEA's scope [31]. However, due to the significance of microstructural evolution; for example, on the thermal cycling reliability, methods to consider microstructural evolution have been developed. Stochastic Monte-Carlo methods based on repeated random sampling can be combined with FEA to analyze the recrystallization of solder interconnection during thermal cycling. Method developed by Li et.al., has been shown to be an accurate method for predicting solder interconnection lifetime based on microstructural evolution [69]. The developed method is based on the accumulation of stored energy in the interconnection during each thermal cycle.

4 Test method for advanced reliability assessment

In following subsections the general overview and application of the method are presented. Furthermore, the known model shortcomings are discussed. The model is based on principles and effects presented in previous sections, and is designed for addressing the effect of temperature on vibration lifetime.

The method consists of several experimental, modeling and analysis stages. But firstly, one is required to estimate the real loading conditions, based on which the test conditions can be established. To generate a relevant lifetime prediction, large enough sample size should be used and acceleration factors should not be too high, as this can easily lead to overly pessimistic and inaccurate results.

With the designed test board multitude of stress conditions can be extracted from a single test board, thus only single test amplitude may be sufficient for good results. The higher the amount of tested components and the wider the stress range, the more accurate and reliable model can be achieved.

FE-modeling is a key part in the procedure as it allows the extraction of stress and strain parameters from detailed locations, such as the solder interconnections, where the failures usually occur. It is shown that even experimental PWB strain values can result in good prediction, however on the product component board proper measurements can be hard to conduct. FE-modeled PWB strain values are shown to suffer from inaccuracy near the boundary condition regions, whereas results from interconnections are still assumed to be accurate at the same region.

Lifetime model is based on the Weibull distribution and the power law lifetime estimation model (modified Coffin-Mason equation). In addition to the lifetime, also the cumulative failure distribution can be estimated with some justifiable assumptions. More detailed method workflow is presented in the next subsection.

In the following sections test method will be utilized to create a lifetime prediction for a D^2PAK component. Results obtained in the experimental tests are used to validate the designed method and to optimize the workflow, as well as to map out the pitfalls, weaknesses and shortcomings of the method.

4.1 Applying the designed test method

In this section the general workflow of the developed method is discussed. Each stage of the model and common pitfalls are explained. Flowchart of the method is presented in figure 9, which is also applicable for many other reliability and lifetime prediction test methods.

Special tools can be used or designed to aid in the process, such as automatic model creation. Even though it may seem as a large amount of work especially in the FE-modeling sector, in many cases the existing results and/or models can be utilized also with other components and in coming projects.

In sections 5 and 6 the conduction of the steps is thoroughly explained. In these sections also the used methods and calculations are explained.

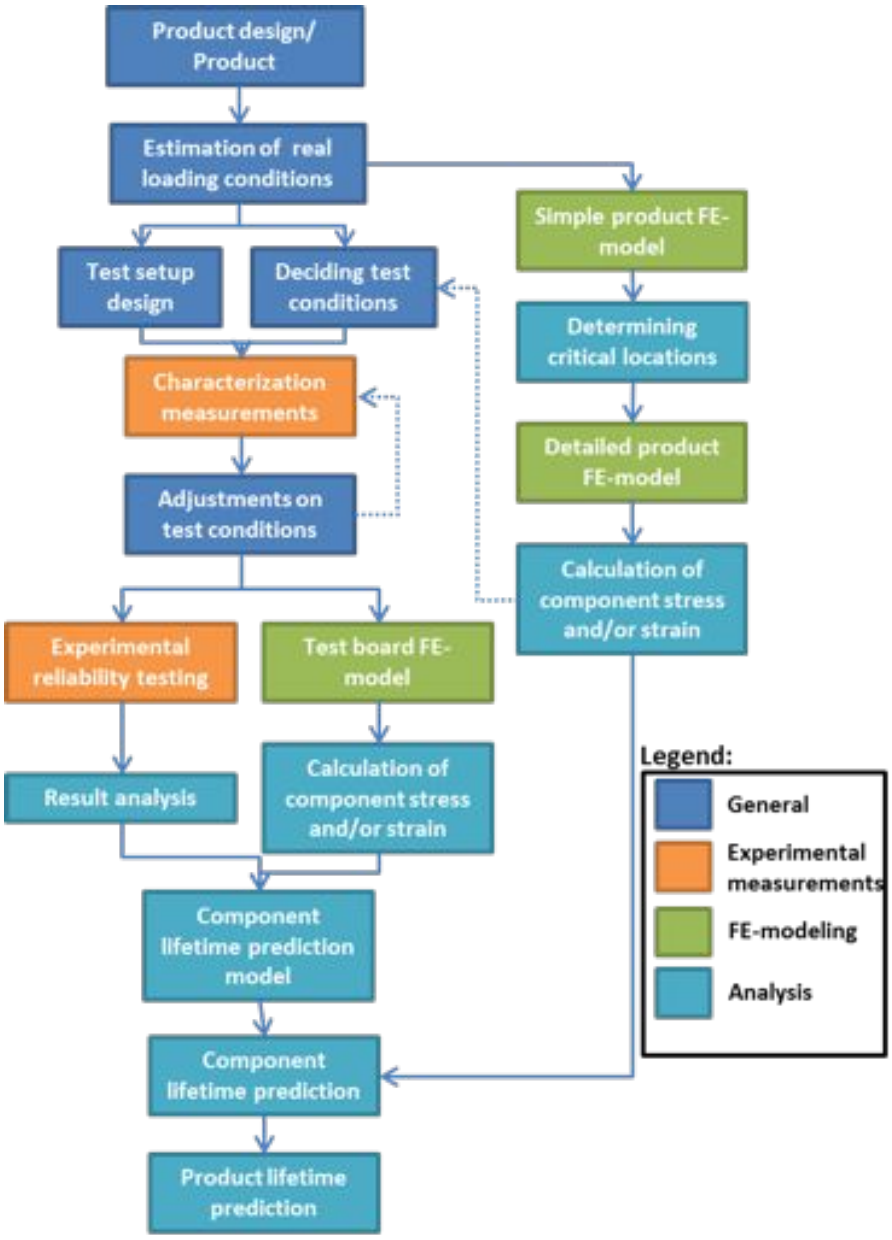

Figure 9: The workflow of the designed test procedure.

Product design/Product

The first step of the lifetime prediction is the design of the product or the actual product. Lifetime predictions should be generated prior to product manufacturing. During the lifetime assessment a need for design changes may raise, altering design after manufacturing usually is impossible. However, commonly the possibilities of design changes are limited, due to limitations created by electrical design.

With comprehensive reliability assessment, guidelines for reliable design can be established. As company adopts in-depth reliability assessment procedures, they can draw guidelines based on the previous assessment results and the field reliability of

the products.

Estimate real loading conditions

The estimation and understanding of the real loading conditions is critical. If one does not know the conditions where the product will be used, creating a good lifetime prediction is difficult.

For the estimation actual on-site data can be used as well as standards. When we have determined the actual product loading conditions we can proceed to determining the component loading conditions and designing the test procedure.

Simple product FE-model

Simple product FE-model can be created using either mass points or simple block models for components. The advantage of simple model is rapid creation and calculation. Critical locations can be assessed using board strain results.

The component board mounting setup should be considered in the analysis. Baseplate's behaviour can affect substantially on the excitation input of the component board. Furthermore, thermal expansion and CTE mismatch between the different parts of the system can also have a substantial effect on the frequency response of the assembly.

The effect of boundary conditions should always be considered. Due to the boundary conditions especially PWB strains may differ from the actual. When model is created with mounting setup, these boundary condition effects can usually be minimized on the component board level.

Determining the critical locations

Critical locations should be assessed by analyzing the PWB strain. Components located in the areas of highest strain concentrations should be considered for testing.

In addition, component type should be considered. In the earlier part of the project, large inductor component was determined to be extremely reliable. Only few failures in component or component interconnection were detected, in most cases PWB failure was the case. Where as large CABGA-256 BGA component failed with similar test amplitudes immediately in nearly all of the locations. To reach reasonable lifetimes test amplitude was dropped to nearly one fourth of the original. In this case the BGA component was expected to be the reliability bottleneck, even though it was not located around the highest strain concentrations. Usually larger components with small interconnections are the most vulnerable ones.

Detailed product FE-model

To extract the actual component interconnection stress and/or strain, detailed model has to be used. Using the detailed model is recommended for the best results, however using the experimental PWB strain results or simplified model results may also lead to acceptable results.

For the detailed model, one or several mass points or block models are replaced with detailed component models. It is often beneficial to do several calculations where only one or two detailed models are used, as a large amount of detailed models will require tremendous calculation capacity and time. It should be noted that even though the amount of different components can be very large in the product or in all of the products manufactured by the company, the amount of component types is usually reasonable. When a detailed component model is created, it can be used also in future with different products.

Calculation of component stress and strain

Depending on the component and the loading conditions, failure location may vary. If model is generated well enough it should give a good indication of the failure location.

Calculation results are used to generate component lifetime prediction and whole product lifetime prediction. Additionally, preliminary results can also be used as an aid when deciding the test conditions.

Deciding test conditions

Test conditions should be decided in respect to the actual usage environment. To represent the real conditions well, the acceleration factor of test should not be too great. For the highest precision in the model, failure modes between the real and accelerated conditions should remain the same. However, during design phase no field data is commonly available, but the data from the previous products or assumptions based on available knowledge can be used. Over accelerated test may result in different failure mode and incorrect results. Low acceleration factor most likely represents the real case well, but results potentially in very long test times, which is not beneficial financially and may postpone product release.

In any case it should be made sure that test subjects face higher stresses compared to the product. Even though standards for combined loading testing do not exist yet, multiple standards on vibration and thermal testing are available which can be used as reference.

For very robust components higher acceleration factors may need to be used to fail the components. Alternatively, based on experience, testing some of the components can be decided to be irrelevant. Components that are considered to be very reliable compared to other components, can be discarded, as they can be assumed not to pose a reliability threat.

Test setup design

The test setup consists of vibration exciter system, thermal chamber and control & monitoring system. It is beneficial to choose vibration exciter system and thermal chamber so that they can be used in various testing conditions; i.e., capability to vibrate high enough weights with high enough amplitudes and possibility to use chamber also for standardized thermal cycling tests.

Even though the test board in this study was not made according to any standards it was proved to yield a high amount of failures during each test run. Similar approach is recommended especially for cases where as short as possible test times are preferred. One board design can be used to test several component orientations and multiple strain levels. Using same basic design with small modifications with different components, reduces the required design work and allows usage of same FE-model with minor modifications. For specific cases special designs and baseplates may need to be used. Simplest possible vibration mode shape is achieved using line clamps at the ends of the test board allowing the board between the clamps to vibrate at a simple and nearly symmetrical mode. In optimal case this mode is a single wavelength sinuous wave, which is usually the first significant resonant mode.

The baseplate should be manufactured from a material with similar CTE to the PWB. Due to weight and mechanical performance aluminum and aluminum alloys are a good choice, despite a small CTE difference. The CTE of steel is closer to FR4 and it has a higher elastic modulus, but also higher density. Based on the CTE and higher elastic modulus, steel would be good option; however, the threefold density may surpass the benefits.

The test setup requires the capability to measure the strain and the acceleration from the boards. These are needed to characterize the board behavior to ensure model accuracy. For the reliability testing, equipment to monitor the failures is needed. Usually the failure criterion is an open circuit. Due to vibration, fracture may only be open during a short period of the cycle. As there can be hundreds of cycles per second, fast detection is required. For example, event detectors allow continuous and fast monitoring of all channels or additionally high speed data acquisition systems can be used as described in [48]. Relay based logger systems are not recommended as they often measure only one channel at a time for a short period of time.

Measurement wire connection should be ensured; for example, by using a two hole connection i.e., wire is fitted through the first hole and soldered to the second. For large scale testing, connectors can be used to reduce the amount of work. However, reliability of connectors should be ensured.

The failure criterion in the standard [48] is three failures withing five drop impacts. Similar approach is recommended to reduce the possibility of erroneous failure indications. In this thesis open circuit during three consecutive two second measurement intervals was used.

Characterization measurements

Characterization measurements are used to analyze the board behavior. PWB strains from several locations and the acceleration of the clamp as a function of frequency should be measured. These allow to determine the first and the simplest significant vibration mode frequency. Strain and acceleration results can be used to adjust the loading conditions to match the designed loading conditions. Furthermore, they are essential in the model tuning.

During the characterization measurements, all or several components can be

monitored to see if failures seem to occur already during the characterization tests. If failures occur already in this stage, loading parameters are likely too high as characterization measurements are relatively short, commonly several minutes.

Characterization measurements should be conducted at all temperature conditions. Before the measurements, assembly should be allowed to relax for some time to stabilize thermal stresses due to temperature ramp-up/down. The relaxation of stresses in solder interconnections will happen as described in section 2.4. One hour relaxation time is assumed to be enough to stabilize the stresses to a sufficient level. The characterization measurements at all temperatures will help reduce the modeling work, as simpler model can be used when temperature effects on board strain are characterized by experimental results. Even if these are also considered in the modeling, measurements can be used to validate the modeling results.

Adjustments on test conditions

If the characterization measurements indicate too high or low strain and/or extremely fast failures, modifications to the test conditions should be conducted. After the modifications, the characterization measurements should be repeated to ensure the correct input and calibration values for the FE-model.

If the behavior is completely unexpected the whole setup may require improvements. Simple factors, such as wire breakdowns or loose screws can cause unexpected results.

Experimental reliability testing

The experimental reliability testing is conducted at point frequency and at static temperature. The frequency should be the first significant resonant mode of the component board. Even though this frequency was measured in the characterization stage, it should be confirmed for each board as some variation between the boards can exist. The tuning of the frequency can be conducted usually by ear but also accelerometer or strain gauge can be used. In addition, the frequency should be set roughly 1 % lower than the actual spike to ensure test staying on resonance spike for the whole test. During the test, the board resonance frequency has been observed to drop, presumably due to the degradation of the board under constant vibration loading. These effects are case specific so the 1% value may not be appropriate in all cases. Other possibilities are the active monitoring of the resonant frequency or using a vibration sweep. Sweep however, can make lifetime prediction more complicated.

Prior to the test start, the assembly should be allowed to relax when temperature is ramped up or down. Stresses due to the thermal expansion will reduce during a short period of relaxation time. This should ensure that the temperature related stresses are stabilized.

Depending on the test board design, several test boards should be tested at every temperature. Enough data points for each orientation and stress combination is required to establish statistical reliability on the results. In addition, having data from several test runs will ease false failure detection. If possible, several test amplitudes should be used. Having more data points increases the model reliability.

It is essential to have data also from lower stress levels, which are more relevant to the actual case. If lifetime model is created using data from relatively high stresses, the extrapolation of the curve to lower stresses is exceedingly more inaccurate.

Result analysis

The results of each test run should be compared to other test runs to point out erroneous failure indications. If board resonance frequency falls enough resulting in a notable drop of acceleration and strain, lifetimes will be significantly higher than they should be.

The results, grouped according to symmetry and conditions, are incorporated to statistical models. Weibull reliability model is suggested, and often also used in other similar applications. By assessing the fit of the Weibull model, some estimations can be done on the result integrity:

- If some points do not fit to curve reasons for this should be analyzed. Possible reasons for bad fit may be changing failure mode, varying test parameters between test runs and erroneous failure indications.
- If data of one test run seems to be out of the trend in various locations, it is likely that something has been wrong with the test parameters during that test run.
- If the variation is large within a single location at all temperatures, grouping and failure modes should be reconsidered.
- In a case, where single data points are out of the curve, a high possibility of erroneous failure detection exists.

Comparison between Weibull models in different temperatures should be conducted. The slope, i.e. parameter β, of the Weibull curve is usually considered to be related to the failure mode. If slope in on location under different temperatures differs, it is likely that there is a difference in failure mode. Same thing is true between the different locations and orientations inside one temperature. Differences can be small but also notable and certain orientations, locations or temperatures may result in notably lower lifetimes due to different failure mode.

Test board FE-model

When the strain and acceleration measurements are conducted at all test temperatures, the effects of thermal expansion can be left out of the model as well as the baseplate. Naturally, change in material properties has to be considered. These simplifications will result in erroneous frequency behavior, but component strain and stress values are expected to be correct. As a result the model is notably simpler and the calculation time will be reduced to the fraction of the full complex model. This kind of approach is recommended only with simple test board assembly, with the product model it is not suggested as the behavior is more complex.

In our test case calculation time for the component board model with 24 component block models and one detailed component model was several hours. When clamps and baseplate were incorporated into the model to analyze the effects of thermal expansion with vibration excitation, results were not reliable. In both cases boundary conditions affect notably on the edges of the board. In this region board strain values are not considered to be accurate, due to boundary condition induced effects on strain gradients and distributions. However, component level results in the same region are considered to be accurate enough. It is possible to loosen the boundary conditions of PWB by modeling the clamp and PWB contact interface and their interactions. On the other hand, this improvement in the model is expected to result in a calculation time of multiple days.

Calculation of component stress and/or strain

Component level stress or strain value should be used as the loading value for each group of components. Even though in our experiments measured PWB strain resulted as the best fit for component lifetime model, its incorporation to product level is difficult. Calculated PWB strains on the other hand were detected to yield erroneous results due to gradient and distribution issues inflicted by the boundary conditions. The component level strain or stress value and its location should be chosen according to the failure mode for the best results. These values can be easily extracted from both, experimental and product, component boards and are assumed to be accurate in both cases.

In this thesis the maximum solder strain and lead stress values were considered. The maximum value is assumed to give accurate results, but also the average value of certain area can be used. Extracted loading values are used to generate component level lifetime prediction.

Component lifetime prediction model

Calculated stress or strain values are combined with respective Weibull lifetime models. Each group should now contain the information about orientation, location, temperature, test frequency and Weibull parameters. Each group now represents a set of very specific conditions. These can then be combined in various combinations to generate a simple power law component lifetime prediction model.

Depending on the desired prediction accuracy, component lifetime model can be created by combining all results or combining similar orientation inside certain temperature. By using the latter method, temperature and orientation dependency can be incorporated in to the model. For the easiest analysis, the most pessimistic model is suggested. Choosing the most pessimistic model should always give results that are equal or pessimistic compared to the actual case. This also minimizes error possibilities, as if more comprehensive model is used, strain orientations and temperatures should be considered.

According to model there should be certain strain or stress level where lifetime approaches to infinity. In reality, infinite lifetime cannot be expected due to other failure modes, but this level can be considered to be the safe level under vibration

loading. The stress and strain levels should be designed to remain below this value if possible to provide as high lifetime as possible.

Component lifetime prediction

Using the generated component lifetime prediction model we can create lifetime prediction for components on the product board. The calculated component stress or strain values are imported to the component lifetime prediction model. As a result we obtain component lifetime in real loading conditions.

The amount of strain cycles is critical to reliability. The frequency of test excitation should be compared to the real product frequency conditions, as in the real conditions frequency may be manifold to the test case.

In Weibull model the lifetime is defined as the point where 63,21 % of the components have failed. Weibull shape parameter β may be used to create a cumulative failure distribution for more comprehensive analysis.

Product lifetime prediction

For the full analysis of product lifetime, separate component lifetimes need to be combined. It should be noted that for the highest accuracy the lifetime of all components should be used, but as this may be often difficult, as product component board may contain hundreds or thousands of components. In cases like this, components with higher lifetimes can be left out. It may be also possible to have combined general prediction for the amount of simple components such as chip resistors, based on MIL or Telcordia parts count method described in section 2.3. Discretion is advised, as overlooking one critical component may render the whole prediction inaccurate and over optimistic.

In this thesis, a method for determining the product cumulative failure has been presented. This method can be used to generate product lifetime and failure rate model.

4.2 Discussion on method weaknesses

Several model weaknesses or possible shortcomings can be distinguished. These should be considered during the application process. When further work is done with this method, these are to be analyzed.

Compared to many standardized tests, all components of the test board instead of the center one were monitored. Due to this the stress distributions below components may vary. This can result in some inaccuracy. However, the actual solder or lead stresses can be calculated using FEA.

The monitoring of multiple component makes the failure analysis more difficult. Components that have failed in the early stage of the test will be vibrated as long as the components failing later. It may be difficult to distinguish which part of the fractures have occurred before failure and which part after it.

In this thesis components were grouped by symmetry to six groups and one location of each group was detailedly modeled. However, the actual stresses may have

minor differences between different locations in the same group. This could be mitigated by detailedly modeling each component separately. Despite the practicality of this method, it often is too time-consuming.

Used lifetime models were very simple, and the effect of using more sophisticated lifetime models was not studied. It is possible that this could increase the accuracy of the model, especially when low amplitude test results are not available.

In addition, the power law lifetime model was created based on the Weibull lifetime models of each symmetry group. Lifetime prediction based on separate component lifetimes was not studied. Also the calculation of error range was discarded due to the usage of Weibull lifetime models. If model created using separate component lifetimes was used, the calculation of error ranges would be simpler. Calculating them based on R^2 values might also be possible.

The shape of the cumulative distribution was calculated by assuming that the Weibull shape parameters of symmetry groups apply also when extrapolating the curves. This should be true as Weibull shape is commonly associated with the failure mode. More accurate shape could probably be calculated if lifetime prediction was created using separate component lifetimes.

Moreover, it might be beneficial to use active monitoring of board acceleration. Active monitoring would ensure that the board behavior is constantly exact match with the modeled case. When using the predetermined point frequency, small differences in the board acceleration are expected due to the deterioration of the board and the resulting shift of resonance frequency.

Based on the results obtained in the experimental analysis it seems that testing will still take a substantial amount of time. Too high acceleration factors increase the inaccuracy when model is extrapolated far beyond these values. However, this is also component specific, i.e. for the more rigid components higher test amplitudes have to be used to fail them in reasonable times.

This approach is developed primarily to investigate the solder interconnections, thus the used test setup may not have been optimal for validation. Main failure mode was determined to be copper lead fracture. Thus the amount of information on solder fractures was limited. This problem will be mitigated in the coming study using a large BGA component. Based on the previous study at room temperature, all failures with the BGA were related to solder fractures.

5 Materials and methods

This thesis is a part of a project with a goal to assess and find ways to improve the reliability of a commercial harsh environment inverter and create guidelines and tools for the rapid reliability assessment and improvement of similar products in as early development stage as possible. The product is designed for harsh environment where it will face high temperatures, temperature cycles, vibration, shock impacts, moisture and dust. Commercial board was studied using vibration excitation and FE-modeling. Using this data, critical locations and components were chosen for further analysis.

A total of four components were used in the earlier part of the project, in which only vibration excitation at room temperature was studied. In this second part, main focus is on the D^2PAK packaged schottky diode component.

5.1 The design of the test board

A specific test board was designed to maximize the amount of failure data in a single test run. The test boards were manufactured and assembled by the subcontractors of the product owner to ensure similar quality to the product. In addition, manufacturing quality could be assessed. Designed PWB is a 2 mm thick high T_g (glass transition temperature) six layer FR-4 board. The dimensions of the board are 210 mm by 380 mm, with a vibrating area of 250 mm between line clamps. On the edges of the board are connections for measurement equipment. Used test component was ON Semiconductor MBRB8H100T4G Schottky power rectifier in 15 mm x 9 mm D^2PAK package. Components were soldered with SAC305 (Sn3,0Ag0,5Cu wt%) solder. In figure 10 the designed test board, named HETB-02, and the used component are presented.

The used test component is not the one as originally intended. The component has only one active lead, instead of intended two. As a result, the amount of available data is smaller than designed.

Components were placed in five different orientations in five rows. Contrary to many test standards e.g., JEDEC JESD22-B111 [48] all of the components were monitored. The different rows were designed to face different strains; the maximum strain in the middle (row 3), half of the maximum in rows 2 and 4, and three quarters of the maximum in rows 1 and 5. This design was created to maximize the amount of failure data and different strain levels during a single test run. By using only one test amplitude and few boards, relatively good coverage could be achieved in a very short testing time.

The desired vibration behavior was as simple and predictable as possible. The FE modal analysis results of HETB-01 are presented in figure 11. HETB-01 is similar to HETB-02, with different components and slightly lower frequencies. Strain measurements and observation with synchronized LED-pulse-lighting support these results. The most significant mode is the mode 1, additionally some mode 3 behavior can be seen when the excitation frequency is around the first mode.

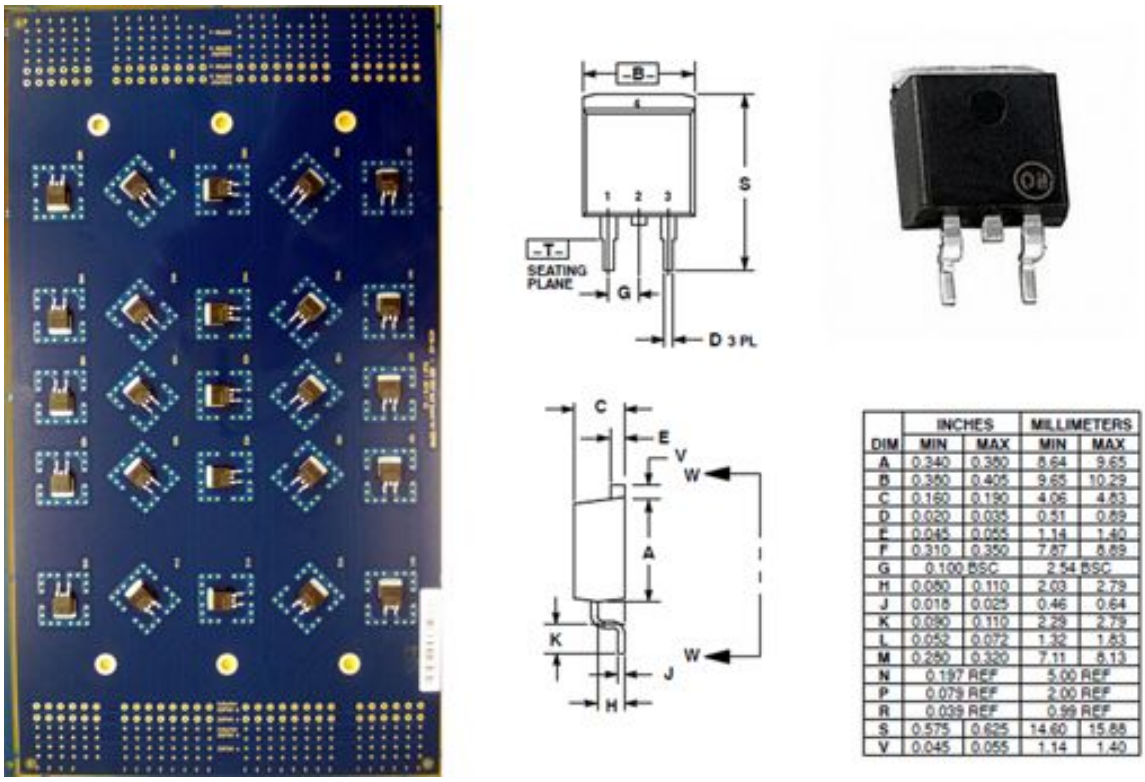

DIM	INCHES MIN	INCHES MAX	MILLIMETERS MIN	MILLIMETERS MAX
A	0.340	0.380	8.64	9.65
B	0.380	0.405	9.65	10.29
C	0.160	0.190	4.06	4.83
D	0.020	0.035	0.51	0.89
E	0.045	0.055	1.14	1.40
F	0.310	0.350	7.87	8.89
G	0.100 BSC		2.54 BSC	
H	0.080	0.110	2.03	2.79
J	0.018	0.025	0.46	0.64
K	0.090	0.110	2.29	2.79
L	0.052	0.072	1.32	1.83
M	0.280	0.320	7.11	8.13
N	0.197 REF		5.00 REF	
P	0.079 REF		2.00 REF	
R	0.039 REF		0.99 REF	
S	0.575	0.625	14.60	15.88
V	0.045	0.055	1.14	1.40

Figure 10: HETB-02 test board and used ON Semiconductor D^2PAK component

5.2 Test setup

To allow vibration testing at different temperatures, modifications to an Arctest ARC-500 thermal cycling chamber were made. The modifications allowed the placement of vibration exciter below the chamber. Aluminum extension shaft was manufactured to enable the placement of the baseplate inside the thermal chamber. Used vibration exciter system was electrodynamic shaker by Brüel & Kjær consisting of permanent magnet body type 4805, mode study head type 4814 and power amplifier (700 W) type 2707. Vibration signal was created using an Agilent 33522A arbitrary waveform generator. Setup is shown in figure 12.

Solid aluminum (al 5754) baseplate was attached to the exciter's shaft. The 220 mm x 300 mm x 8 mm baseplate was manufactured by Protoshop Ltd. For the testing of the commercial board, 20 mm high steel mounting post were used and for test board polyacetal (POM) line clamps were used. The size of the POM clamps was h: 22 mm w: 15 mm l: 210 mm, the test board was clamped between two clamps from both sides and tightened with screws.

Testing was conducted at four different temperatures: $-35°C$, $20°C$, $60°C$ and $95°C$. Used temperatures ranged from the thermal cycling chamber's lower limit to the higher limit; i.e., the maximum capability was used.

Heat transfer along the extended shaft was FE-modeled, to see if heat from the chamber would transfer to the vibration exciter and possibly affect the performance. According to the simulation natural air cooling is enough to cool the shaft and no

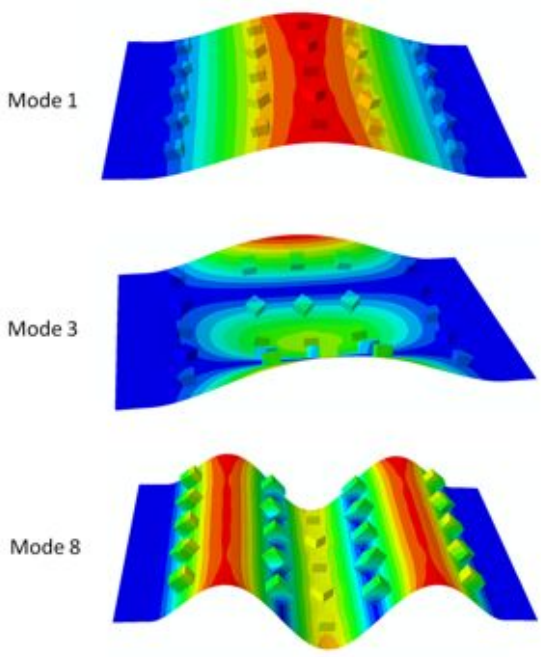

Mode	Effective Mass (g)	Frequency (Hz)
1	2.4E+02	94.1
2	6.2E-20	123.0
3	6.0E-02	237.4
4	1.3E-21	267.2
5	4.6E-18	314.0
6	7.5E-19	456.3
7	1.2E-23	483.0
8	4.8E+01	530.1
9	1.1E-20	586.9
10	2.1E-19	713.7

Figure 11: The vibration modes of HETB-01 (similar to HETB-02)

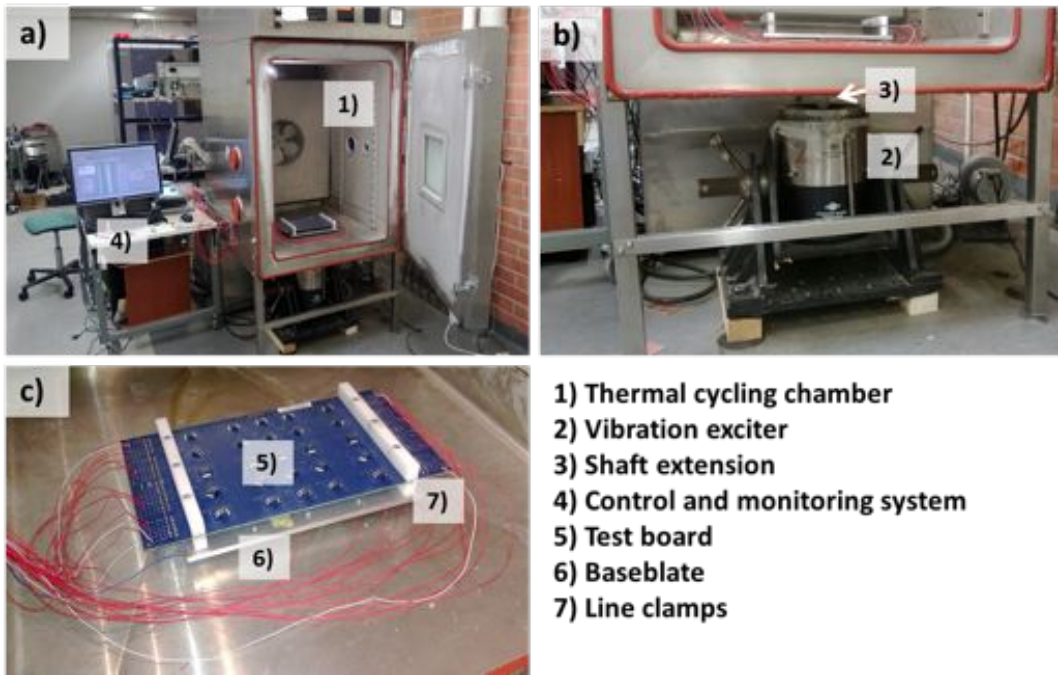

Figure 12: Used test setup for reliability testing

thermal energy will be transferred to exciter.

When tested at $-35°C$ some ice build-up was observed around the inlet, fabricated for the extended shaft. This was expected to have some effect on the performance, as the friction would increase.

Characterization measurement setup

Characterization measurements were conducted to assess the real component loading conditions on the commercial board and the behavior of the baseplate, commercial board and test board. The measurements were done using strain gages and an accelerometer. The employed setup is presented in table 1.

Table 1: Used measurement equipment for characterization tests

Task	**Equipment**
Strain measurements	Kyowa biaxial strain gages (KFG-2-120-D16-11L3M2S), 7 installed on each tested board. Grid dimensions 2 mm x 1,2 mm
Acceleration measurements	PCB Piezotronics 352B01 accelerometer
Data acquisition	NI Labview measurement suite (PXI-6052E/ SCI-1520/ SCI-1314/ Labview)

With the component boards the main focus was on strain, as it is the stress parameter failing the component or the component board. Acceleration measurements were used only as a control. However, with the baseplate, only the accelerometer results were used for the characterization. Acceleration measured from the clamp is used as the test board's acceleration input. All characterization results were used to estimate the loading conditions of both component boards as well as to optimize the FE-models of the boards.

Lifetime test measurement setup

Lifetime test setup was the same as before, excluding the monitoring setup. During the lifetime testing each of the components was separately monitored using specifically designed NI Labview program and Analysis Tech Model 128/256 STD event detector. The program retrieved event detector data every two seconds. Three consecutive failures was used as a failure criterion. Three consecutive failures was used to eliminate erroneous inputs, similar policy is used in e.g., JEDEC JESD22-B111 [48].

Even with this precaution, some erroneous failures were recorded. These erroneous failures could be discarded from the results using short post test check up run (i.e. an additional test run of several minutes) and the fact that in the case of erroneous results, usually several failures were recorded at the same second. When such occurrences were noticed, test was restarted to continue the monitoring of these components. These erroneous failure indications were assumed to occur solely due to the employed event detector, presumably malfunction or unknown properties related to the measurement of diodes.

The test frequency was optimized separately for each board as small differences between boards were found to exist in the previous project. The excitation frequency

was determined based on the characterization measurements and tuned by using ear, as the resonance spike could clearly be located by listening the sound that the board makes. The chosen test frequency was 1 Hz below the preliminary resonance spike due to the board degradation. During the test, resonance frequency was found to decrease due to the changes in the structure of the board e.g., failing component leads. In most cases, falling down from resonance spike could be avoided, thus ensuring proper excitation during the complete test.

Test amplitude was chosen to be 3 V which results in approximately 7 - 8 G acceleration input. With chosen input component board lifetime would be optimal, considering the tight test schedule. Due to the time limitations, a maximum of two days of testing time per board was allocated. With chosen amplitude this would be the case at all of the temperatures and around 20 of 25 components would fail during the test.

5.3 FE-modelling

An FE-model of the test board was generated using a global-local approach. Only the studied component was detailedly modeled, whereas other parts were only roughly modeled. The models were created with Abaqus 6.12.

FE-models have been used to evaluate behavior and to extract parameters. For example, all strain values are based on the FE-models. The experimental characterization results have been used to adjust the models to be as accurate as possible.

5.4 Failure analysis methods

Failures were analyzed using Olympus BX51M optical microscope equipped with Leica DFC420 camera and JEOL JSM-6330F Field Emission Scannig Electron Microscope (SEM). Cross-sectional samples were investigated using optical microscope and fracture surfaces using SEM.

Failed components were cut out using a diamond saw. Components with PWB were molded into epoxy. After curing, samples were extracted from sample cups and then ground to expose the active lead and the larger pad. To achieve a smooth finish, the samples were polished using a Struers RotoPol-22 equipped with a RotoForce-4 automatic sample holder and rotation & force applying system.

To inspect the fracture surfaces, several samples were prepared by cutting the lead from the component body with a Dremel rotary tool. The leads were placed in holes drilled in a copper button. Contact was ensured using a small amount of conducting silver paint.

6 Results and discussion

A comprehensive reliability study was conducted using the principles described in section 4. These principles were further developed based on the results and the findings from the experimental tests.

Experimental testing consisted of characterization measurements, lifetime tests, modeling and an in-depth failure analysis. These results are presented in following subsections.

6.1 Characterization results

The behavior of the baseplate, commercial product and the used test board were analyzed. Characterization results are presented and discussed as follows.

Baseplate characterization

Characterization was started with the analysis of the baseplate. The behavior of the baseplate was analyzed under different temperatures using the same input signal. In addition, the effect of the changes made to the setup were investigated i.e. the extended shaft and the chamber. The acceleration profile of the baseplate at all test temperatures, using 5 V sinusoidal linear frequency sweep from 5 Hz to 2000 Hz, is presented in figure 13. The acceleration has been measured from the corner of the baseplate. The baseplate behaves expectedly: resonant frequencies decrease and acceleration amplitude increases when the temperature is increased. This happens because of the change in material properties due to the changing temperature; e.g., Young's modulus will decrease when temperature is increased [32].

Compared to the new setup, the old setup has roughly 10% higher resonance frequencies, but the amplitude is around the same. This can be explained by the added mass of the extended shaft and the small changes in mechanical structure.

Product component board characterization

After the baseplate, the actual product was characterized. The product component board was attached with screws to baseplate's steel mounting posts from 20 locations. All 20 mounting points are distributed in a nearly symmetric 4 by 5 matrix evenly around the PWB. For characterization a 5 Hz - 2000 Hz linear sine sweep, with 5 V input amplitude was used.

Product behavior under vibration loading is heavily dominated by the behavior of the baseplate's natural frequencies (around 400 Hz, 800 Hz and 1600 Hz). According to the modeling results, product has numerous critical natural frequency modes around 1000 Hz -1200 Hz. Depending on frequency, different parts of the component board are affected. In figure 14 the input from one strain gauge placed around several investigated components is presented. Spikes around baseplate natural frequencies can be expected to be highly affected by baseplate. Around 1000 Hz strain values can be assumed to occur mostly due to the actual component board behavior. By looking at the strain graphs around 1000 Hz it seems that the behavior is as expected

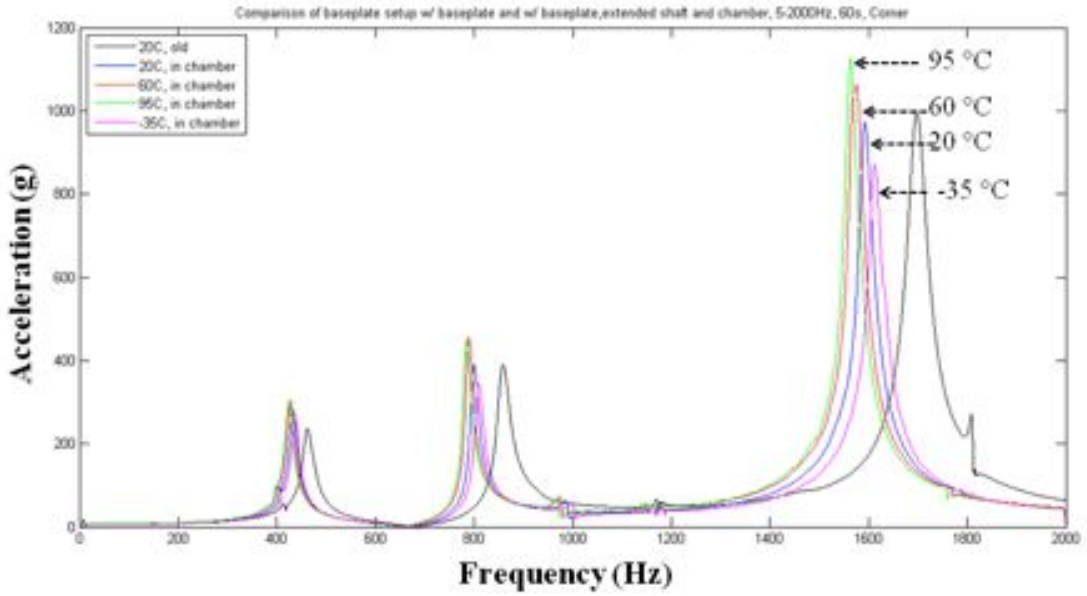

Figure 13: Baseplate acceleration profile, 5 Hz - 2000 Hz 5 V input. Measured from baseplate corner.

when considering the frequency, at $-35°C$ frequencies seem to be the highest and at $95°C$ the lowest. Strains at the baseplate's natural frequencies are notably higher, roughly doubled, compared to the component board natural frequencies.

One conclusion can be drawn from these results: baseplate behavior is critical. This means that when considering the lifetime and reliability of the finished product, baseplate and/or chassis design is most likely extremely important. In other words, when modeling the component board for the vibration reliability analysis, the chassis should also be modeled. In a case where the chassis and the component board have significant natural frequencies at approximately same frequencies, board strains can increase dramatically. In the figure 13 we can see that acceleration in baseplate corner is roughly an order of magnitude higher on the resonant frequencies. If this increased acceleration excites the component board natural frequency, strains can increase by one order of magnitude compared to figure 14, which can result in a very rapid failure. Even in our test case, where the baseplate and the component board natural frequencies do not overlap, strains are significantly higher at the baseplate induced frequencies. When designing the component board reliability, discarding the effects of mounting can lead to over optimistic results.

For a more simplified analysis the maximum strains were extracted from two strain gauges in both directions. These strain results and the respective frequencies are presented in table 2 and a graphical illustration in figure 15. Even though these results are not directly comparable as they are extracted from different frequencies they still allow the comparison of the different temperatures. In the reliability point of view, the most relevant factor is the maximum strain as it will be the factor failing

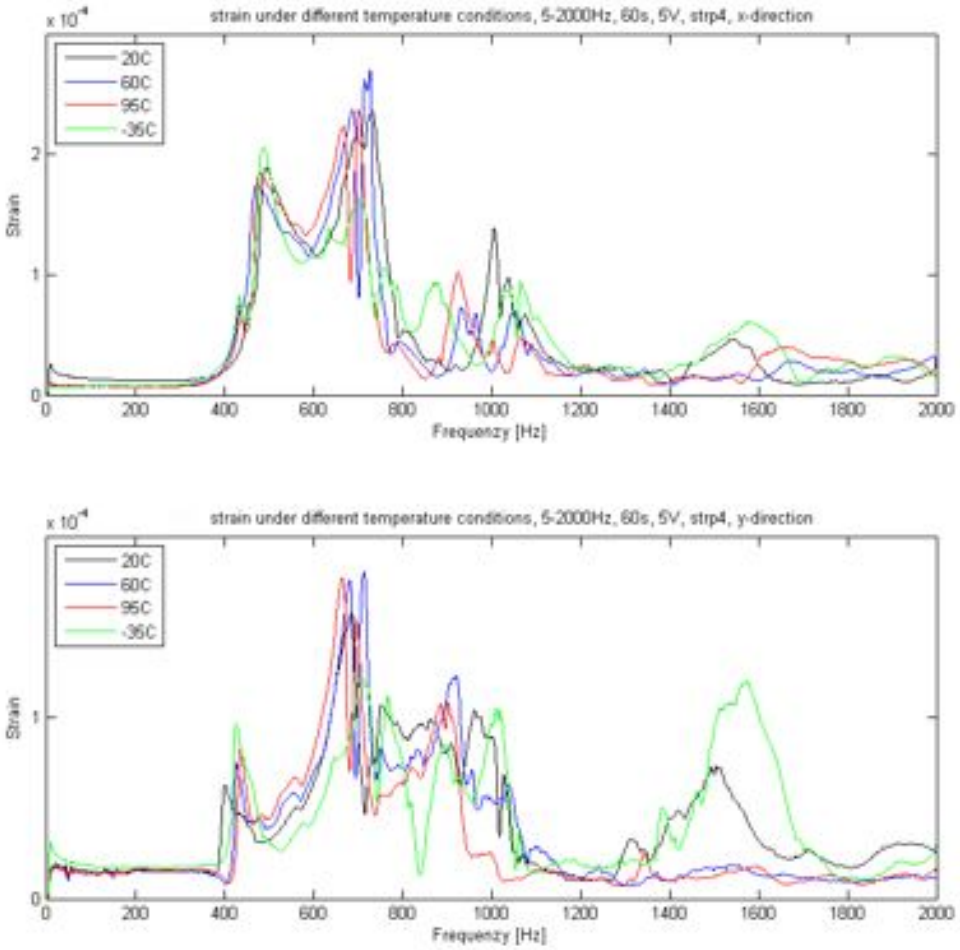

Figure 14: Product component board strain profile, 5 Hz - 2000 Hz 5 V input. Measured from area where several investigated components are located.

the board ultimately, provided that all frequencies are excited evenly. From these simplified results we can draw a conclusion that the acceleration is significantly lower in lower temperatures. This is assumed to occur mostly due to the increased rigidity and the ice build-up in the shaft inlet and thus increased friction. Another factor is that the mass of the baseplate and the component board is relatively high, thus they produce recoil like effect. When baseplate starts to vibrate it will also excite the mounting point of the baseplate and due to the large mass some of the vibration will be transferred to vibration exciter. This effect may strengthen or weaken the actual input depending on the frequency. However, the magnitude of this effect is unknown and the effect of temperature on it is even more unclear.

Figure 15 also tells that the strains are the highest at 60 $°C$ and the lowest in -35 $°C$. Differences are small, except in the case of Strain#2_y where in 60 $°C$ notably large strain value can be observed.

In addition, it should be noted that the experimental strain measurements cannot give the complete picture of the strain and stress distributions on the PWB. Simple board strain measurements should only be used for comparison and model

Table 2: Maximum strain values in two locations on product PWB at different temperatures and their respective frequencies with 5 V input

	Temp ($°C$)	**Freq (Hz) x**	**Strain x**	**Freq (Hz) y**	**Strain y**
Strain #2	-35	1569	4,91E-05	1029	1,26E-04
	20	1529	3,78E-05	724	2,61E-04
	60	715	5,94E-05	709	3,577E-04
	95	693	4,71E-05	696	3,204E-04
Strain #4	-35	491	2,060E-04	713	1,234E-04
	20	734	2,361E-04	691	1,573E-04
	60	733	2,696E-04	691	1,806E-04
	95	702	2,377E-04	671	1,769E-04

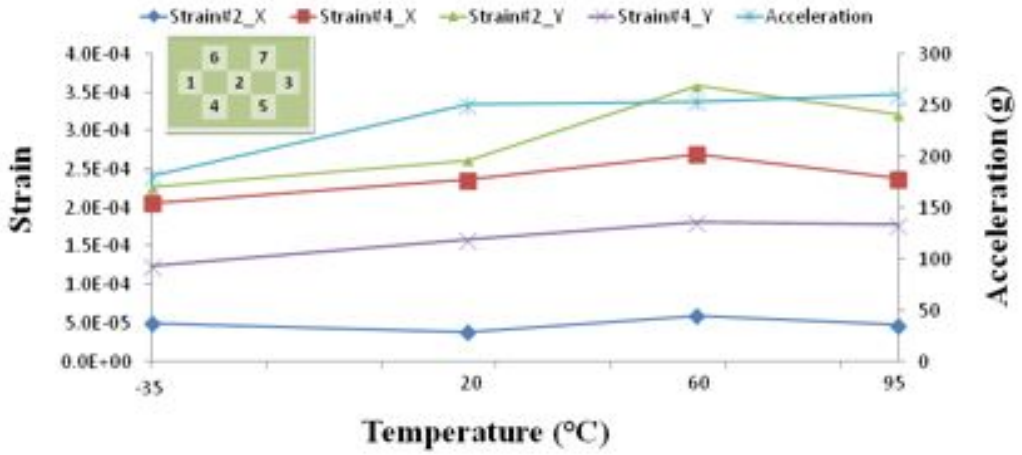

Figure 15: Maximum strain values in product PWB at different temperatures from two locations, x and y directions and maximum shaft acceleration input with 5 V input. A schematic representation of strain gauge locations is located in upper left corner.

optimization. From a proper FE-model the whole PWB strain distribution can be extracted as well as the actual strains in the interconnections. The interconnection strains, i.e. solder strain and lead strain, are the critical parameters for the reliability as they are usually associated with the failing locations.

The effect of temperature is not limited to change in material parameters, it will also result in thermal expansion that can cause significant stresses and strain by itself. According to the FE-simulation presented in figure 16 strain occurring due to uniform temperature change can be up to an order of magnitude higher than the strain induced during the vibration excitation (5 V, table 2). This high static strain is not critical as usually the strain cycles are required for crack propagation. Temperature cycling will naturally produce also cyclic strain, but the frequency is

usually very low. For example, in the test system heating the thermal chamber from 20 $°C$ to 95 $°C$ takes roughly 45 minutes. So a full cycle time between these temperatures would be 90 minutes if dwell time is zero. During this, almost 4 million strain cycles occur, if 700 Hz frequency is considered. In the real application the effect of both is important due to the long life time.

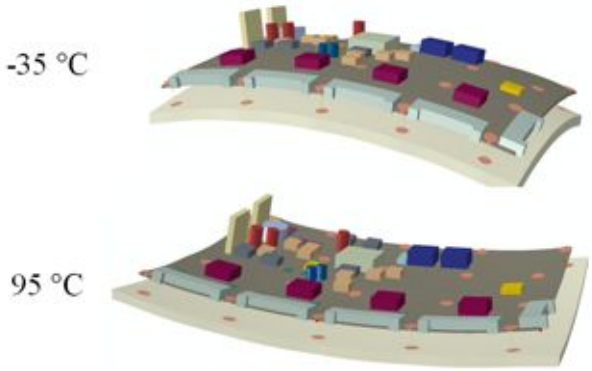

Temperature °C	Deflection (mm)	Strain#2_x	Strain#2_y	Strain#4_x	Strain#4_y
-35	0.159	1.02E-03	9.16E-04	9.78E-04	9.74E-04
20	0	0	0	0	0
60	-0.0857	6.19E-04	5.22E-04	5.86E-04	5.80E-04
95	-0.1677	1.25E-03	1.04E-03	1.18E-03	1.17E-03

Figure 16: FE-simulation of Product component board and baseplate subjected to uniform temperature change. Deformations in maximum and minimum temperatures are shown and strain results in locations #2 and #4 are shown in table.

Test board characterization

As a final part of the characterization, the test board was analyzed. The mechanical response of HETB-02 board was analyzed using the vibration test setup with five strain gauges and one accelerometer. The characterization measurements were conducted at all four test temperatures. Used test profile was sinusoidal sweep from 70 Hz to 110 Hz with the voltage amplitude of 5V. The strain measurement results and the schematical representation of the strain gauge locations is shown in figure 17.

According to the measured results presented in figure 17 strain values are nearly the same at temperatures of 20 $°C$, 60 $°C$ and 95 $°C$. Accelerations in these cases are also similar. At -35 $°C$ the strain and the acceleration values are notably lower, this is expected to happen due to the ice build-up. Interestingly, the frequencies behave opposite to expected: higher the temperature, higher the frequency. In table 3 in addition to the experimental results, also FE-modeled strain and frequency results are presented. In the modeled case, the frequencies behave as expected: lower the temperature, higher the frequency.

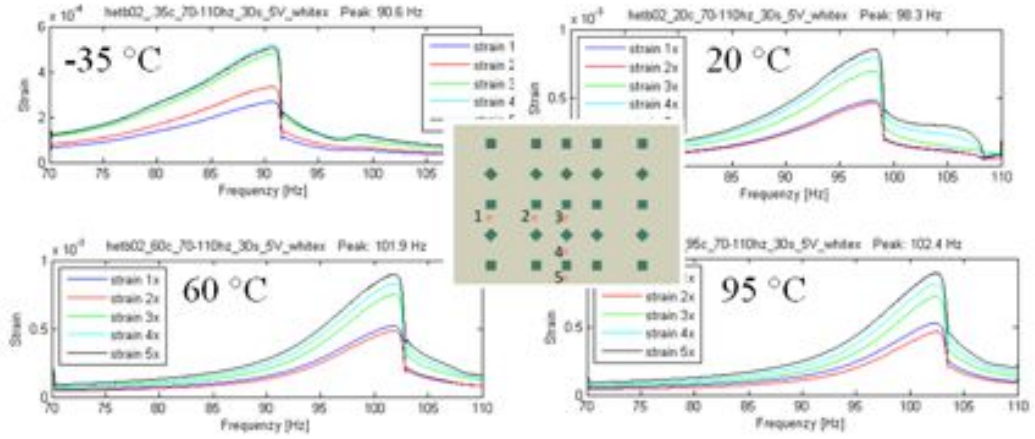

Figure 17: HETB-02 Strain measurement results under different temperatures and the schematical representation of strain gage locations.

The figure 17 also shows the importance of using the initially 1% lower test frequency compared to the peak value. Due to degradation, the resonant frequency will slightly drop during the lifetime test. Only a slight increase of frequency will result in steep drop in board strain.

Table 3: The comparison of HETB-02 experimental measurements and FE-simulation results

Temp. ($°C$)	**Acc.** **(G)**	**Exp. Freq.** **(Hz)**	**FEM freq.** **(Hz)**	**Exp. strain** **(gauge #5)**	**FEM strain** **(gauge #5)**
-35	8,29	90,6	118,0	5,06E-04	5.11E-04
20	10,88	98,3	93,8	8,55E-04	8,44E-04
60	10,54	101,9	86,5	8,99E-04	9,02E-04
95	10,66	102,4	81,3	8,94E-04	8,99E-04

Difference in the frequencies can be explained by differences between the FE-model and the real setup. In the FE-model it is expected that everything else remains the same except the material properties. This is the case, for example, in figure 13, but in HETB-02 setup the case is different due to increased structural complexity. High T_g FR4 PWB is attached to the aluminum baseplate using steel bolts and polyacetal line clamps. All these materials have different material properties, in this case the most relevant property is the coefficient of thermal expansion (CTE). In table 4 these values are presented.

Using the data provided in the table 4, simple calculations can be used to estimate the effects of the temperature change via equation 4. In the table 5 the relative change in size due to temperature change from 20 $°C$ to 95 $°C$ and -35 $°C$ is presented. Using these results simple estimations of the stresses in structures can

Table 4: CTEs of material used in HETB-02 test setup

material	**usage**	**CTE (ppm/$^\circ C$)**
FR4	PWB	14 (x- & y-axis) 175 (z-axis)
aluminum (Al)	baseplate	23,1
Polyacetal (POM)	line clamps	135
Steel	clamp tightening	17,3

be generated. Actual stresses are dependent on the material properties and they are not considered here. POM clamp with PWB would expand over 1 % in size if allowed to, but the screw used to tighten the clamp will only lengthen 0,13 %, thus preventing the clamp from expanding. This difference will create stress and deformation on the clamp and the PWB. Some marks of deformation can be seen in the clamps e.g., cracks in clamp around the screw location. Clamps will tighten or loosen significantly due to temperature change and this may affect on frequency behavior thus partly explaining the unexpected behaviour of the resonance frequencies.

$$\Delta l = \alpha_l \Delta T \tag{4}$$

In addition to clamps, temperature will also affect the baseplate and PWB. From tables 4 and 5 it can be seen that the baseplate will expand more than the PWB. In the case of increased temperature this will create tension on the PWB. The tension is assumed to result in a guitar string like effect. The increased tension will increase component board's resonant frequency. Furthermore, the baseplate (and the component board) will bend slightly, and this may also affect the vibration behavior. Similarly, in lower temperatures the baseplate will induce compressive stress on the PWB.

In the FE-model, the line clamp was assumed to be connected from the whole distance. However, in the real case clamp is connected only with three bolts on both sides. This difference combined with the deformation of the clamps due to thermal expansion, may also have affected the frequency behavior.

Table 5: Relative changes in size in several structures under the change of temperature from 20 $^\circ C$ to 95 $^\circ C$ and -35 $^\circ C$

structure	Δl ($\Delta T = +75^\circ C$)	Δl ($\Delta T = -55^\circ C$)
POM clamp + PWB	1,03 %	-0,74 %
Al clamp + PWB	0,23 %	-0,17 %
Steel screw	0,13 %	-0,10 %
Baseplate	0,17 %	-0,13 %
PWB	0,11 %	-0,08 %

To further investigate these effects, additional aluminum clamps were fabricated.

The results from the Al clamp measurements and comparison to the POM clamps is presented in table 6. Results at the neutral conditions (20 $°C$), where no stresses due to thermal effects should exist, show a slight acceleration drop. This effect is assumed to happen mainly due to the added mass and possibly slightly due to the structural differences i.e. the Al clamps are significantly more rigid compared to the POM clamps. Minor increase in the frequency is expected to happen for the same reasons. Whereas no significant change in the strain values can be seen.

At -35 $°C$, acceleration drop of the same magnitude occurs as at 20 $°C$. Also here, the difference can be explained by the added mass and the slight change in structural rigidity. However, at the colder temperature, larger increase of frequency and a marked increase in strain values can be seen. In the higher temperatures the increase of the acceleration is notable compared to the old results (POM clamp) and the neutral conditions. As the added mass is expected to lower the acceleration, the increase of the acceleration has to happen due to the structural differences. It is likely that the POM clamps will show a notable drop in the elastic modulus at the higher temperatures. Presumably, with the Al clamps this effect is nearly insignificant. Additionally, the rise of resonant frequency at the higher temperatures is notable.

Table 6: The comparison of HETB-02 experimental measurements using polyacetal (POM) and aluminum (Al) clamps

Temp. ($°C$)	**Acc. (G) POM/Al**	**Exp. Freq. (Hz) POM/Al**	**Exp. strain (gauge #5) POM/Al**
-35	8,29 / 7,65	90,6 / 93,5	5,06E-04 / 7,89E-04
20	10,88 / 9,44	98,3 / 99,9	8,55E-04 / 8,70E-04
60	10,54 / 10,75	101,9 / 105,7	8,99E-04 / 8,74E-04
95	10,66 / 11,48	102,4 / 108,2	8,94E-04 / 8,77E-04

Based on these observations it is clear that the unexpected change in the resonant frequency does not happen due to the clamp tightening and loosening. The change of the frequency is larger when using the Al clamps, which suggests that the expansion of the baseplate is the main reason. The POM clamps probably deform and bend due to this stress thus reducing the tension in the PWB, whereas the Al clamps are more rigid and the tension on the PWB is higher. The loosening of the clamps seems to have had notable effect on the strain at -35 $°C$ temperature, but the tightening seems irrelevant.

6.2 FE-simulation of combined loads

Stress and strain in the solder interconnection and in the component lead was investigated with FE-simulation. The simulations were conducted for both cases i.e. components on the product component board and HETB-02 test board.

For the stress and strain simulation a detailed model of the D^2PAK components was placed on the PWB. The detailed model was used only in the investigated

location, other components were modeled only with a simple block models. Average element size in detailed model was 0,05 mm. Simulations were done in two steps: first a thermomechanical stress simulation with uniform temperature change was run, followed by a vibration sweep simulation.

Product component board

For the stress and strain analysis the test components in two locations and orientations were investigated. The component location and naming with the detailed model can be seen in figure 18.

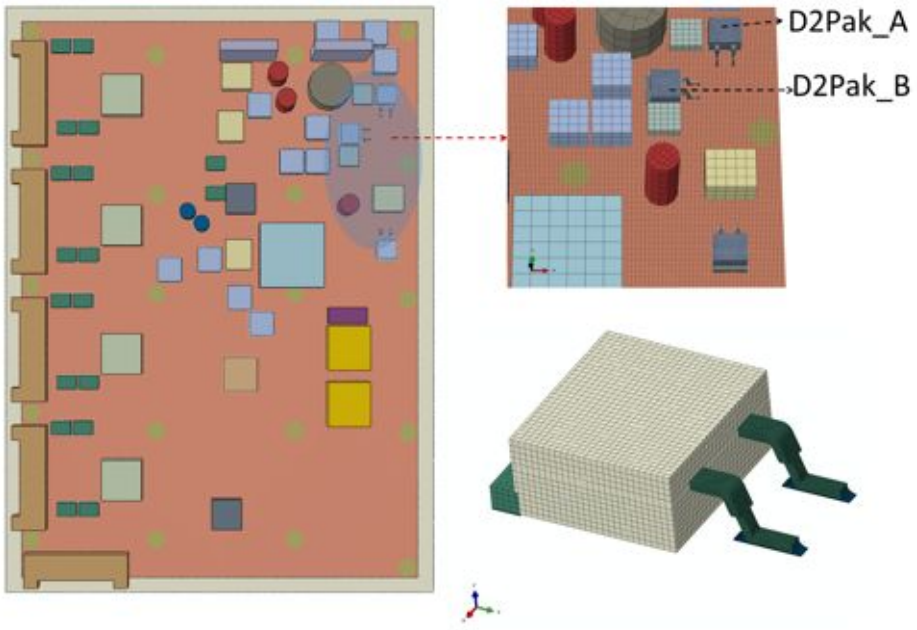

Figure 18: Two detailed component models, D^2PAK_A and D^2PAK_B, placed on product component board model. Detailed model presented in the lower right corner.

Thermomechanical stress and strain data is shown in figure 19. The stress distribution in the model is not dependent on the testing temperature so only the distribution at -35 $°C$ is shown. Room temperature was used as a zero stress state, as a result the stress and strain increase while moving further from the room temperature. There was no significant difference in the thermomechanical stress and strain between these two locations and orientations.

After the thermomechanical analysis the effect of vibration was investigated in the same analysis. Thus the thermomechanical stress and deformation are also considered in the simulation. Frequency sweep from 300 Hz to 1300 Hz was utilized with an input acceleration of 1 G. The maximum solder strains are shown in table 7. At the 20 $°C$, simulation yields lowest strain values, as no residual thermomechanical stress is present. It is also found that the increasing testing temperature will increase

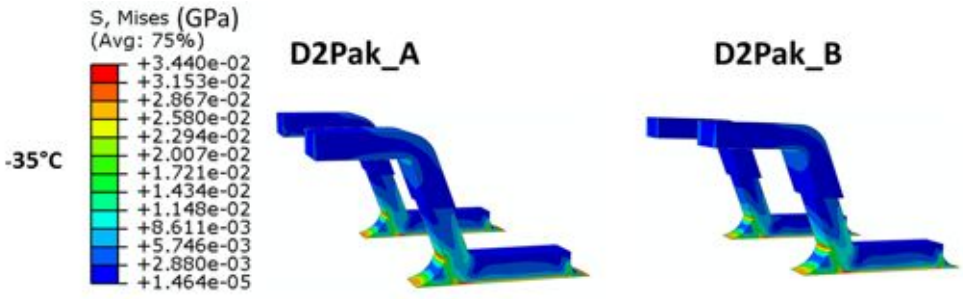

Temperature (°C)	Stress (MPa)	Strain
-35	34.4	-1.292E-3
60	19.8	1.071E-3
95	38.2	2.165E-3

Figure 19: Thermomechanical stress and strain of D^2PAK on the product component board components under the uniform temperature change.

the strain value and finally lead to a shorter lifetime. This is due to the fact that the materials are softened at high temperatures and the deformation of the materials are increased. Compared to the D^2PAK_A, the D^2PAK_B experienced much lower strains during the vibration.

The locations of the two components are shown in figure 18. According to a previous study with HETB-02, we have already made the conclusion that the assembly orientation parallel to the long edge of the component board (D^2PAK_A in this case) will lead to shorter lifetime. Besides, compared to D^2PAK_A, D^2PAK_B is surrounded by more components and located further away from the free edge of the component board. Therefore, the difference can be the result of these known factors: different assembly orientation, the influence from the nearby components, the screw locations, and the distance to the free edge. As a conclusion we can say that if a component is surrounded by other large components it will face lower stresses. At least in this case the structural reinforcement effects of larger components surpass the effect of the higher mass. A component near the free edge of the component board may experience higher stress and strain. Component's location in respect to mounting points also plays a large role.

Table 7: Maximum solder strains in product component board

Temperature ($°C$)	**D^2PAK_A strain**	**D^2PAK_B strain**	**difference (%)**
-35	4,70E-05	3,68E-05	28
20	1,64E-05	1,10E-05	49
60	8,37E-05	6,29E-05	33
95	9,35E-05	6,99E-05	34

HETB-02 test board

HETB-02 test board was modeled at all test temperatures. In the HETB-02 simulations thermomechanical residual stresses were not considered. Only the change in the material properties at different temperatures was considered. The simulated stress and strain distributions are shown in figure 20. The change of temperature will only affect the magnitude of stress and strain, thus distribution is similar in all temperatures. As can be seen in figure 20, the stress and strain concentrations are located in the lower turning point of the component lead. Components parallel to strain direction (Vx1) will face largest stresses and strain and thus be the most vulnerable components. Components placed in 45 ° orientations compared to strain direction (Vx2) will face slightly lower stresses and strain compared to the parallelly oriented components. Components placed perpendicular to strain direction (Vx3) will face significantly lower stresses and strain i.e. from one quarter to one fifth compared to two previous ones. The large difference can be explained by the large solder interconnection below the component body. It will locally make the system more rigid, thus reducing the strains in the PWB and in the lead interconnection.

In the parallel and perpendicular orientations stress and strain distributions are nearly identical in both of the leads. At 45 ° orientations only one lead has significant stress and strain concentrations. The lead with the higher stress and strain concentration is the outer lead. The inner lead is inside the area where the large body interconnection will reinforce the PWB thus reducing the stress on the lead. Very high lifetimes are expected in locations where the monitored leg is protected by the large body interconnection.

Figure 21 compares the maximum solder strains of all the calculated components. Two dashed lines divide the graph into three groups and each group represents one assembly orientation (e.g., Vx1 includes V31, V41, and V51 in the graph). Regardless of the testing temperature, the orientation group Vx1 has the highest strains and the group Vx3 has lowest strains. Each curve represents solder strain in one temperature. According to simulation, the test performs nearly as designed, from single test board we can extract lifetime data with 3 different strain values in each direction. The differences between these strains are not as large as intended, but it is considered to be sufficient.

Strains are highest at 20 $^{\circ}C$ and lowest at -35 $^{\circ}C$. At 60 $^{\circ}C$ and 95 $^{\circ}C$ strain values are nearly identical. Curve shape stays similar, independent of temperature, indicating that the behavior of the test board stays the same in all temperatures. Tests were conducted with 3 V voltage input, thus there may have been differences in the acceleration input. Changing material parameters and ice build-up may have affected the acceleration input. For this reason, strain values are not comparable. However, this is not a concern for the reliability of the actual test. Lifetime models will be composed in respect to strain and lifetime.

To justify the simulated strain results, comparison between the experimental and the FE-modeled board strain values is presented in table 8. We can see that board strain values are nearly an exact match. Due to good match in board strain, simulated lead/solder stresses and strains can be assumed to be close to the real

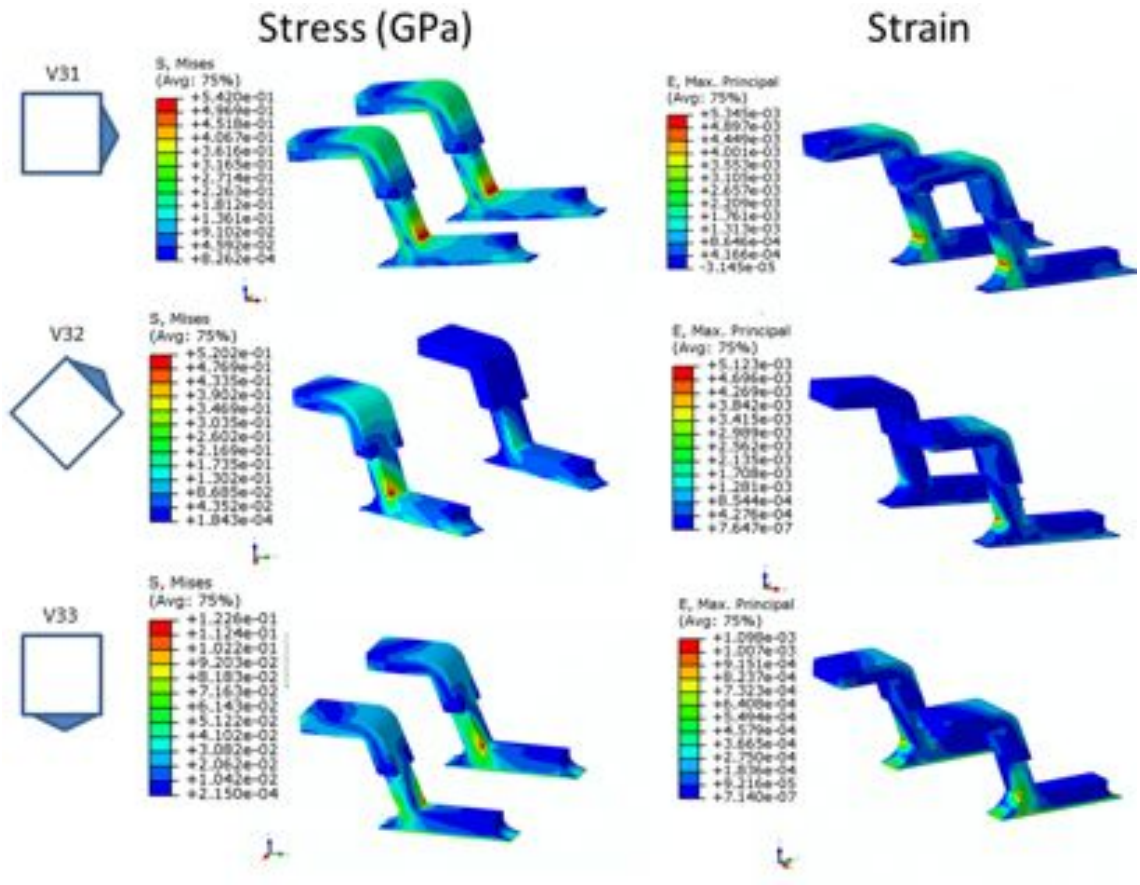

Figure 20: The stress and strain distributions of D^2PAK components on HETB-02 board under vibration loading at room temperature .

case. However, there is no way to measure the stress or strain in component lead due to small dimensions and varying geometry. FEA is the only method that allows studying stresses in these small interconnections

Table 8: Measured and FE-modeled maximum board strain under different temperatures with 3V voltage input.

Temperature ($°C$)	**Strain (gauge #5)**	**FEM strain (gauge #5)**
-35	5,04E-04	5,04E-04
20	7,40E-04	7,30E-04
60	6,37E-04	6,39E-04
95	6,54E-04	6,47E-04

6.3 Lifetime test results

Lifetime testing was conducted using a point frequency excitation at four different temperatures as described in section 5.2. At each testing temperature three or four

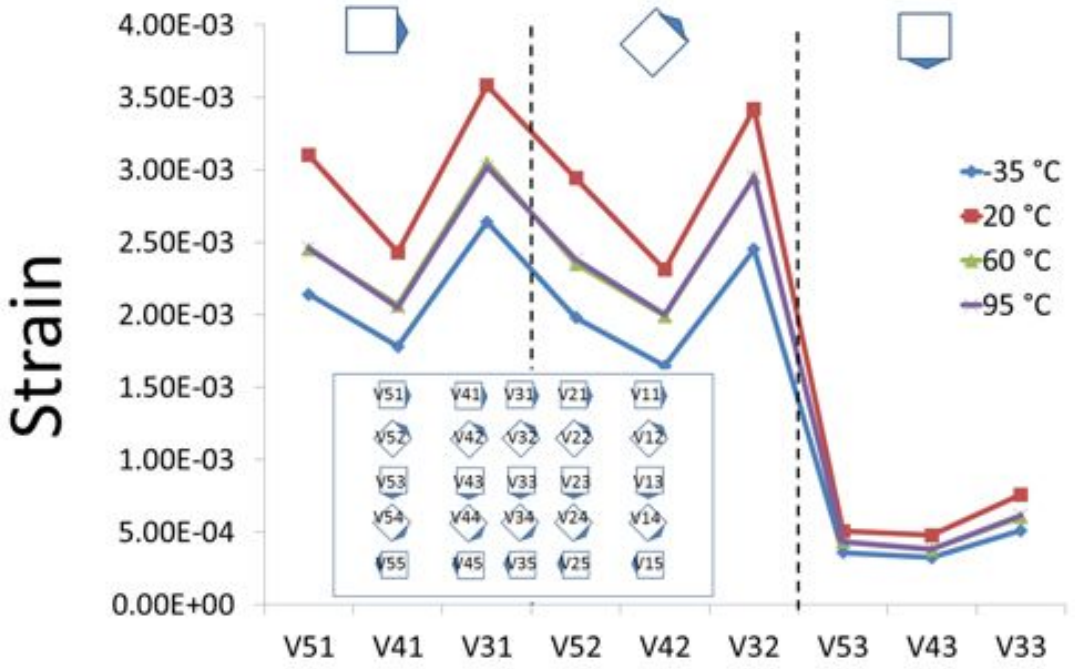

Figure 21: Maximum simulated solder strain at different locations, orientations under combined vibration and thermal loading.

successful test runs were conducted. Several test runs determined to be unsuccessful due to dropping off from the resonant frequency spike. The dropping off from the resonance results in very low excitation amplitude and naturally very long lifetime. Despite the precautions taken to avoid erroneous event detector outputs, several erroneous failure indications were observed. Both falling from the resonance and the erroneous event detector outputs could be easily detected and discarded from the results. In some cases part of the data was considered as sensory data and in most severe cases the whole test run was discarded.

As described in the previous subsection the strains are very low when component is placed perpendicular to strain direction and in 45° orientation the leg that is protected by the large component body interconnection will also face only small strains. For these reasons, main focus was on components Vx1, Vx2 and Vx5 as these will face largest strains and fail during the test time. In figure 22 component orientations are presented with strain direction.

Test results are presented as Weibull cumulative distributions, according to equation 1. Weibull fitting was determined to be good ($R^2 > 0,95$) in most cases, but in all cases at least acceptable ($R^2 > 0,9$). However, in some cases the amount of the available failure data was very low. These cases cannot be considered to be statistically reliable. Weibull distributions are graphically illustrated in figures 23 - 26 and parameters are listed in tables 9 - 12.

The Weibull plot of group V21, V25, V41, V45 at -35°C (figure 23 and table 9) yields the goodness of fit of 0,91. By looking at the curve and data points we can

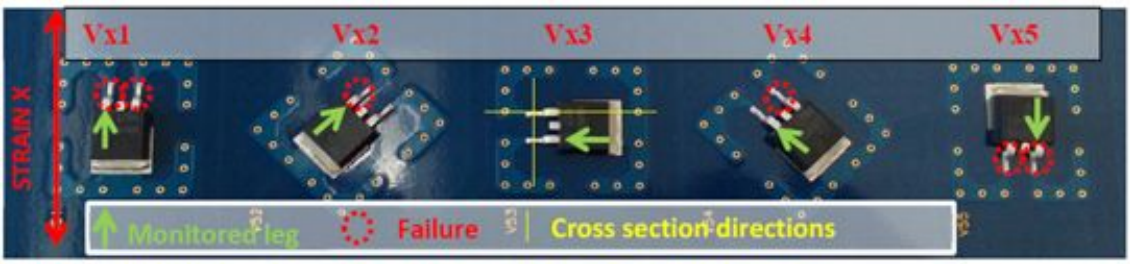

Figure 22: HETB-02 component lines, monitored legs and the locations of detected failures.

see that the data could be separated into two groups (first six and last eight data points). This suggest that there may be two separate failure modes present in this location under these conditions. Additionally, based on data it seems that the V25 and V45 have longer lifetime compared to V21 and V41, this may indicate that the symmetry assumption between these location is at least partly false. As a result it is possible that the separation of group can be explained by small differences in the stress conditions.

According to [70] the β value of approximately one can also indicate the presence of multiple failure modes. For example, in location V22, V42 at $20°C$ (figure 24 and table 10) we can see a β of 1,08. By looking at the plot we can see that in that location, only four data points are available. These four data points could be divided into two groups where both groups would result in Weibull curve parallel to other curves in the plot. Similarly to previous case, the two with shorter lifetime are from location V22 and longer lifetimes from V42. Also in this case it seems that the symmetry is not as accurate as expected. It is obvious that with different component, such as symmetrical BGA, symmetry should be more accurate. As a conclusion component orientations should be more carefully designed, especially if non symmetric component, as in here, is used.

Additionally, in Vx1 and Vx5 locations, where components are placed parallel to strain direction, some variation may occur. As only one lead is monitored, the failure in the second lead may cause some uncertainty.

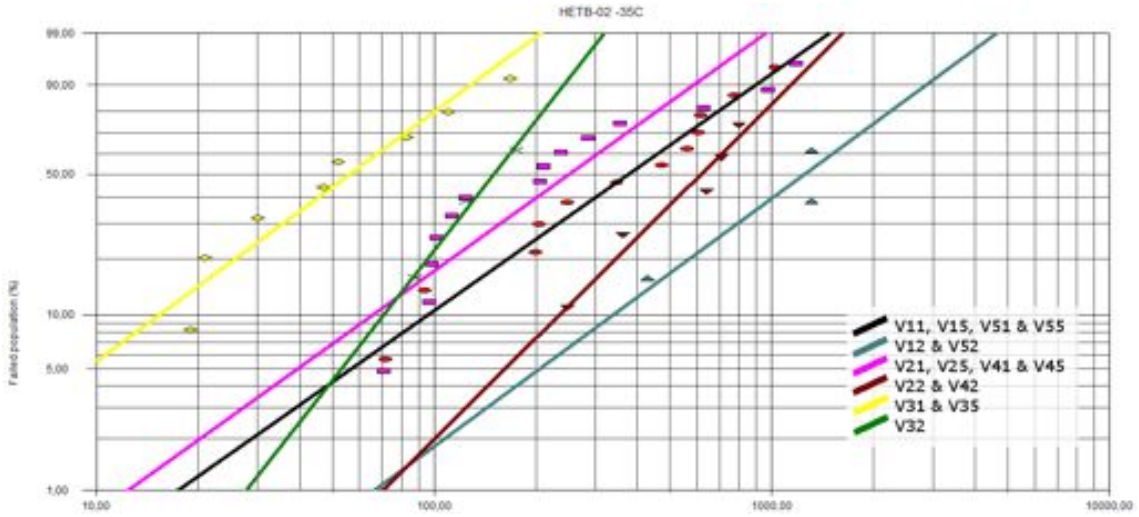

Figure 23: HETB-02 lifetime results in Weibull form (-35°C). Failed population versus time (min).

Table 9: HETB-02 Weibull parameters and simulated solder strain at -35°C.

-35°C	**solder strain**	η	β	R^2
V11, V15, V51, V55	2,14E-03	490	1,38	0,99
V12, V52	1,98E-03	1613	1,44	0,92
V21, V25, V41, V45	1,78E-03	326	1,41	0,91
V22, V42	1,65E-03	744	1,95	0,98
V31, V35	2,64E-03	73	1,45	0,96
V32	2,45E-03	174	2,51	0,99

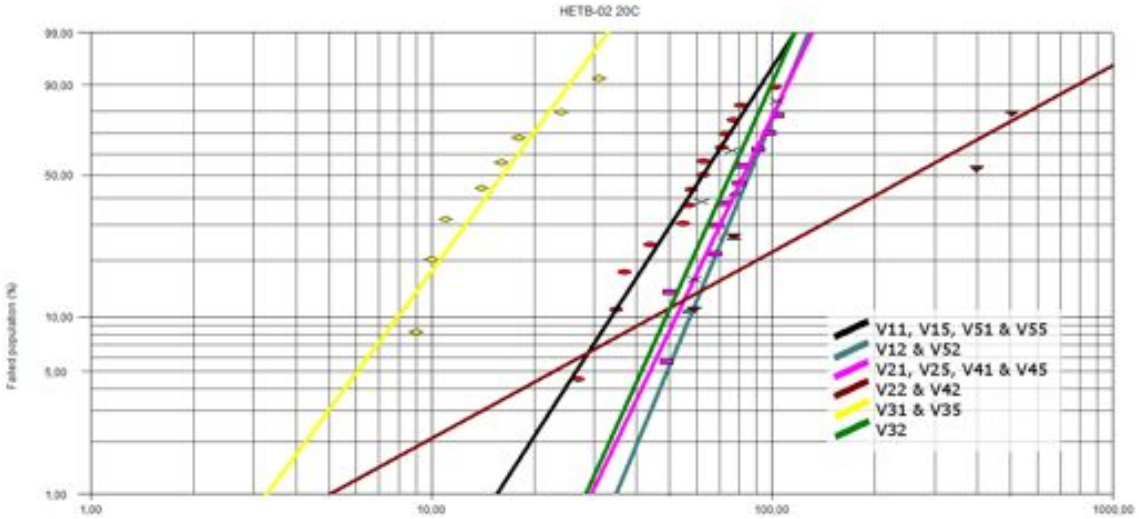

Figure 24: HETB-02 lifetime results in Weibull form (20°C). Failed population versus time (min).

Table 10: HETB-02 Weibull parameters and simulated solder strain at 20°C.

20°C	**solder strain**	η	β	R^2
V11, V15, V51, V55	3,10E-03	71	3,04	0,99
V12, V52	2,94E-03	93	4,7	0,94
V21, V25, V41, V45	2,43E-03	90	4,11	0,97
V22, V42	2,31E-03	365	1,08	0,95
V31, V35	3,58E-03	19	2,66	0,95
V32	3,42E-03	82	4,34	0,92

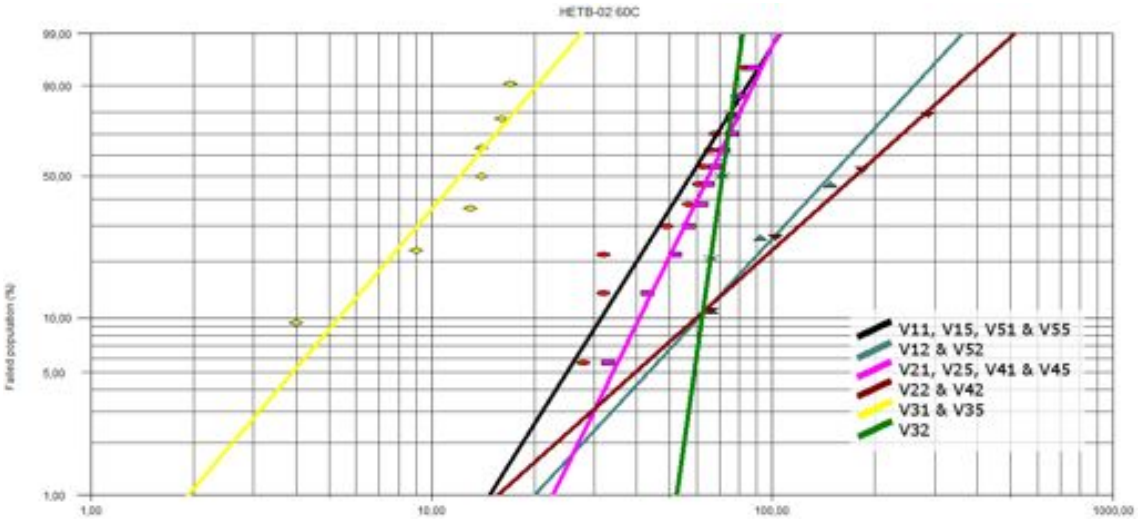

Figure 25: HETB-02 lifetime results in Weibull form (60°C). Failed population versus time (min).

Table 11: HETB-02 Weibull parameters and simulated solder strain at 60°C.

60°C	**solder strain**	η	β	R^2
V11, V15, V51, V55	2,45E-03	65	3,12	0,96
V12, V52	2,35E-03	176	2,12	0,98
V21, V25, V41, V45	2,07E-03	71	4,02	0,99
V22, V42	1,99E-03	215	1,75	0,99
V31, V35	3,05E-03	14	2,03	0,93
V32	2,95E-03	73	13,69	0,99

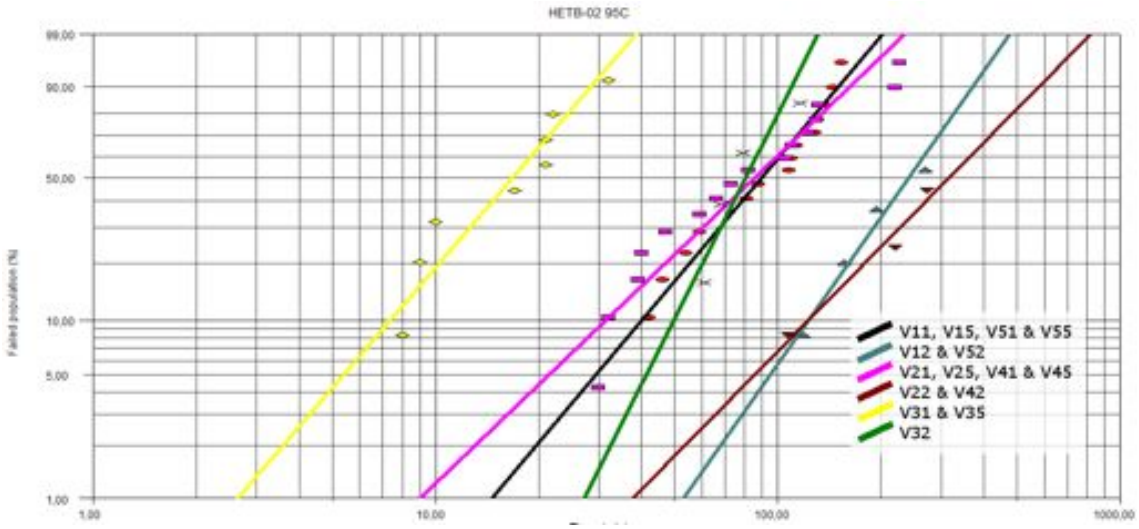

Figure 26: HETB-02 lifetime results in Weibull form (95°C). Failed population versus time (min).

Table 12: HETB-02 Weibull parameters and simulated solder strain at 95°C.

95°C	**solder strain**	η	β	R^2
V11, V15, V51, V55	2,14E-03	105	2,33	0,98
V12, V52	1,98E-03	275	2,79	0,98
V21, V25, V41, V45	1,78E-03	104	1,88	0,96
V22, V42	1,65E-03	380	1,99	0,98
V31, V35	2,64E-03	20	2,29	0,95
V32	2,45E-03	89	3,89	0,92

Depending on the amount of successfull test runs, three or four data points were available from each of the component locations. This means that in the best case, group V11, V15, V51 & V55 may contain up to 16 data points; whereas, group V32 can only contain the maximum of 4 data points. Exact time to failure was used as the value. The components that did not fail were used as sensory data with the value of test ending time. Sensory data will not be presented as data points in Weibull plots; nonetheless, it is still considered in calculation and affects on the probability values linked to each failure.

At 20 °C and 60 °C, simulated strains behave as expected (highest in line V3x and lowest in line V2x). Component lifetimes behave as strains suggest (Shorter lifetimes with lower strains). At -35 °C and 95 °C strains behave as expected; however, compared to V1x, lifetimes are shorter or same in row V2x. There is no clear explanation for this but it is assumed to be related to the fact that the model does not incorporate the effects of thermal expansion. These may have some effect on the mode shape thus shifting the strain values.

To compare different temperatures, Weibull lifetime results from location V21, V25, V41 & V45 are presented in figure 27. Weibull lines at 20°C and 60 °C are nearly parallel, suggesting that the failure mechanism would be exactly the same.

At -35 $°C$ and 95 $°C$ slope is slightly different, this would suggest that there is at least some difference in failure mode. Comprehensive failure analysis can be found from section 6.5. Additionally, we can see that the first data points at -35 $°C$ and 95 $°C$ could form a Weibull graph with similar slope compared to 20$°C$ and 60 $°C$, this option is represented with the dashed lines in figure 27. As discussed earlier, this suggests that there is a possibility of changing failure mode. The behavior of the slope parameters is similar in most of the locations. However, in locations where the amount of data points is low, variations are higher and cannot be assumed to be completely reliable.

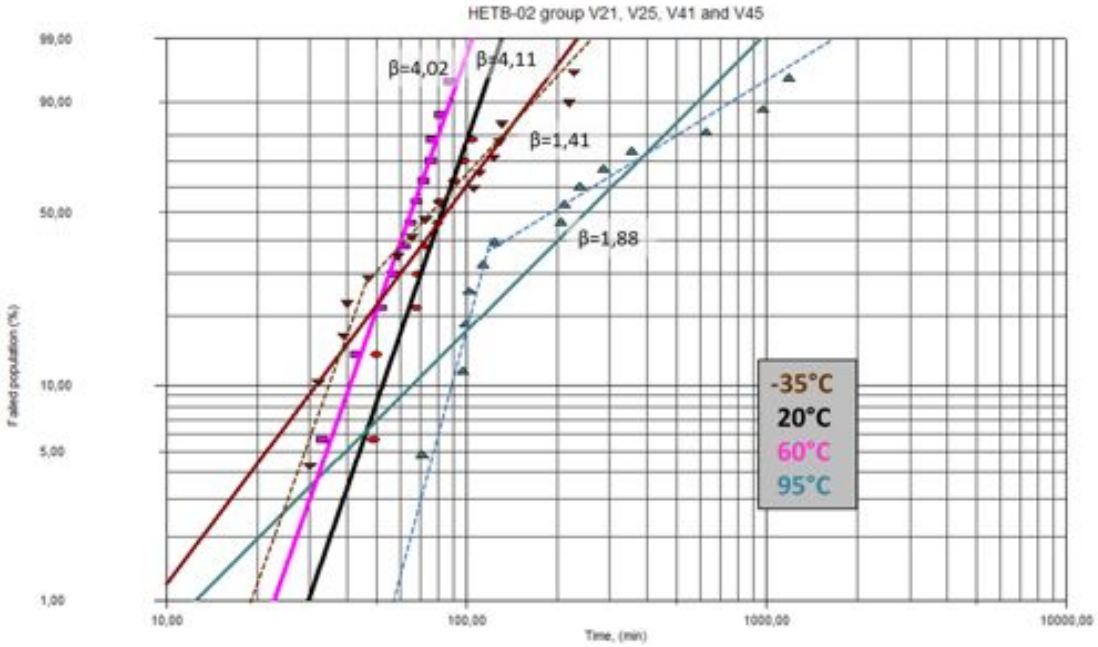

Figure 27: Comparison of Weibull lifetime results in location V21, V25, V41 & V45 in respect to temperature.

As the amount of experimental data is relatively low in many locations, small variations may have notable effects. Thus it is possible that the characteristics suggesting changing failure modes, may only be variation between samples. Possible sources for this variations include: symmetry assumptions, small variation in test run parameters, small variations in component lead or joint geometry and undetected erroneous failure indications.

6.4 Lifetime predictions

Component lifetime prediction

The lifetime test results presented in the previous subsection were used to create lifetime models. Power law lifetime estimation model was used to establish general lifetime prediction. The power law lifetime model equation is presented in equation 5, where ϵ is strain or stress, η lifetime and a & b are two fitting parameters. Used

model is a modified Coffin-Manson lifetime prediction. Three different strain or stress parameters have been used to analyze which of these yields most reliable results.

$$\epsilon = a\eta^{-b} \tag{5}$$

Measured PWB strain, calculated solder strain and calculated copper lead stress were investigated. The benefit of the measured PWB strain is that it is easy to extract with simple experimental strain gauge measurements. The other two parameters require modeling work. The calculated solder strain and lead stress are expected to yield the best results as they are calculated from the actual failure location.

In addition, also calculated PWB strains from block model and detailed model were considered. However, results from these cannot be used. Components located beside the clamps were heavily affected by the boundary condition. Boundary condition alters the PWB strain behavior near the edge. Strain distribution and gradient do not behave expectedly, thus the maximum strain from this area is too high and the average strain of the area too low compared to experimental results. However, component behavior is still expected to be quite accurate, and thus also the lead stress and solder strain. They behave as expected according to the design, measured results and lifetime results.

Strain gauges were placed on the HETB-02 PWB as shown in figure 17. Based on the measurements, strains are higher at the edge of the PWB compared to the center. Strain for location V35 was calculated as an average of strain gauges #4 and #5, as it is located between these two gauges. Due to symmetry, location V31 strain was assumed to be the same. Location V32 was calculated as an average from gauges #3 and #4 as its symmetrical to component V34 that is placed between these two gauges. Stains for other groups were calculated with the same scaling and symmetry assumptions. As there are only five strain gauges on the board other lines were assumed to behave as the center line gauges; i.e., gauges #3, #4 and #5. For example, strain at the board edge on line two was assumed to be equally larger than the strain gauge #2 reading as the gauge #5 reading is larger than the #3.

The component solder strain and lead stress was calculated at all temperatures using detailed component FE-models. Achieved results were used to generate the simple power law lifetime estimates.

To compare the goodness of power law fit, R^2s between different measurement or calculation methods and different groupings are presented in table 13. Five different combinations are considered. The first group "All separate" is the average of eight R^2s from all four temperatures and two different orientation and σ their standard deviation. "Temp. separated" is similar, except the orientations are combined to same group. 90° and 45° are fits when all temperatures are grouped to same lifetime model and only orientations are separated. In "all", all results are combined to the same model.

Comparison between the results obtained with different methods is presented table 13. Best fit is achieved using the measured PWB strain. This is contrary to the expectation and may indicate that model accuracy is not perfect. Modeled

results give the strain or stress in the actual failure location, and thus are expected to be most accurate method. This may mean that, due to boundary conditions model is slightly off as with the PWB strain model results were clearly erroneous in edge region. This suggest that some improvements should be done to the test board design and/or model.

Table 13: Power law lifetime model goodness of fits and standard deviation in averaged cases.

	Measured PWB strain		**Calculated solder strain**		**Calculated lead stress**	
Combination	R^2	σ	R^2	σ	R^2	σ
all separate (avg)	0,89	0,19	0,77	0,17	0,66	0,21
temp. separate (avg)	0,73	0,07	0,56	0,06	0,49	0,10
90°	0,90	-	0,65	-	0,54	-
45°	0,85	-	0,72	-	0,65	-
all	0,79	-	0,59	-	0,52	-

Incorporating baseplate and clamp structures to the model was investigated. If clamp elements are simply connected to PWB elements behavior did not improve but seemed even more obscure. One option is to model the system without connecting the PWB and clamp elements to each other and use contact definitions. However, this method requires explicit integration in time domain and would make the model much more complex and is expected to increase calculation time from few hours to multiple days or even weeks. Within this thesis, 24 models were calculated, thus total calculation time would have been months. Such long calculation time is infeasible and inefficient. As a result, it is critical to understand this effect and always evaluate all the results calculated. Easy fix would be changing the board layout, by moving components closer to center line thus allowing more space between boundary and the closest component lines.

Even though the measured PWB strain results in best fit, it is impractical for real application. Used test board design is simplest possible to ensure easy and accurate analysis. In the actual product the comprehensive PWB strain measurements require a large amount of gauges, and due to more complex vibration modes placing them is less straight forward. For these reasons using modeled values is recommended for more accurate and easier analysis.

From the two modeled methods solder strain seem to yield the better fit even though the dominating failure mode is initiated at the location of highest lead stress concentration. Due to assumed better representativeness we will use lead stress as the condition for lifetime calculations. Same calculation methods will apply to both types and the decision of used parameter has to be done in each case considering representativeness, assumed result reliability and practicality. For example, when considering the lifetimes of different products it may be practical to use the same criterion for each component.

Combining the different orientations does not seem to produce good fit according

to results in table 13. The fit values of "all separate", 90 ° and 45 ° are consistently higher compared to "temp separate" and "all", in which different orientation are combined.

The lifetime models for separate orientations and temperatures are presented in figure 28. The amount of data points for each model is very low. Higher accuracy prediction could be obtained using a higher amount of data points. To achieve this, several test amplitudes or different test board design can be used, which allows larger strain value span.

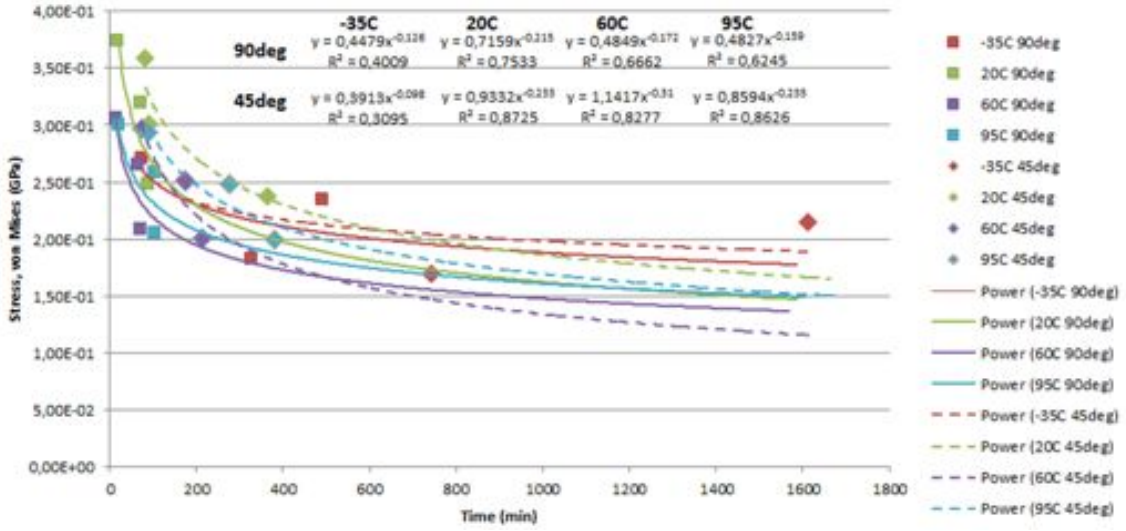

Figure 28: Separate power law lifetime models for each orientation and temperature.

At all temperatures, the lifetime of 90 ° orientation can be expected to be the shortest at higher stress and strain values. At the lower strain values and higher lifetimes seems that 45 ° orientation lifetime will fall below 90 ° orientation at 60 °C and 95 °C at stresses below 0,15 GPa. However, this effect can be just a coincidence due to the low amount of data points at the lower strain values.

To create a model that considers the temperature dependencies of power law model parameters a and b (equation 5) were investigated. For 45 °, second order polynomial equation gives good fit but for 90 °, 3rd order equation is required to achieve fit. It is peculiar that the behavior of the parameters of the two orientations is so different. Explanation may lie in the insufficient amount of data as it seems unlikely that so large difference would occur due to the orientation and only at certain temperatures. The fitting of the parameters in respect to the temperature is presented in figure 29.

The calculated temperature dependent models for a and b can be used to calculate component lifetimes in different temperatures. However, lifetime calculations become complicated if the second or third order polynomial are used. In addition, no simple orientation dependency can be established. Depending on the strain orientation in respect to component relevant equation can be chosen. If the strain orientation is not simple to determine, the most conservative model is suggested.

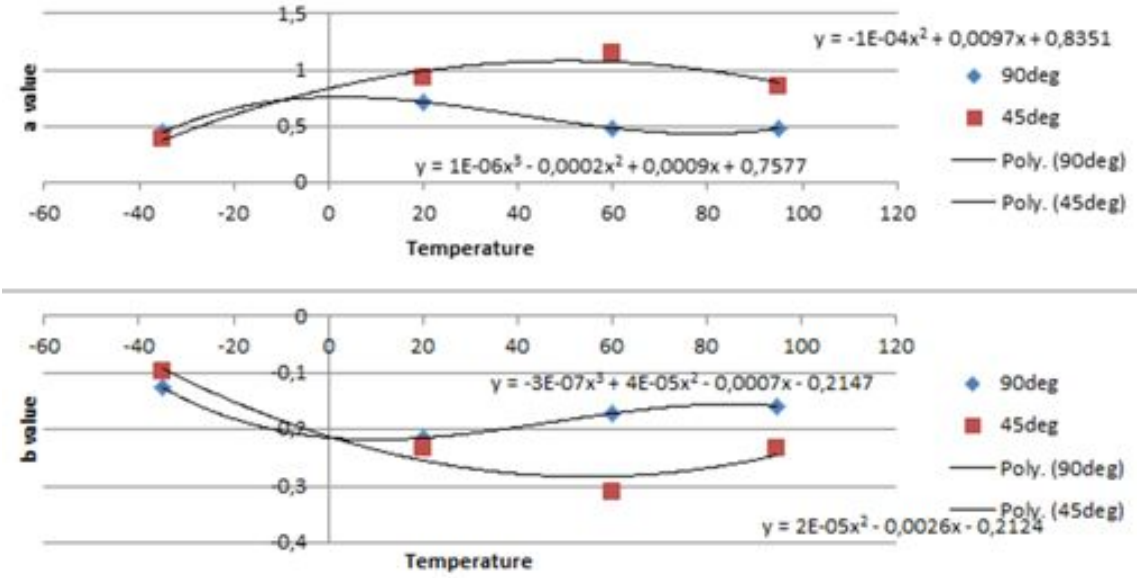

Figure 29: The temperature dependency of separate power law lifetime models. a (upper) and b (lower) in respect to temperature.

Instead of using polynomial equations it may be more convenient to just use the most relevant equation parameters; i.e., when around 60 $°C$ using the most relevant single parameters instead of the equations.

To further simplify the analysis, combined temperature independent models can be used. Three possible alternatives exist: the combination of all and two orientation specific models. Models are presented in figure 30. Below stresses of 0,2 GPa, the model that combines all is the most optimistic, thus it is suggested that orientation specific models can be used to increase prediction pessimism, i.e. safer prediction. Depending on the orientation, proper model can be chosen, the second option is to use the most pessimistic prediction. At stresses above 0,16 GPa, the 90 ° model yields most pessimistic results and at stresses below 0,16 GPa, the 45 ° should be used.

Compared to separate lifetime models, combined models yield optimistic results, especially when compared to the 60 $°C$ model. Accordingly, the most pessimistic results can be obtained using 60 $°C$ model. The two orientation specific models intersect at stress around 0,16 GPa. Thus 90 ° model is recommended for stresses above 0,16 GPa and 45 ° below that. Using these parameters the most pessimistic prediction can be obtained. In addition, according to thermal imaging results provided by the product manufacturer, temperature around the components with the same D^2PAK package operate generally in temperatures around 60 $°C$.

A single test board was tested at 60 $°C$ with a lower excitation amplitude. Although, these results cannot be considered to be reliable, due to the low amount of data and the fact that only one temperature was tested, they result in a need of reconsidering the model reliability. If data from this single test run is added to the 60 $°C$ models notable change in behavior is observed. These results affect notably

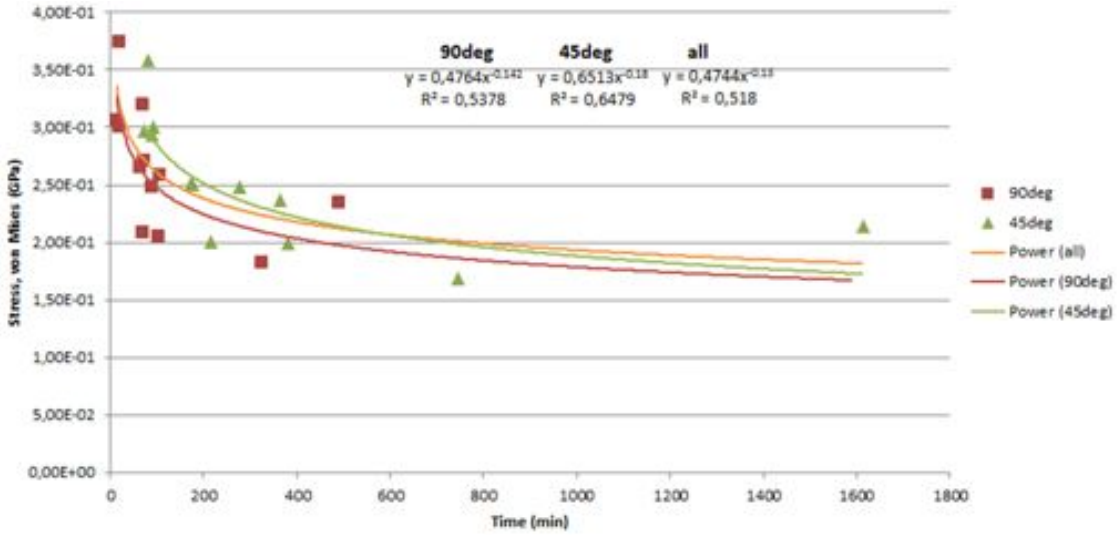

Figure 30: Power law lifetime models for both orientations and their combination.

on the lifetime prediction, with the added low amplitude data, 60 $°C$ predictions change from most pessimistic ones to nearly the most optimistic ones. As a clear conclusion we can say that all of the prediction may be tremendously too pessimistic. In addition, it seems clear that low amplitude tests are required for accurate lifetime predictions. This, however, will increase the required testing time significantly.

Extrapolation of results to far beyond the used data points, can result in erroneous predictions. This is a common problem with lifetime models. Thus it seems that several high amplitude tests combined with lower amplitude tests is the optimal approach. To reach the maximum accuracy of lifetime models, as low as possible amplitude should be used. Furthermore, it may be sufficient to test a lower amount of temperatures. This however, is probably case specific and requires some experience on the developed method. The amplitude of lower amplitude test should be decided based on available testing time and maximum amplitude present in field conditions.

Due to the discovered potential excessive pessimism of the models, in this case, using temperature independent models is recommended. Temperature independent models are expected to result in as good prediction as possible considering the available data. To increase the model accuracy and reliability several low amplitude tests are required at all temperatures.

Independent of the usage of the stress or strain as the loading condition, the amount of cycles is important. The amount of stress or strain cycles is the failing factor rather than duration under the stress or strain exposure. Thus, component reliability model should be adjusted according to the frequencies of the test and the actual usage. The frequencies can be considered before generating the component lifetime models or when product lifetime is calculated. By multiplying component lifetime with test frequency and lifetime step in seconds (in our case 60 as lifetime was measured in minutes) component lifetime in cycles can be calculated. This can be especially convenient when using temperature dependent model where test

Table 14: Power law lifetime model coefficients a and b in different models

Model	**a**	**b**
-35°C 90°	0,448	0,126
-35°C 45°	0,391	0,098
20°C 90°	0,716	0,215
20°C 45°	0,933	0,233
60°C 90°	0,485	0,172
60°C 45°	1,142	0,310
95°C 90°	0,483	0,159
95°C 45°	0,859	0,235
temp. dependent 90°	1e-06T^3−2e-04T^2 +9e-04T+0,758	3e-07T^3−4e-05T^2 +7e-04T+0,215
temp. dependent 45°	−1e-04T^2+9,7e-03T+0,835	−2e-05T^2+2,6e-03T+0,212
all combined	0,474	0,130
90° no temp.	0,476	0,142
45° no temp.	0,651	0,180
recommended	0,476 (σ,Mises >0,16 GPa) 0,651 (σ,Mises <0,16 GPa)	0,142 (σ,Mises >0,16 GPa) 0,180 (σ,Mises <0,16 GPa)

frequencies differ. Other option is to use lifetime model presented in equation 6, where x is the stress (σ) or strain (ε), f_t is the used test frequency, f_r frequency in real usage environment and t_c is time conversion coefficient i.e. to convert lifetime from minutes to hours value is 60 and to days 1440. If lifetime is measured in stress cycles $f_t = 1$ and t_c has to be calculated from seconds. In addition, if we want to consider usage time we need to have parameter α in the equation i.e. if product is under use for 12 hours per day we would use $\alpha = 0,5$

$$\eta = \frac{f_t}{f_r t_c \alpha} \left(\frac{a}{x}\right)^{\frac{1}{b}} \tag{6}$$

For example, D^{2}PAK component on an imaginary board, with operation temperature of 60 °C, is operated for 18hours per day ($\alpha = 0,75$) and faces the maximum stress of $\sigma = 0,015GPa$ at frequency $f_r = 1200Hz$. using the recommended more pessimistic temperature independent model with 45 ° orientation ($a = 0,651$ and $b = 0,18$). With these assumptions component lifetime would be around 265 years.

The generated lifetime prediction is potentially inaccurate, due to the lack of low amplitude data. Despite this, results suggest that accurate prediction can be generated with the developed method. Quality of the prediction is highly dependent on the quality of the test results, as well as the relevance of the used test amplitudes.

Product lifetime prediction

Product lifetime prediction is the final step of this method. To calculate the lifetime of the whole product lifetime models of all components should be known. However,

as the most unreliable components will dominate, good results can be achieved only by considering the most critical components. If a single component is notably more unreliable than the others, its lifetime will be close or equal to product lifetime.

Lifetime results were shown to follow the Weibull distribution. The shape of the distribution is defined by the shape parameter β. For each data point of the lifetime prediction model there is one matching lifetime and shape parameter. Several options exist for choosing the shape parameter for each prediction. In any case, using value that has the higher amount of data points is suggested as they can be assumed to be most accurate. In addition, β values from data with similar or closest stress will most likely be accurate. However, actual stresses may be significantly lower compared to in-test stresses. Most pessimistic results will be obtained by using as low β value as possible, thus using the lowest compatible value may be beneficial.

Average of all relevant data points is expected to give good estimation on overall β. An example calculation is presented using a hypothetical product with five D^2PAK components placed around the board and assuming all the other components to be significantly more reliable and thus discarded from calculation. Components are presented in table 15. For components A, B and C 45 ° temperature independent model with a β of 3,52 was chosen. For components D and E 90 ° model with a β of 2,48 was chosen. We assume that for these two components clear 90 ° strain orientation is found. Components are placed in the different regions of the board thus variation in frequencies exist. Daily operation time is assumed to be 18 hours.

Table 15: Five components on the imaginary board, their max lead stress,frequency and used chosen model

Component	**stress, σ (GPa)**	frequency (Hz)	**chosen prediction model**
A	0,015	1200	45° no temp.$\beta = 3,52$
B	0,016	1100	45° no temp.$\beta = 3,52$
C	0,016	1300	45° no temp.$\beta = 3,52$
D	0,019	1200	90° no temp.$\beta = 2,48$
E	0,026	1000	90° no temp.$\beta = 2,48$

Cumulative Weibull distribution function is given in equation 7. Where t is elapsed time, β the chosen shape parameter and η is the component lifetime calculated with equation 6. Cumulative Weibull distribution can be used to calculate the component failure distribution, which then can be used to calculate the product failure distribution and lifetime.

$$F(t;\beta;\eta) = 1 - e^{-(t/\eta)^{\beta}} \tag{7}$$

Equation 7 gives the probability of component failure $P(c)$ at a certain time t. With basic probabilistic calculations we can determine that the probability of product failure, i.e. one or more failed components, to form as $P(p) = 1 - (1 - P(c_1))(1 - P(c_2))...(1 - P(c_n))$ i.e. $1 - P(nonefailed)$. Based on this we can derive equation to calculate the failure distribution of the product. Derived equation is

presented in equation 8, which is based on equation 7 and in addition n represents each of the investigated components.

$$F(t;\beta;\eta;n) = 1 - \prod_{n=1}^{x} e^{-(t/\eta_n)^{\beta_n}} \tag{8}$$

The results of the lifetime prediction are presented in figure 31. According to prediction product lifetime would be 129 years. However, after 60 years roughly 10 % of the products have failed. If the model is expected to be accurate, the product could be expected to be very reliable. However, in the actual case other components cannot be ignored. Furthermore, other failure mechanisms would have likely failed the component by that time e.g., thermal cycles, corrosion, electrical failures or shock impacts. Moreover, during long lifetimes effect of microstructural evolution can't be neglected.

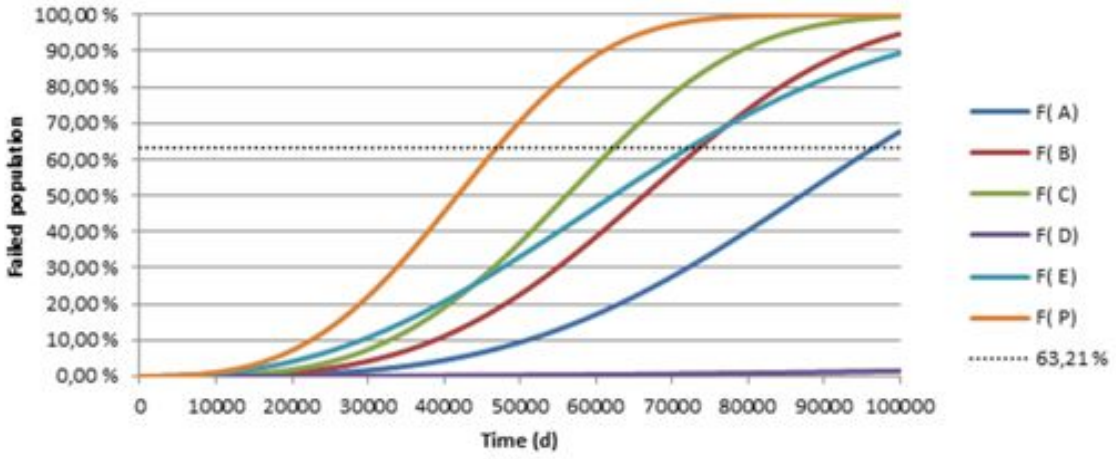

Figure 31: Product (P) and component (A - E) failure probability in respect to time (days).

For a comparison, the studied components on the real product assembly would face stresses as high as in the example with around 40 G acceleration. However, it should be noted that the result in the actual mounting system may be different. With the more probable excitation levels of 10 G and 1 G stresses would be around 0,005 GPa and 0,0005 GPa respectively. Some examples of component lifetimes using different models and stress values are presented in table 16. In the calculations same frequency with the experimental test and 100 % duty cycle are used. The results in the table show the immense variation between different models. Most important observation is the difference between 60 $°C$ 45 $°$ model and the same model with few lower amplitude data points. At highest stress the difference is five orders of magnitude i.e. from few days to few hundred years, and even more with lower strain levels. Conclusively, accuracy of the model and the accurate loading parameters are critical for good predictions.

Variation between the models is large in most of the cases. Some variation is expected due to differences between different temperatures and orientation. However,

Table 16: The comparison of component lifetimes between the different models and several magnitudes of stress.

	lifetime (a)			
Model / stress	σ =5E-2 GPa	σ =5E-3 GPa	σ =5E-4 GPa	σ =5E-5 GPa
-35$°C$ **45°**	3E+2	5E+12	8E+22	1E+33
20$°C$ **45°**	7E-2	1E+3	3E+7	5E+11
60$°C$ **45°**	6E-3	1E-1	1E+4	3E+7
60$°C$ **45° w/low**	2E+2	4E+11	1E+21	3E+30
60$°C$ **90°**	1E-1	9E+4	6E+10	4E+16
95$°C$ **45°**	5E-2	8E+2	1E+7	3E+11
45° no temp.	4E-1	1E+5	5E+10	2E+16
90° no temp.	2E+0	2E+7	2E+14	3E+21

new lower amplitude tests would be required to confirm these differences, i.e. which part of the difference is due to the temperature and orientation and which part due to the model inaccuracy caused by the insufficient data. A few test runs in each temperature with a lower amplitude should provide enough results to increase the model accuracy significantly.

As a conclusion we can say that even though it seems that predictions may not be accurate, they are usable. Results suggest that the temperature independent predictions are pessimistic. In this case, using recommended models will result in a prediction that suggest too short lifetime. If this predicted lifetime is high enough, in reality it should be even higher. For future use the increasing size of the test board component matrix is recommended. This results in a larger amount of data points per board thus reducing the amount of required test runs and increasing accuracy. In addition, at least two different test amplitudes should be used to further increase the amount of data points for lifetime prediction. With these improvements to used setup, significantly more accurate lifetime predictions can be achieved.

6.5 Failure analysis

The physical failure analysis of the boards was conducted using optical microscopy for the cross-sectional samples and SEM for the fracture surface investigation. The total of 40 cross-sectional samples and 15 fracture surface samples were fabricated. Cross-sectional samples were analyzed using a Olympus BX51M optical microscope.

Cross-section analysis

In nearly all of the cases the failure occurred due to a fracture in component's copper lead. This indicates that the test may have been over accelerated, as usually substantially weaker solder material is expected to fail. In figure 32 cross-sectional images of failed leads at different temperatures are presented. In figure 33 images with higher magnification (20X) are presented from the area where copper (Cu) lead

crack and solder crack interconnect. Failures at 20 $°C$ and 60 $°C$ are very similar. The fracture resulting in the failure has propagated through the copper lead. Two incomplete fractures were detected, based on these the copper lead fracture has initiated at the top side of the lead. Additionally, small amounts of solder cracking along the lower edge of the lead exist, partly along the interface and partly in the bulk solder.

Solder interface was investigated using EDS (energy-dispersive X-ray spectroscopy) analysis. Results show that, as expected, only Cu_6Sn_5 IMC-layer is present on the copper lead and solder interface. The thickness of the layer was around 3 μm. No visible amounts of Cu_3Sn was observed.

At -35 $°C$ copper lead fracture is slightly smoother and has propagated in lower angle compared to other cases. The amount of solder cracking seem smaller and less bifurcation compared to higher temperatures can be seen. Copper lead fracture at 95 $°C$ sample seem to be in all ways similar to 20 $°C$ and 60 $°C$ cases. However, the amount of solder cracking is significantly higher compared to all other temperatures.

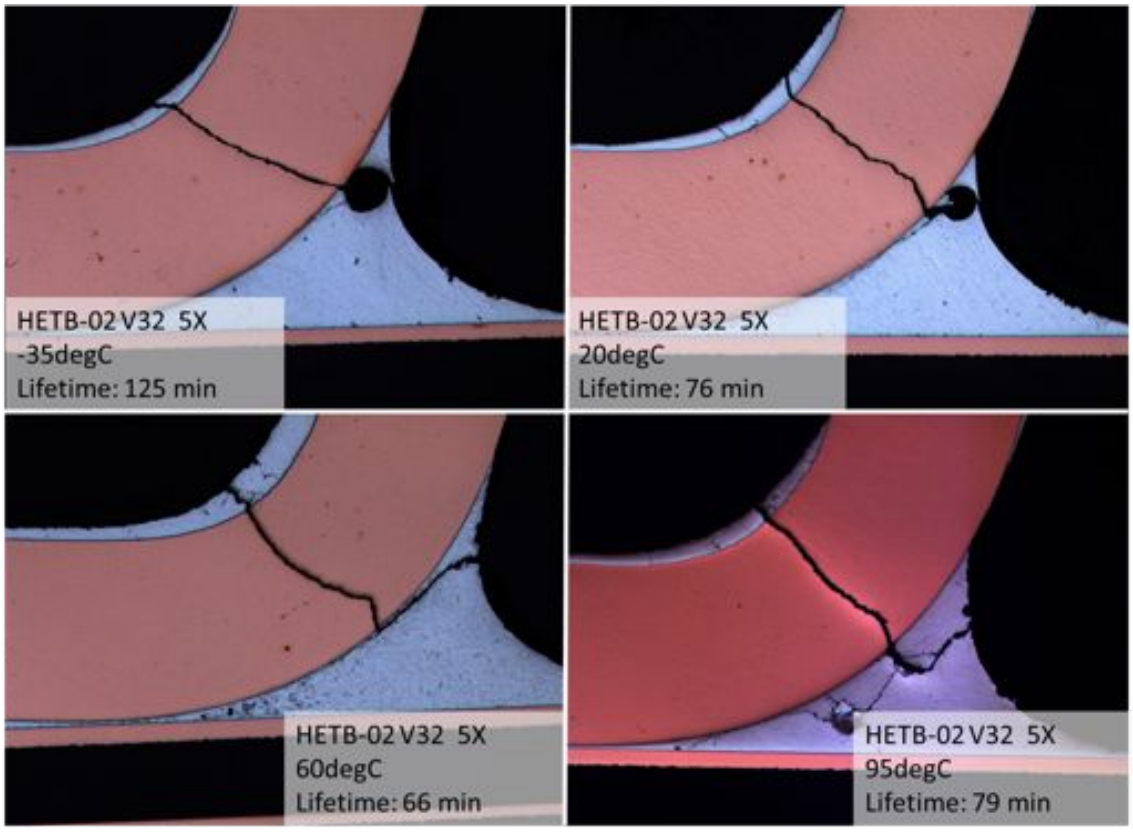

Figure 32: Cross sections from failed D^{2}PAK component leads location V32 from all temperatures and similar lifetimes, 5X magnification.

These differences would fit to the prediction made in section 6.3 where the different slopes of the Weibull curves were discussed to indicate some differences in failure modes. It is evident that some, albeit small, differences exist in the failure mechanisms. Similar observations were made also from other samples; although,

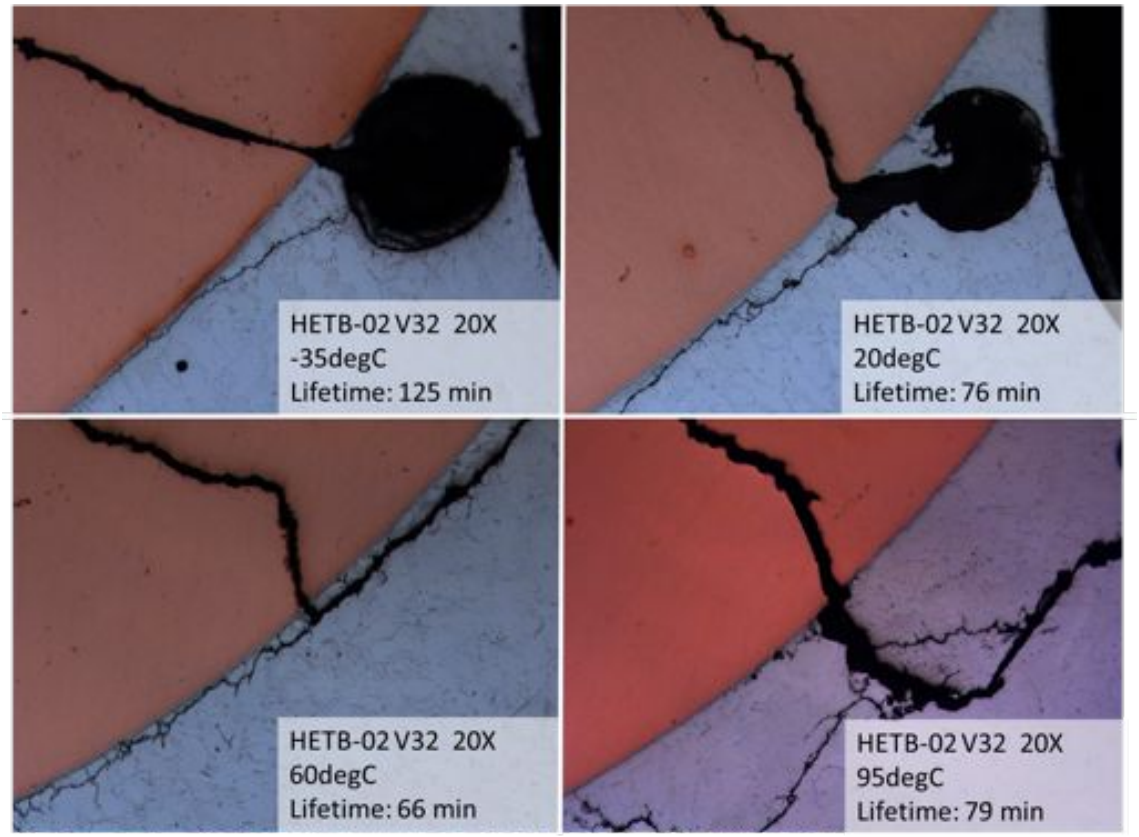

Figure 33: Cross sections from failed D^{2}PAK component leads location V32 from all temperatures and similar lifetimes, 20X magnification.

some variation existed. It is conclusive that the amount of solder cracking increases with increased temperature. However, the lower angle of the lead fracture seem more controversial. Lower crack angle was observed in several cases at -35 $°C$ but also in couple cases at 20 $°C$. In all other samples crack angle was higher. Even higher crack angles were observed, mainly in 95 $°C$. Variation is large but there seems to be pattern in crack angle increasing with the temperature.

The reason for the increasing amount of solder cracking lies in the change of material properties due to temperature change, as discussed in section 2.4. This results in a case, where crack propagation in solder is faster in higher temperatures and thus the amount of it will increase with temperature. The stress in the copper lead will remain the same or nearly the same and similar fracture will form independent of test temperature, provided that solder will remain strong enough not to fail before the lead.

Even if the crack angle is at least partly dependent on the temperature, as it seems, it cannot be explained by change in material properties, as according to simulations, stress and strain distributions are independent of the temperature. However, as the effects of thermal expansion were not considered in the model, they may offer an explanation for the change in crack angle. Thermal expansion can result in significant deformation. In this case, the system between the component package,

lead, solder and PWB is considered. Temperature changes will induce stresses and deformation on the system. As the local system is deformed and/or pre-stressed, the strain and stress distribution due to the vibration loading may change. Even small changes may result in the variations of crack nucleation location and propagation path.

Compared to location V32, in location V31 we can see a higher amount of solder fracturing. Location V31 is on the same line as V32, but due to orientation difference, the stress and strain in the lead are higher even when the board strain value is nearly the same. The lifetime in this location is much shorter compared to V32. Cross-section micrographs from location V31 are presented in figure 34. In this case, -35 $°C$ fracture has similar angle as in two medium temperatures, in the highest temperature (95 $°C$) crack angle is slightly higher compared to other samples.

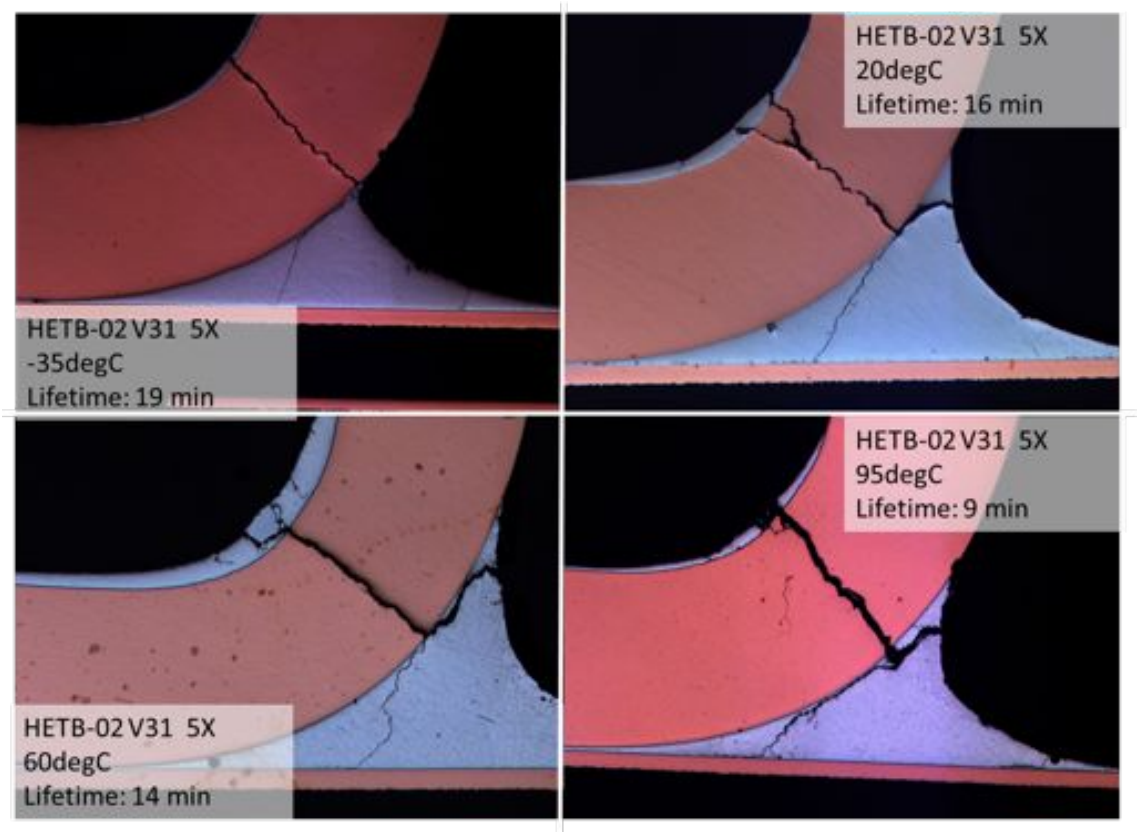

Figure 34: Cross sections from failed D^{2}PAK component leads location V31 from all temperatures and similar lifetimes, 5X magnification.

At -35 $°C$ solder fracture has propagated to PWB copper pad, as has also happened with all other samples. At 20 $°C$ voiding along the the PWB pad and solder interface can be seen, although, poorly visible in the presented microsections. At 60 $°C$ already small cracking can be observed along the interface, whereas at 95 $°C$ fracture is larger.

Large amount of fracturing was detected under the lead tip in a single sample

from location V31 at 95 $°C$. Micrographs from the cracking below lead tip are presented in figure 35. The crack has propagated to around the halfway point of the solder interconnection. As the crack has also propagated from the other side as was discussed above, only under a quarter of the interconnection is still intact. Notable amount of vertical bifurcations can be seen between the two fracture paths. The formation of these possibly happens either during or after the crack formation. If they occur after the both cracks have formed, it is possible that the part of the solder is partly separated from the bulk and is allowed to vibrate freely between the two fracture surfaces. In this case, the continuous impacts or increased strain due to freer movement would shatter the solder creating the bifurcations. Other possible explanation is that while the second fracture propagates it occasionally connects to the other fracture, but still continuing on it's horizontal path. However, it is not clear whether the fracturing below lead tip has happened before or after the actual failure.

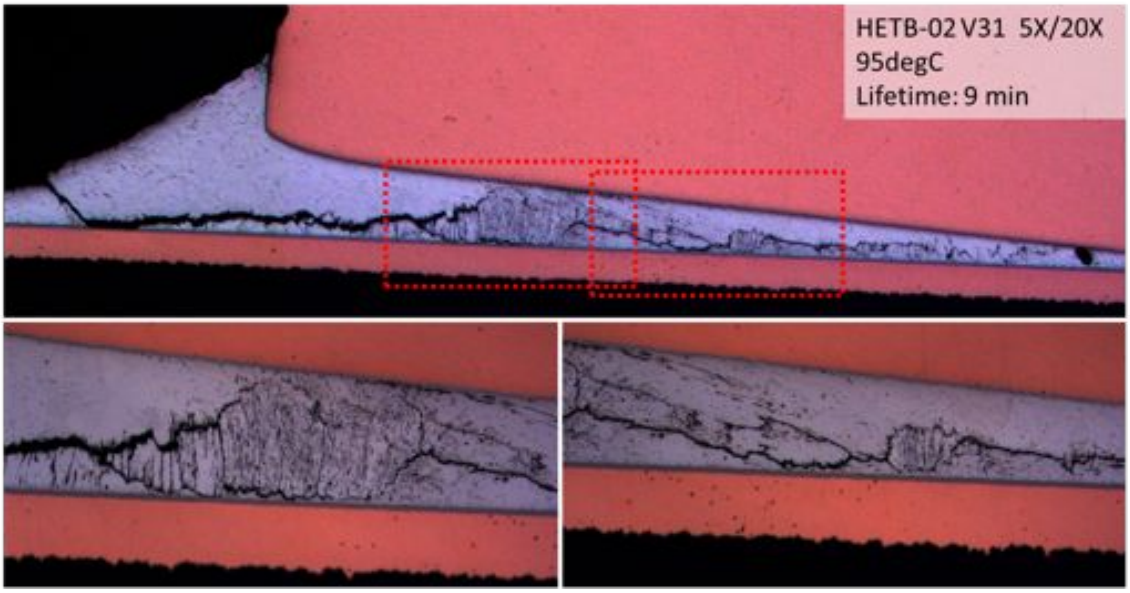

Figure 35: A large amount of solder cracking below lead tip in location V31 at 95$°C$, 5X magnification, close ups with 20X magnification.

In most of the samples some solder cracking around the lead tip was detected. However, the extent of that was minimal compared to one shown in figure 35, usually a small crack from solder surface had propagated through solder down to the PWB pad. The small crack usually resembles the beginning of the crack in figure 35; i.e., the 45 ° part. In several cases cracks had propagated along the interface of solder and PWB pad but rarely beyond the actual tip of the lead.

From all cross-sectional samples, two solder failures were detected. These both had happened at 95 $°C$ with long lifetimes and in a low stress locations. One in location V22 with a lifetime of 3021 minutes and the other one in location V52 with a lifetime of 833 minutes. Latter is presented in figure 36. We can see that fracture has mostly propagated along the interfacial region. The fracture has propagated

from both directions simultaneously: along the solder and PWB pad interface from the tip side and along the lead and solder interface from the component side. The two fracture paths have propagated passing each other horizontally and eventually connected vertically near the tip of the lead. This supports the assumption that the larger stresses occur on the component side of the interconnection.

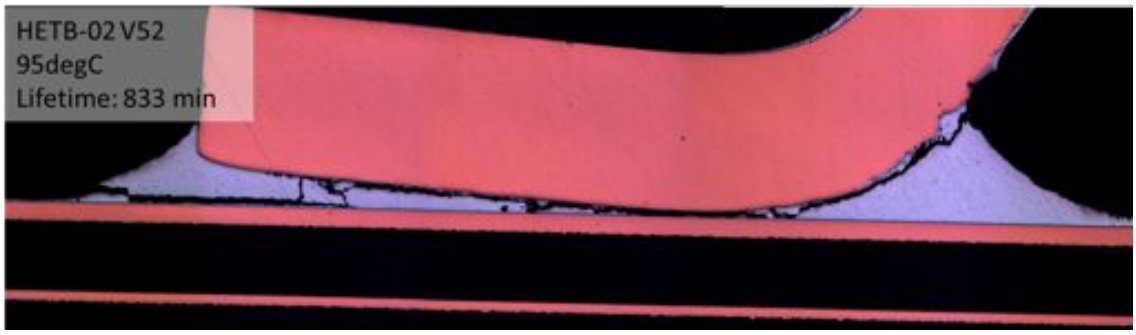

Figure 36: Solder failure location V52 at 95 $°C$, 5X magnification.

Detected solder failures support the assumption that the test has been over accelerated. With lower stress and strain magnitudes it is possible that the solder failure might be the dominating failure mode, at least under some conditions, such as elevated temperature with low vibration excitation level. To further investigate this, lower amplitude test was conducted at 60 $°C$ using an excitation amplitude of 2,2 V. With the used test amplitude solder strains were around 70 % of the 3 V amplitude test strains. 60 $°C$ was used due to being the most relevant in respect to the real application.

In the lower amplitude test, lead failure still remains dominant, with similar characteristics to higher amplitude tests; e.g., leads with several day lifetimes appeared similar to leads with lifetimes of under an hour. In addition, a single solder failure was detected. Lifetimes were notably longer, as expected. During the 20 day test only 11 confirmed failures were detected, whereas in the higher amplitude tests generally around 18 components failed in under two days. Depending on the location, lifetimes in the lower amplitude test ranged from threefold to hundredfold, compared to main test amplitude. One of the components that had not failed was prepared as cross-section and only small noncritical fractures could be seen. Conclusively, to confirm the possibility of solder failure being the dominant failure mode, even lower amplitude testing would be required.

The large component body pad results in a very rigid connection as in only one sample severe fractures were detected. In other cases only minor fractures were found on the edges of the solder formation. Figure 37 presents micrographs below component body pad in location V31 at 95 $°C$. The fractures have propagated from the both ends of the pad covering roughly a half of the whole interconnection. On the back side (right) of the component fracture has propagated mostly along the large amount of voids but also past the void formations in bulk solder. On the lead side (left) fracture has propagated partly in the bulk solder near the the interfacial region and partly along the interface. Vertical bifurcations are visible

along the crack. Compared to the bifurcations seen in the lead interconnection of the same component (fig. 35) their nature seems different. Here bifurcations are clear and wide with notable distance between them, whereas below lead tip bifurcations are narrower and very densely located. In this case the bifurcations aren't between two fracture paths, but are separate bifurcations from the main crack with similar orientation and length to each other. Possible factors affecting on bifurcation formation are voids, grain boundaries, and IMCs. Similar bifurcations have been reported in [71]; however, no explanation for these was presented.

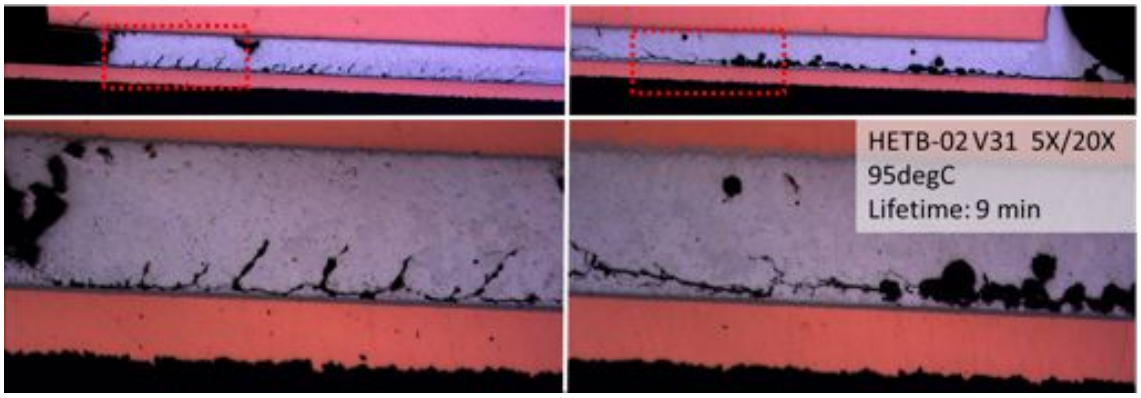

Figure 37: Solder cracking below large component body pad in location V31 at 95 $^{\circ}C$, 5X magnification, close-ups with 20X magnification.

Fracture surface analysis

As a part of the failure analysis also a total of 15 fracture surfaces were analyzed. The fracture surfaces were analyzed using a JEOL JSM-6330F SEM. The schematic illustration of the fracture surface is shown in figure 40

SEM micrographs from the location V32 with similar lifetimes are presented in figure 38. On the left side of the micrograph a clear line can be seen, indicated with dashed arrow in $20^{\circ}C$ micrograph (similar also with other micrographs). On the right side of the line is the actual copper lead and on the left side is the solder area. Depending on the shape of the fracture in the solder, the area may be smaller, larger or in different angle compared to the copper fracture surface.

From the samples shown in figure 38 no clear fracture initiation location could be seen. Only at $20^{\circ}C$ beach formations are present. Beach formations are usually considered to indicate the initiation point of the fatigue fracture and to happen during the first stage of fatigue fracture. Formations can be seen near the right edge, slightly under the halfway point of the lead cross-section. According to the modeling results the most probable fracture initiation location would be the outermost corner of the lead. In these micrographs that location is the lower right corner of the lead.

It is expected that fracture propagation will start slower and continue to second phase. In the second phase propagation is faster as the overall strength has lowered and the amount of plastic deformation increases. Ultimately, the cyclic stress will exceed the fracture strength leading to overstress failure.

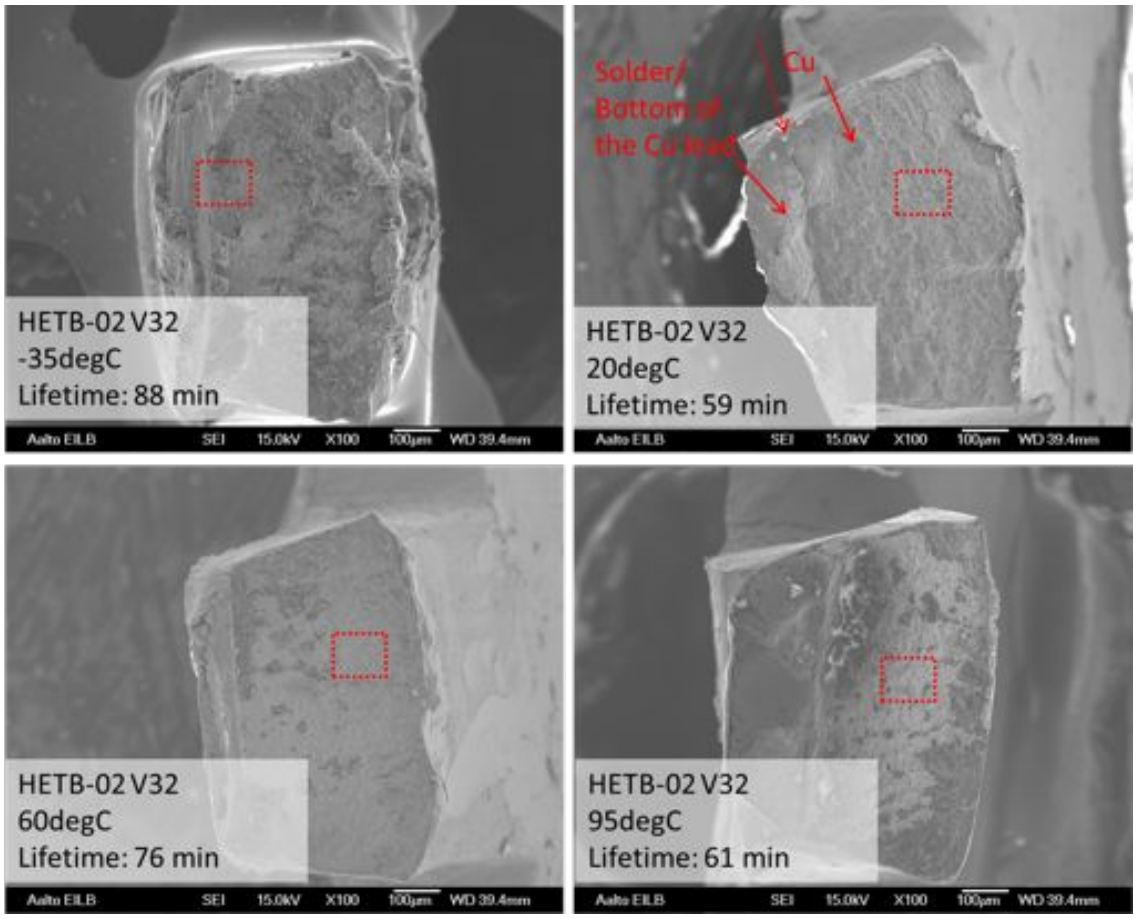

Figure 38: Fracture surfaces form location V32 at different temperatures with similar lifetimes, 100x magnification. Higher magnifications from marked areas are presented in figure 39.

Between different micrographs, differences in color cannot be compared by color as there may be differences in the SEM parameters. However, inside one micrograph different colorations most likely indicate some differences in surface roughness. In all samples we can see some color differences in lower right corner and/or left upper corner. At -35 $°C$ and 95 $°C$ here is very clear difference in lower right corner and at 60 $°C$in the upper left corner. In addition, there are many small local sites where these differences exist.

It seems that some differences in the fracture surfaces exist in the right side of the lead (in figure 38). For example, in 95 $°C$, there is a clear color difference on the right side of the lead. Additionally, in 60 $°C$ case there seems to be some differences in surface formation, not so much in color.

Micrographs with 1000x magnification are presented in figure 39. In these micrographs the most dominant fracture surface types are investigated. Based on appearance and lifetime, main failure mode is fatigue induced transgranular cracking [72]. It should be noted that the left side of the -35 $°C$ is solder fracture, but the right side represents the copper fracture surface well. All of the micrographs show

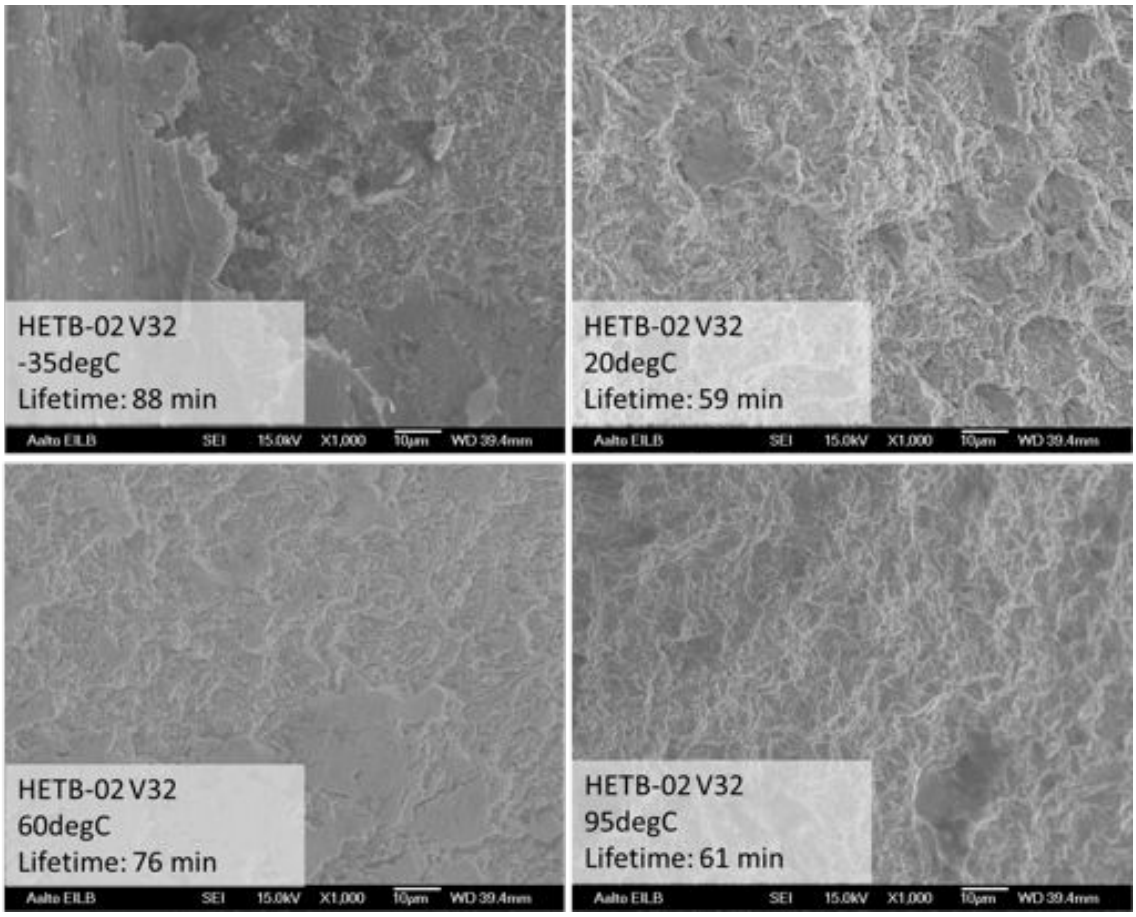

Figure 39: Fracture surfaces form location V32 at different temperatures with similar lifetimes, 1000x magnification.

similar characteristics: Very uneven surface with a high amount of small ridges. At 60 $°C$ there seems to be a large amount of smoother surfaces, which may indicate local intergranular cracking, whereas dominant mode seems to be transgranular cracking. Clear differences in surface roughness between different temperatures can be distinguished. However, clear trend can not be established.

As stated earlier, no clear pattern can be established between different temperatures. Fracture surfaces from components with lower stress values and longer lifetime share the same characteristics. However, in many cases they seemed smoother. Variation in smoothness was large between samples even in similar conditions. The smoothness indicates slower crack propagation.

Failure modes

A schematic representation of the component cross-section is presented in figure 40. As discussed, main failure mode is component lead fracture in the second bend, this is marked with red. Main failure mode was determined to be caused by transgranular copper lead fatigue fracture due to cyclic loading. Strain-rate in this test was approximately 0,1/s. No clear signs of ductile or brittle fractures due to overstress

were observed. Additionally, also solder damage was observed. Pink color is indicating the second failure mode, solder failure below component lead tip. Green lines are representing non failing, rare but critical large fractures, which would likely soon result in failure. Last group is common but noncritical small fractures visible in most of the samples. All fracture types/locations were not necessarily detected in all of the samples.

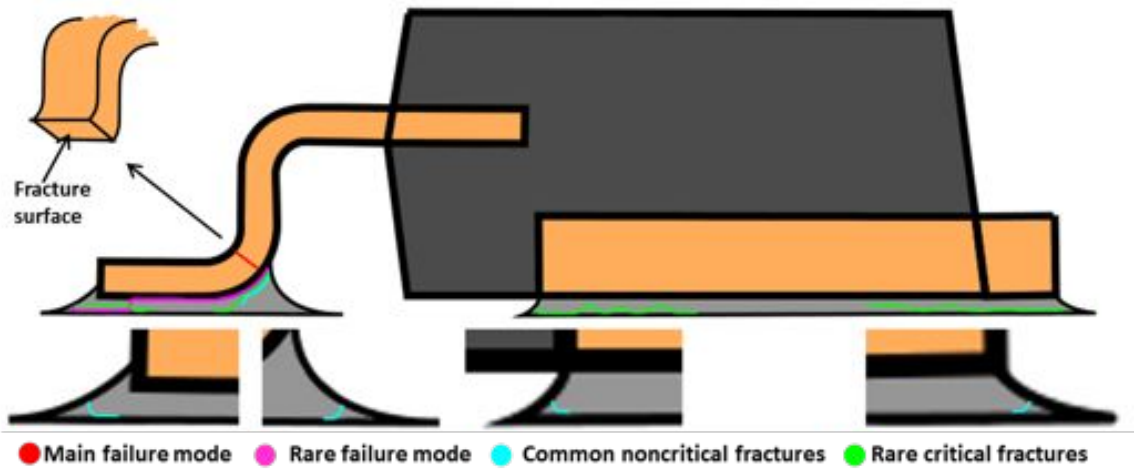

Figure 40: Schematic illustration of D^2PAK component's cross-section with detected failure modes and fractures.

Small solder fractures and larger fractures in beginning are due to solder fatigue. In larger solder fractures also ductile fracture behaviour was observed. The cracks have propagated along the IMC and bulk solder interface, as well as in the IMC layer. IMC layer cracking is commonly related to high strain rates, commonly above 1/s [5]. It is possible that after some solder fatigue and ductile cracking locally strains may increase substantially and result in brittle IMC cracking.

It seems that at high temperatures, under low amplitude vibration, solder fractures may become more common. However, with lower amplitude at 60 $°C$ copper lead failure still remained dominant, and no notable change in the amount of solder damage was observed. In this 20 day test only one solder failure was observed. Thus it seems that the copper lead failures will be the dominant failure mode in most cases as components that survived showed no significant amount of solder cracking or copper lead cracking.

Relevance of the dominant failure mode is questionable. In literature no discussion on copper lead fatigue with D^2PAK components could be found, suggesting that this failure mode may not be relevant in real applications. With TSOP package under similar lifetimes solder fatigue has been shown to be main failure mode [57]. With QFP package both, solder and lead fatigue has been observed [57]. Both packages have similar joint geometry as D^2PAK.

7 Future work

Method used in this thesis was based on vibration excitation at different temperatures. A more comprehensive test plan was designed to further develop the test method, improve the reliability of the studied commercial product and to create tools and guidelines to be used with other products. This test plan is designed to last up to one year.

These tests will be conducted using the HETB-03 test board. This board is similar to HETB-02 board but is designed for large BGA component. The used component is Amkor A-CABGA256-1.0-17, a 256 I/O BGA dummy component with a daisy chain network. FPGA component in same package can be found from the studied commercial board and is considered to be the one of the most critical components. Designed test board and component is presented in figure 41

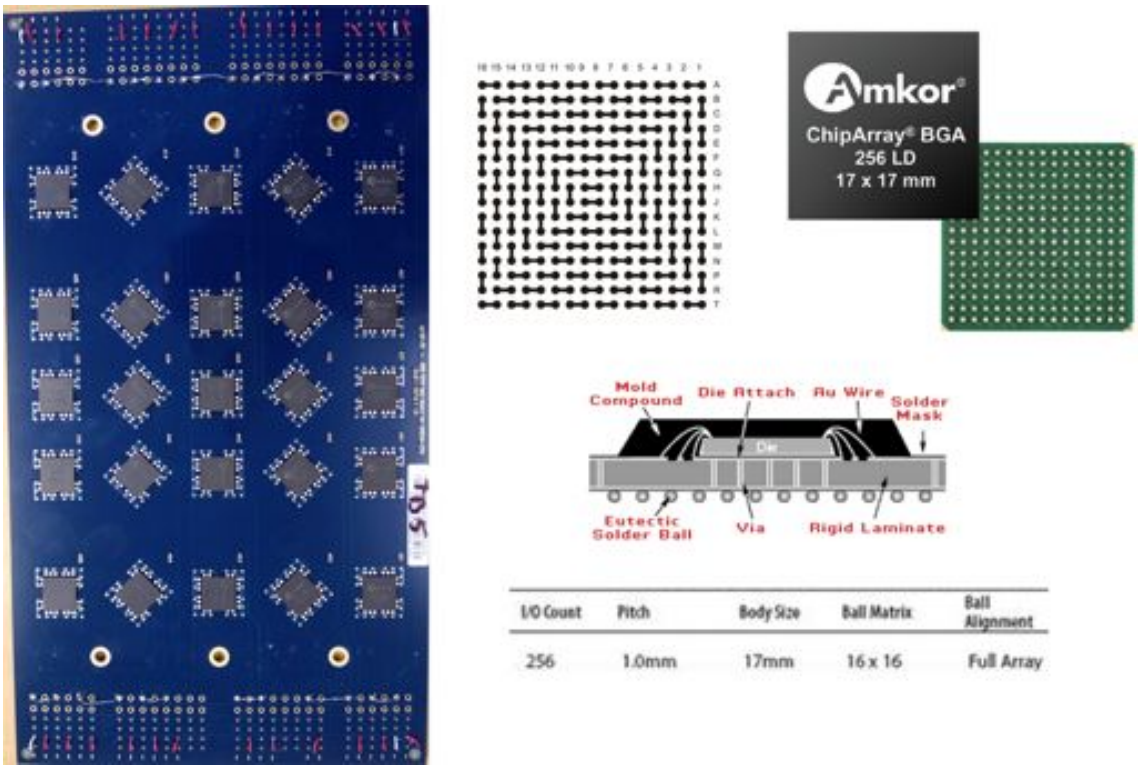

Figure 41: HETB-03 test board and used Amkor CABGA256 component.

Test will be started using similar workflow as described in this thesis. First, two test boards will be tested in each of the four test temperatures using a point frequency excitation. Results will be then analyzed using the same methods as in this thesis. Due to the increased amount of testing time, lower test amplitude is used to prevent the usage of too high acceleration factor.

The goal is to combine vibration loading with thermal cycling. Due to the fact that generally thermal cycling tests may last months and vibration test only a significantly shorter period of time, careful adjustment of stresses has to be conducted. Too high or low vibration amplitude will result in an unbalanced test, where one

stress will dominate the results. Two tests will be conducted as a preliminary study: thermal cycling and vibration sweep lifetime test. Thermal cycling test will be conducted in similar conditions as the final testing i.e. the temperature profile will be the same and the test board is connected to the baseplate assembly. Due to the resonant frequency's dependence on the temperature, vibration sweep will be used. Sweep will be adjusted so that at all temperatures resonant frequency will be excited. Using frequency sweep will also reduce the vibration stress during the test, as the stresses will be at the maximum level only for a part of the sweep.

After the stress parameters have been established for the combined loading test i.e. lifetimes in separate tests are on the same level, combined thermal cycling and vibration sweep tests will be conducted for several test boards. Lifetime is expected to be notably shorter compared to the individual tests.

Moreover, the effect of microstructural evolution, due to isothermal annealing, will be investigated. SAC solder microstructural evolution activation energy is assumed to be 0,715 ± 0,052 eV [73]. Test boards will be annealed in 130°C for 1000h and 2500h, which according to equation 9 will be equivalent to 8,5 ± 3 years and 21,5 ± 8 years in 60°C respectively. Arrhenius equation presented as equation 9 is used to model temperature's influence on the speed of chemical reactions. Annealed boards will be subjected to testing, one to vibration alone and several to combined thermal cycling and vibration.

$$k = Ae^{-E_a/k_bT} \tag{9}$$

With the presented test plan comprehensive understanding of the component reliability under combined vibration and temperature loading is achieved. These results can be used to study the mechanisms in combined loading testing and validate the dynamic temperature and vibration test. In addition, results will be used to improve the reliability of commercial inverter board and act as an aid in tool and design guideline development.

8 Conclusions

This thesis developed a novel approach for rapid reliability assessment of power electronics under concurrent vibration and thermal loading. With the model, comprehensive lifetime prediction under complex conditions can be generated in a relatively short time. Study addresses the effect of temperature on vibration lifetime, which is usually out of the focus of traditional single parameter tests.

In many standardized vibration tests (e.g., JEDEC) only a single component per test board is monitored. In the developed method, the amount of measurement data is maximized by using a specific test board design, where numerous components can be monitored during a single test run. The approach used in the developed method allows notably more efficient testing, as several stress magnitudes and numerous components can be simultaneously tested on a single board. Stress and strain in each component location or symmetry group can be accurately modeled using FEA.

The developed lifetime prediction is based on the Weibull equation and a simple power law equation, similar to the Coffin-Manson equation. Experimental lifetime data results are obtained under combined vibration excitation and thermal loading conditions. Test boards are vibrated at several constant temperatures. This allows the generation of temperature dependent vibration lifetime model.

The study consisted of the theory part, presentation of the developed method and experimental analysis, which applies and validates the method. The thesis offers the following main contribution:

- An approach was developed that can be effectively used for comprehensive reliability assessment for power electronics under concurrent vibration and thermal loading conditions in a short time.

Other significant findings:

- The temperature has a marked effect on vibration lifetime.
- The vulnerability of solder increases with temperature.
- The effect of mounting should not be ignored when designing a product.

Based on this study and on the literature review, temperature can have a tremendous effect on the vibration lifetime. The results indicate that it is clearly insufficient to conduct vibration tests only under room temperature, especially for harsh environment applications. Currently no standardized test methods exist (except HALT) that incorporate the effect of temperature on vibration loading. However, HALT should only be used as design aid not for lifetime assessment. New comprehensive testing methods and standards are required in order to effectively improve the reliability under harsh environments.

The developed method was validated using a D^2PAK power electronics component. The validation results show that the model works as expected and can be used to create a comprehensive lifetime prediction model. Furthermore, the experimental testing was used to develop the method and to map out possible pitfalls during test

execution and product design. However, further development of the method is still beneficial.

In the experimental test, the main failure mode of the D^2PAK component was found to be copper lead fatigue. Additionally, varying amounts of solder damage was observed in most of the samples. The amount of solder damage increased with temperature. Albeit only few solder failures were detected, it is clear that their occurrence increases in higher temperatures and lower vibration excitation levels. Under low amplitude vibration excitation and high temperature, it is possible that they can be the dominant failure mode. Evidently, the change of temperature can significantly affect solder alloy's behavior. Moreover, the long term effects; e.g., microstructural evolution, may substantially weaken the reliability of interconnection.

The designed approach was used to establish a lifetime prediction for the D2PAK component. Despite the possibility of temperature dependent model, temperature independent model was recommended. Based on a single low amplitude test, the models were found to be pessimistic. This presumably occurs due to a too high test acceleration factor and insufficient data on the lower amplitudes. Despite the pessimism, results suggest that tested component is very reliable: the lifetime of over 100 years was predicted under very harsh field conditions.

In this thesis also the importance of the mounting was demonstrated. Notably higher component board strain levels were measured at the baseplate natural frequencies, compared to the component board natural frequencies. The baseplate resonant modes increased the component board acceleration input by an order of magnitude. Conclusively, if the baseplate's behavior is not considered in the design, the consequences can be catastrophic to the reliability.

Based on the findings, this study designed a new test program. In the upcoming study, a BGA component will be used for more comprehensive study of solder failures. In addition, the upcoming study will investigate the effect of microstructural evolution due to thermal cycling and isothermal annealing. Furthermore, it will compare thermal cycling and constant temperature loading combined with vibration excitation.

By following the presented guidelines, accurate and reliable lifetime prediction can be created for power electronics. Nonetheless, the accuracy of the model is heavily dependent on the quality of the experimental testing and the relevance between used test loading and the field conditions. Furthermore, utilizing the conclusions of this thesis during product design can be highly beneficial when designing products for harsh environments.

References

[1] D. W. Hart, *Power Electronics*. McGraw-Hill, 2011.

[2] R. W. Johnson, J. L. Evans, P. Jacobsen, J. R. Thompson, and M. Cristopher, "The Changing Automotive Environment: High-Temperature Electronics," *IEEE Transaction on Electronic Packaging Manufacturin*, vol. 27, pp. 164–176, 2004.

[3] H. A. Chan and P. J. Englert, *Accelerated Stress Testing Handbook - Guide for achieving quality products*. IEEE Press, New York, 2001.

[4] T. Laurila, V. Vuorinen, T. T. Mattila, M. Turunen, M. Paulasto-Kröckel, and J. K. Kivilahti, *Interfacial Compatibility in Microelectronics Moving Away from the Trial and Error Approach*. Springer-Verlag London, 2012.

[5] T. T. Mattila and M. Paulasto-Kröckel, "Toward Comprehensive Reliability Assesment of Electronics by a Combined Loading Approach," *Microelectronics Reliability*, vol. 51, pp. 1077–1091, 2011.

[6] J. Karppinen, *Reliability Assesment of Electronic Assemblies under Multiple Interacting Loading Conditions*. PhD thesis, Aalto University, 2013.

[7] J. Karppinen, J. Li, and M. Paulasto-Kröckel, "The Effects of Concurrent Power and Vibration Loads on the Reliability of Board-level Interconnection in Power Electronic Assemblies," *IEEE Transactions on Device and Materials Reliability*, vol. 13 (1), pp. 167–176, 2013.

[8] F. Jensen, *Electronic Component Reliability*. John Wiley & Sons, 1995.

[9] Trafi, "Ajoneuvojen takasinkutsukampanjat 2003-2010." Retrieved 20.11.2013, Url: http://www.trafi.fi/filebank/a/1317714212/838e3d4566f2d89f55f378721cd290e8/194-Takaisinkutsut20032010.pdf.

[10] Trafi, "Takaisinkutsukampajat." Retrieved 20.11.2013, Url: http://www.trafi.fi/tieliikenne/luvat_ja_hyvaksynnat/takaisinkutsut.

[11] C. Bunis, D. Crowe, P. Ersland, and A. Feinberg, *Design For Reliability*. CRC Press, 2000.

[12] W. D. Brown, *Advanced Electronic Packaging: With Emphasis on Multichip Modules*. IEEE Press, New York, 1999.

[13] M. T. Thompson, "Introduction To Power Electronics," 2005-2007. Retrieved. 15.12.2013, Url: http://www.thompsonrd.com/NOTES%2001%20INTRODUCTION%20TO%20POWER%20ELECTRONICS.pdf.

[14] C. C. Chan, "The State of the Art of Electric, Hybrid, and Fuel Cell Vehicles," *Proceedings of IEEE*, vol. 95, Issue 4, pp. 746–765, 2007.

[15] Z. Q. Zhu and D. Howe, "Electrical Machines and Drives for Electric, Hybrid, and Fuel Cell Vehicles," *Proceedings of IEEE*, vol. 95, Issue 4, pp. 746–765, 2007.

[16] Infineon, "IGBT Modules: Discover the range - Infineon Technologies," 2014. Retrieved: 28.1.2014, Url: http://www.infineon.com/cms/en/product/igbts/igbt-modules/channel.html?channel=db3a30433afc7e3e013b22a5aeae5917.

[17] "MIL-HDBK-217F, Military handbook - Reliability Prediction of Electronic Equipment."

[18] S. S. Manson, "Behavior of Materials Under Conditions of Thermal Stress," *National Advisory Committee for Aeronautics*, vol. Report 1170, pp. 317–350, 1953.

[19] L. F. Coffin, "A Study of the Effects of Cyclic Thermal Stresses on a Ductile Metal," *Transaction of ASME*, vol. 76, pp. 931–950, 1954.

[20] O. Basquin, "The Exponential Law of Endurance Test," *Proceedings of american Society of Testing and Maaerials*, vol. 10, pp. 625–630, 1910.

[21] T. Kilinski, J.R.Lesniak, and B. Sandor, *Modern Approaches to Fatigue Life Prediction of SMT Sodler Joints in Solder Joint Reliability Therory and Application.* Van Nostrand Reinhold, 1991.

[22] W. Engelmaier, "Effects of Power Cycling on Leadless Chip Carrier Mounting Reliability and Technology," in *Proceedings of International Electronics Packaging Conference*, 1982.

[23] P. Chauhan, M. Osterman, W. S. R. Lee, and M. Pecht, "Critical Review of the Engelmaier Model for Solder Joint Creep Fatigue," *IEEE Transactions on Components and Packaging Technologies*, vol. 32, pp. 693–700, 2009.

[24] R. Darveaux, "Effect of Simulation Methodology on Solder Joint Crack Growth Correlation," in *Proceedings of 50th Electronics Components And Technology Conference*, 2000.

[25] J. Liang, N. Gollhardt, P. S. Lee, S. Heinrich, and S. Schroder, "An Integrated Fatigue Life Prediction Methodology for Optimum Design and Reliability Assesment of Solder Interconnections," in *Advances in Electronic Packaging, Proceeding of the Pacific Rim/ASME International Intersociety Electronic and Photonic Packaging Conference*, 1997.

[26] A. Syed, "Predicting Solder Joint Reliability for Thermal, Power, & Bend Cycle within 25% Accuracy," in *Proceedings of the 51st Electronic Components ans TEchnology Conference*, 2001.

[27] A. Palmgren, "Die Lebensdauer von Kugellagern (The Service Life of Ball Bearings)," *Zeitschrift des Vereins Deutscher Ingenieure*, vol. 68, pp. 339–341, 1924.

[28] M. A. Miner, "Cumulative Damage in Fatigue," *Journal of Applied Mechanics*, vol. 12, pp. 159–164, 1945.

[29] B. S. Shelton, M. K. Pabisz, T. G. Zhu, L. Liu, and B. Peres, "Package for Semiconductor Devices," U.S. Patent US20100140627 A1, Oct, 8, 2009.

[30] T. Laurila, V. Vuorinen, and J. Kivilahti, "Interfacial Reactions between Lead-free Solders and Common Base Materials," *Materials Science and Engineering Reports*, vol. 49, pp. 1–60, 2005.

[31] J. Li, *Numerical Simulations for Reliability Assesment of Lead-Free Solder interconnections in BGA Packages*. PhD thesis, Aalto University, 2011.

[32] A. Schubert, H. Walter, R. Dudek, B. Michel, G. Lefranc, J. Otto, and G. Mitic, "Thermo-Mechanical Properties and Creep Deformation of Lead-Containing and Lead-Free Solders," in *2001 International Symposium on Advanced Packaging Materials*, 2001.

[33] "ASME B31.1-1995 Edition (Power Piping ASME Code for Pressure Piping, B31 AN american national standard)."

[34] J. Cadek, *Creep in Metallic Materials*. Elsevier, Amsterdam, 1988.

[35] J. H. Lau and Y. H. Pao, *Solder joints reliability of BGA, CSP, Flip-chip, and Fine Pitch SMT assemblies*. McGraw-Hill, New York, 1997.

[36] M. Mustafa, Z. Cai, J. C. Roberts, J. C. Suhling, and P. Lall, "Evolution of The Tension/Compression And Shear Cyclic Stress-Strain Behaviour of Lead-Free Solder Subjected to Isothermal Aging," in *13th IEEE ITHERM Conference*, 2012.

[37] J. Glazer, "Metallurgy of Low Temprerature Pb-free Solders for Electronic Assembly," *International Materials reviews*, vol. 40, pp. 65 – 93, 1995.

[38] C. Z. Wang, Z. N. Cheng, K. Becker, and J. Wilde, "Applying Anand Model to Represent the Viscoplastic Deformation Behaviour of Solder Alloys," *Journal of Electronic Packaging*, vol. 123, pp. 247 – 253, 2001.

[39] H. Qi, "Effects of Printed Circuit Board Materials on Lead-free Interconnect Durability," in *Polymers and Adhesives in Microelectronics and Photonics, Polytronic, 2005. Polytronic 2005. 5th International Conference on*, 2005.

[40] Y.-L. Lee, J. Pan, R. B. Hathaway, and M. E. Barkey, *Fatigue Testing and Analysis*. Elsevier, 2005.

[41] P. D. T. O'Connor, D. Newton, and R. Bromley, *Practical Relibility Engineering*. John Wiley & Sons, 1991.

[42] G. Totten, "Fatiqu Crack Propagation," *ASM International - Advanced Materials & Processes*, vol. May, pp. 39–41, 2008.

[43] T. O. Reinikainen, P. Marjamäki, and J. K. Kivilahti, "Deformation Characteristics and Microstructural Evolution of SnAgCu Solder Joints," in *Proceedings of the 6th International Conference on Thermal, Mechanical and Multi-Physics Simulation and Experiments in Micro-Electronics and Micro-Systems - EuroSimE 2005*, 2005.

[44] "JEDEC Standard - Temperature Cycling JESD22-A104C."

[45] "JEDEC Standard - Temperature Shock JESD22-A106B."

[46] "JEDEC Standard - High Temperature Storage Life JESD22-A103D."

[47] "JEDEC Standard - Low Temperature Storage Life JESD22-A119."

[48] "JEDEC Standard - Board Level Drop Test Method of Components for Handheld Electronic Products JESD22-B111."

[49] "JEDEC Standard - Mechanical shock JESD22-B104C."

[50] T. T. Mattila, L. Suotula, and J. K. Kivilahti, "Replacement of the Drop Test with the Vibration Test - The Effect of Test Temperature on Reliability," in *2008 Electronic Components and Technology Conference*, 2008.

[51] "JEDEC Standard - Vibration, Variable Frequency JESD22-B103B."

[52] T. Laurila, J. Karppinen, V. Vuorinen, J.Li, A.Paul, and M. Paulasto-Kröckel, "Effect of Isothermal Aging and Electromigration on the Microstructural Evolution of Solder Interconnection During Thermomechanical Loading," *Journal of Electronic Materials*, vol. 41(11), pp. 3179–3195, 2012.

[53] T. Laurila, J. Karppinen, J. Li, V. Vuorinen, and M. Paulasto-Kröckel, "Effect of Isothermal Annealing and Electromigration Pre-treatments on the Reliability of Solder Interconnections under Vibration Loading," *Journal of Materials Science: Materials in Electronics*, vol. 24(2), pp. 644–653, 2013.

[54] J. Karppinen, T. Laurila, T. T. Mattila, and M. Paulasto-Kröckel, "The Combined Effect of Shock Impacts and Operational Power Cycles on the Reliability of Handheld Device Component Board Interconnections," *Journal of Electronic Materials*, vol. 41(11), pp. 3232–3246, 2012.

[55] T. T. Mattila and J. K. Kivilahti, "Reliability of Lead-free Interconnections under Consecutive Thermal and Mechanical Loadings," *Journal of Electronic Materials*, vol. 35(2), pp. 250–256, 2006.

[56] C. Choi and A. Dasgupta, "Effect of Temperature on Vibration Durability of SAC305 Printed Wiring Assemblies," in *13th IEEE ITHERM conference*, 2012.

[57] P. Lall, G. Limaye, J. Suhling, M. Murtuza, P. Palmer, and W. Cooper, "Reliability of lead-free SAC electronics under simultaneous exposure to high temperature and vibration," in *InterSociety Conference on Thermal and Thermomechanical Phenomena in Electronic Systems, ITHERM*, 2012.

[58] T. Eckert, W. H. Müller, N. F. Nissen, and H. Reichl, "Modeling Solder Joint Fatigue in Combined Environmental Reliability Tests with Concurrent Vibration and Thermal Cycling," in *2009 11th Electronics Packaging Technology Conference*, 2009.

[59] O. Wittler, J. Jaeschke, O. Bochow-Neß, A. Middendorf, and K.-D. Lang, "Combined Reliability Testing: An approach to assure reliability under complex loading conditions," in *Integrated Power Electronics Systems (CIPS), 2012 7th International Conference*, 2012.

[60] P. Yang, D. Liu, Y. Zhao, Y. Tang, and H. Wang, "Approach on the Life-Prediction of Solder Joint for Electronic Packaging Under Combined Loading," to be published. Early Access.

[61] H. Qi, M. Osterman, and M.Pecht, "Modeling of Combined Temperature Cycling and Vibration Loading on PBGA Solder Joints Using an Incremental Damage Superposition Approach," *IEEE Transactions on Advanced packaging*, vol. 31(3), pp. 463–72, 2008.

[62] J. H. L. Pang, F. L. Wong, K. T. Heng, Y. S. Chua, and C. E. Long, "Combined Vibration and Thermal Cycling Fatigue Analysis for SAC305 Lead Free Solder Assemblies," in *Proceedings - Electronic Components and Technology Conference*, 2013.

[63] G. K. Hobbs, *Accelerated reliability engineering: HALT and HASS*. John Wiley & Sons, 2000.

[64] D. V. Hutton, *Fundamental of Finite Element Analysis*. McGraw-Hill, 2004.

[65] A. Hrennikoff, "Solution of Problems of Elasticity by the Frame-Work Method," *ASME Journal of Applied Mechanics*, vol. 8, pp. 619–715, 1941.

[66] R. L. Courant, "Variational Methods fot the Solution of Problems of Equilibrium and Vibration," *Bulletin of the American Mathematical Society*, vol. 49, pp. 1–23, 1943.

[67] G. Strang and G. J. Fix, *An Analysis of the Finite Element Method. Automatic Computation*. Prentice-Hall, 1973.

[68] D. Roylance, "Finite Element Analysis," *Course Material: MIT, Department of Materials Science and Engineering, Mechanics of Materials*, 2001.

[69] J. Li, T. Mattila, and J. K. Kivilahti, "Multiscale Simulation of Microstructural Changes in Solder Interconnection During Thermal Cycling," *Journal of Electronic Materials*, vol. 39, pp. 77–84, 2009.

[70] R. D. Abernethy, *The New Weibull Handbook 4th Edition*. Robert D. Abernethy, 2005.

[71] L. Xu and J. H. L. Pang, "Effect of Intermetallic and Kirkendall Voids Growth on Board Level Drop Reliability for SnAgCu lead-free BGA Solder Joint," in *2006 Electronic Components and Technology Conference*, 2006.

[72] A. International, *ASM Handbook - Volume 9 Metallography and Microstructures*. ASM International, 20204.

[73] S. Allen, M. Notis, R. Chromik, and R. Vinci, "Microstructural evolution in lead-free solder alloys: Part I. Cast Sn-Ag-Cu eutectic," *Journal of materials Research*, vol. 19, pp. 1417–1424, 2004.